

The University of Nottingham  
School of Chemistry



# Asymmetric Amine-Carboxylic Acid Organic- Inorganic Hybrid Wells Dawson Polyoxometalates

Noor Mohammad Alnahdi

A thesis submitted for the degree of Master of Research

January 2023

## **Acknowledgements**

I would like to express my gratitude to Dr. Graham Newton, my Master of Research supervisor and mentor, for allowing me to participate in and gain an in-depth understanding of research conducted in this field. As a result, both my knowledge and my experience have been expanded. In addition, I want to convey my appreciation to him for the incredible support and direction he has provided me throughout my academic year, the consistent encouragement he has provided, and his willingness to assist in any way he can.

I would like to express my sincere thanks to Dr. Kieran Jones for his direction and for sharing his knowledge and experience, which were of tremendous assistance in finishing this review to a high degree. In addition, I want to show my appreciation to him for his service, his willingness to help me whenever it was available during the year, as well as his patience in responding to any queries I had.

I would also like to thank Dr. Jack Jordan for his help and direction with the Cyclic voltammetry (CV) experiments and his help in the lab.

I would like to extend my gratitude to the other people who are a part of the Newton and NAMI groups, especially Ph.D. students Nicole Tsang, and Margaret Smith, for their help in the laboratory, with equipment and in scientific discussions.

On a personal level, I want to express my appreciation and respect for my family and my husband. They have never stopped pushing me to achieve my full potential and have given me their unwavering support.

Noor Mohammad Alnahd

# Table of Contents

Acknowledgements.....	I
Abbreviations.....	II
Abstract.....	I
<b>1 Introduction.....</b>	<b>2</b>
1.1 Polyoxometalates.....	2
1.1.2 The Wells-Dawson Structures .....	5
1.2 Organofunctionalisation of POMs.....	11
1.3 Asymmetric Hybrid POMs: Synergistic Function .....	17
1.4 Synthetic Methods for Asymmetric Functionalisation.....	19
<b>2 Aims.....</b>	<b>27</b>
<b>3 Results and Discussion.....</b>	<b>28</b>
Asymmetric Amine-Carboxylic Acid Hybrid Wells Dawson Polyoxometalates.....	28
3.1 Synthesis and Characterisation of Symmetric Hybrid POMs [P <sub>2</sub> W <sub>17</sub> O <sub>57</sub> {(PPA) <sub>2</sub> }] (1) and [P <sub>2</sub> W <sub>17</sub> O <sub>57</sub> {(AEP) <sub>2</sub> }] (2).....	28
3.2 Attempt Synthesis and Characterisation of Asymmetric Hybrid POM [P <sub>2</sub> W <sub>17</sub> O <sub>57</sub> {(PPA)(AEP)}] (3) .....	40
3.3 Purification of Asymmetric Hybrid POM [P <sub>2</sub> W <sub>17</sub> O <sub>57</sub> {(TPY)(C <sub>18</sub> )}].....	44
3.4 Exploring Photo-/Electro-Chemical Properties.....	51
3.5 Experimental.....	54
<b>4 Preparation of Symmetric Hybrid POM [P<sub>2</sub>W<sub>17</sub>O<sub>57</sub>{(RuTPY)<sub>2</sub>}] .....</b>	<b>64</b>
4.1 Synthesis of RuTPY Ligand.....	64
4.2 Experimental.....	70
<b>5 Conclusion.....</b>	<b>74</b>
5.1 List of references .....	75

## Abbreviations

$\delta$  – Chemical shift (parts per milion)

$^{\circ}\text{C}$  – Degrees Celsius

aq. – Aqueous

ATR-IR – Attenuated total reflectance infra-red

bpy – 2,2'-Bipyridine

Calc – Calculated

CV – Cyclic Voltammetry/Voltammogram

DMA – Dimethylammonium

dmbpy – 4,4'-Dimethyl-2,2'-bipyridine

DMF – Dimethylformamide

DMSO – Dimethylsulfoxide

eq. – Equivalentents

ESI-MS – Electrospray Ionisation Mass Spectrometry

$\text{Et}_2\text{O}$  – Diethyl ether

EtOH – Ethanol

Hz – Hertz

IR – Infrared (Spectroscopy)

IPA – Isopropyl alcohol

$J$  – Coupling constant in NMR spectroscopy

M – Molar

$m/z$  – Mass-to-charge ratio

Me – Methyl

MeCN – Acetonitrile

MeNO<sub>2</sub> – Nitromethane

MeOH – Methanol

MW – Molecular Weight

NMR – Nuclear Magnetic Resonance

obs – Observed

POM – Polyoxometalate

PPA – 3-Phosphonopropionic acid

ppm – Parts per million

RT – Room temperature

TBA – Tetra-n-butylammonium

TEA – Triethylamine

TMSBr- Trimethylsilyl bromide

tpy – 2,2':6',2''-Terpyridine

TRIS – Tris(hydroxymethylmethane)  $-(\text{OCH}_2)_3\text{C}-$

UV-Vis – Ultraviolet-Visible

## Abstract

Symmetric organofunctionalised polyoxometalates have been widely studied in recent years, due to their desirable characteristics, including catalytic properties and varied redox behaviour. However, limited research has been conducted into the design, synthesis and characterisation of asymmetric organofunctionalised hybrid POMs. These are of increasing interest because of their tunable electronic properties and ability to access precise functionality.

This work discusses the process of successful synthesis and characterisation of symmetric hybrid Polyoxometalates  $[P_2W_{17}O_{57}\{(PPA)_2\}]$  and  $[P_2W_{17}O_{57}\{(AEP)_2\}]$  and designing accessible synthetic processes for creating multifunctional hybrid materials that provide good control in modifying their structure and characteristics is a persistent issue. The availability of asymmetrically organofunctionalised hybrid polyoxometalates (POMs) offers the potential for developing new molecular materials with various functions that can be adapted to meet the needs of specialised applications.

A simple, low-cost, and high-yielding one-pot synthesis technique based on the Wells–Dawson anion was attempted to be employed in the process of isolating a novel asymmetric hybrid POM  $[P_2W_{17}O_{57}\{(PPA)(AEP)\}]$ . This thesis discusses the development of the synthetic method as well as the characterisation of the asymmetric bi-functionalised hybrid polyoxometalates structure that the hybrid molecule has.

The inclusion of transition metal functionality into the asymmetric hybrid POM at the attached chelating group is investigated, and synthetic strategies are described. As an organophosphonate ligand, a ruthenium(II) polypyridyl complex is produced for direct grafting to the cluster anion during a modified one-pot synthesis.

# 1 Introduction

## 1.1 Polyoxometalates

Polyoxometalates (POMs) are a fascinating family of discrete anionic metal oxide clusters. They consist of a broad class metal oxide clusters of group 5 and 6 transition metals bound by linked and terminal oxo ligands in their maximum oxidation state. Using the basic formula  $MO_x$ ,  $M = Mo$  (VI),  $W$  (VI), and  $V$  (V).<sup>1,2</sup> These species have shown promise in various applications, including conventional, magnetism<sup>3</sup>, catalysis<sup>4</sup>, energy conversion<sup>5</sup>, medicine.<sup>6</sup> They are excellent building blocks for functional materials due to their extensive structural diversity, excellent stability, and adaptability in chemical and physical properties.<sup>7,8</sup>

### 1.1.1 General POM Structure, Bonding and Assembly

There is a vast library of polyoxometalate structures with varying shapes, sizes, and compositions, and it is possible to generalise to understand POM synthesis and bonding.<sup>9</sup> POMs are anionic by nature, and when linked with charge-balancing cations, the entire structure, including the polyanion cluster, counterions, and solvating molecules of the hydration shell, is seen as a single entity. The fundamental building blocks of the metal oxide framework are  $\{MO_x\}$  coordination polyhedra, where  $x$  can be anywhere from 4 to 7, such as four in the Wells-Dawson and Keggin structures and six in the Anderson-Evans ("Anderson") structure, to create tetrahedral or octahedral geometries, respectively. However, the typical coordination number is 6 in a pseudo-octahedral arrangement. In general, POMs are produced by acid-mediated condensation processes of these  $\{MO_x\}$  polyhedra, culminating in their polymerisation via corner-, edge-, or exceptionally rarely face-sharing M-O bonds. Fundamentally, a significant trans effect of the unshared terminal M-O bonds limits the amount of oxo-groups that may occupy terminal positions in each polyhedron. One terminal oxo-ligand is seen the majority of the time in octahedral  $\{MO_6\}$  addenda, which are often located in iso- and hetero-polyanions. However, according to "Lipscomb's Principle,"<sup>10</sup> there can only be a maximum of two unshared oxygen atoms detected in these structures. With the remaining oxygen atoms used to bridge being shared with the other addenda. Because of the movement of the metal centre toward the terminal oxo-ligand, the terminal M=O bonds at the

cluster surface have a substantial polarisation in the direction of the addenda atom. This is due to the trans-effect weakening the opposing M-O bond and distorting the octahedron. This crucially reduces the basicity of the polyoxoanion surface, which restricts the polymerization of the polyhedra by additional protonation, limits the amount of condensation of the metal oxide framework, and explains their existence as molecular species. Isopolyoxoanions comprise purely of a metal oxide framework, which is denoted by the generic formula  $[M_mO_y]^{n-}$ , where M is the metal atom. One or more heteroanions,  $\{XO_y\}^{n-}$ , are inserted into the metal oxide structure to create heteropolyoxoanions,  $[X_xM_mO_y]^{n-}$ , where X is frequently the main group element, such as P, S, or Si. The ratio of X/M determines unique structures.<sup>11</sup> (**Figure 1A**).

The radii of the atoms in the  $\{MO_x\}$  polyhedra and the polyhedral connections play an intricate role in balancing the Coulombic forces that control the discrete cluster formation of polyoxometalates. The ability to form terminal metal oxygen bonds via d-p orbital interactions and

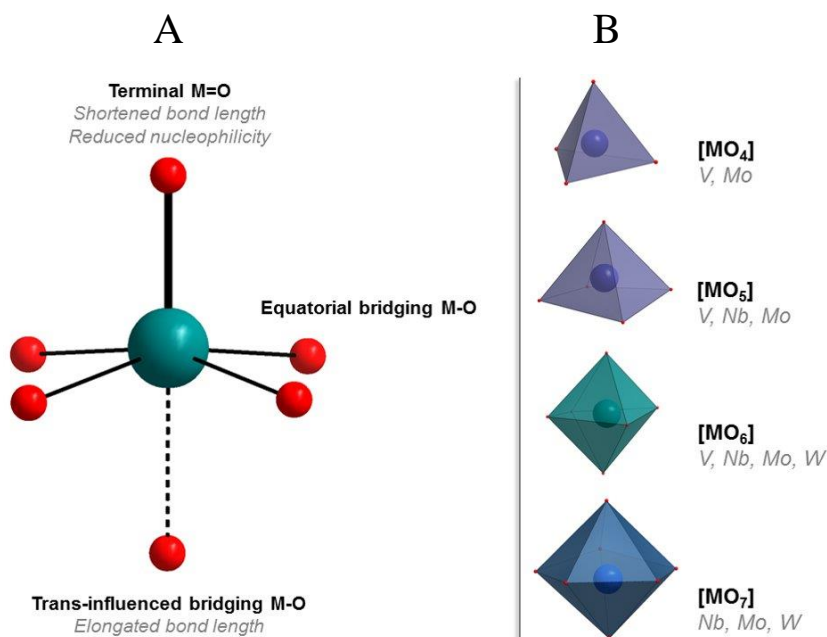


**Figure 1.** A) A representation in visual form of the trans-effect on the metal's coordination environment in polyoxometalates | B) Polyhedral units frequently found as POM structure building blocks.

high coordinate bonding to hard ligand oxygen atoms depends on the availability of vacant d-orbitals and appropriately large ionic radii in the transition metal centres. Given these considerations, early transition metals from groups V and VI, with a  $d^0$  or  $d^1$ , in their maximum oxidation state configuration are the metal ions typically involved in polyoxoanion formation.<sup>12</sup>

Oxo-ligands, which comprise the polyhedron's vertices, are the structurally versatile components of the POM, serving as bridging atoms between metals to permit polycondensation while preventing the POM from expanding indefinitely into infinite metal oxide structures through stable terminal multiple bonds. In a typical octahedral configuration, the terminal oxo ligands exhibit a strong thermodynamic trans-effect by weakening the bond to the bridging oxygen atom that shares its orbitals, located at the opposite vertex of the octahedron. This is the main reason for the high stability of many POM clusters. Structurally, this leads to the displacement of the metal centre towards the terminal oxo-ligand, therefore, away from the idealised octahedral geometry (**Figure 1B**). The high polarisation of the terminal oxo-groups toward the addenda atom (relative to the bridging oxo-ligands) has electronic implications. This in turn significantly lowers the basicity of the oxide surface, preventing protonation and reducing the tendency for further acid-mediated condensation reactions. The result of this trans-effect weakening the opposing M-O bond and distorting the octahedron.

POMs are typically created through self-assembly in a "one-pot" synthesis that involves acidifying an aqueous solution of salts containing the metal oxo anions, including  $\text{Na}_2\text{WO}_4$  or  $\text{NaHVO}_3$ . The metal oxide fragments increase nuclearity and are protonated to form oxide hydroxide compounds as the pH decreases and the solution becomes more acidic. These compounds subsequently condense into intermediate units blocks before forming the polyoxoanion structure (**Figure 2**).<sup>1</sup> The salt of the heteroanion, such as a phosphate or silicate, is also added, acting as a templating anion around which the metal oxide polyhedra condense.

The synthesis methods and other factors influencing the POM self-assembly process remain of great research interest.<sup>13,14</sup> In addition to the choice of metal ion and heteroanion, experimental variables, including the relative concentrations (or stoichiometric ratio, M/X) of the anions, pH, temperature, solvent, pressure, and the presence of any ligands or reducing agents, can affect the self-assembly and nature of the resulting POM.<sup>15,16</sup>

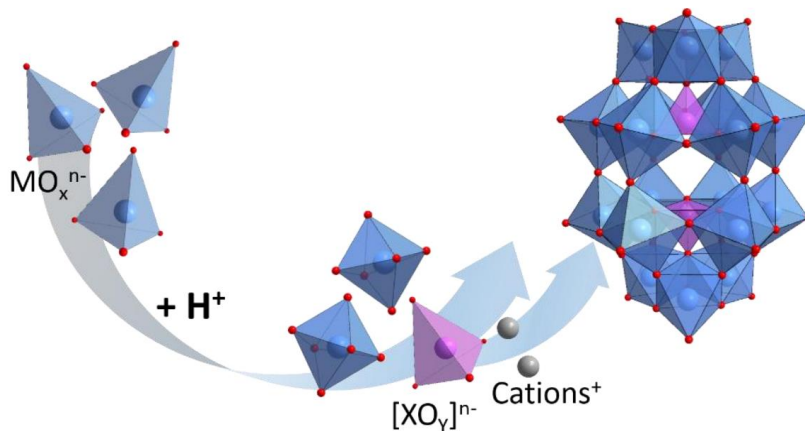


**Figure 2.** A diagram showing the self-assembly process by which metal-oxo particles condense into polyoxometalates (POMs).

POMs are typically isolated in the solid state from solution by precipitation after the addition of an alkali metal (typically  $Na^+$  or  $K^+$ ), ammonium, or organic tetraalkylammonium salts. The choice of counterion is important for controlling solubility and therefore, is crucial for successful crystallisation. Numerous studies have shown that the counterion's influence over cluster behaviour, particularly reactivity and assembly/ aggregation.<sup>17,18</sup>

### 1.1.2 Wells-Dawson and Keggin Structures

The simplest and most established heteropolyanion structure, the Keggin, was first identified in 1933 using the -phosphotungstate anion  $[PW_{12}O_{40}]^{3-}$  (**Figure 3**).<sup>19</sup> It consists of a core tetrahedral heteroanion  $\{XO_4\}^-$ , surrounded by 12 octahedral  $\{MO_6\}$  polyhedra arranged in 4 units comprised of three grouped octahedra,  $\{M_3O_{13}\}$ .<sup>20</sup> The Keggin structure can exist as five isomers,  $\alpha$ ,  $\beta$ ,  $\gamma$ ,  $\delta$ , and  $\epsilon$ , due to the different orientations of the  $\{M_3O_{13}\}$  units, which can be rotated  $60^\circ$  around three symmetry axes.<sup>21</sup> An equilibrium, which depends on the heteroatom and the solvent environment, controls the propensity of Keggin-type POMs to self-assemble as the  $\alpha$ ,  $\beta$  isomer.<sup>22-24</sup> The  $\gamma$ ,<sup>25</sup>  $\delta$ ,<sup>26</sup> and  $\epsilon$  isomers,<sup>27</sup> on the other hand, have very few examples because their isolation frequently requires specialised synthetic techniques.

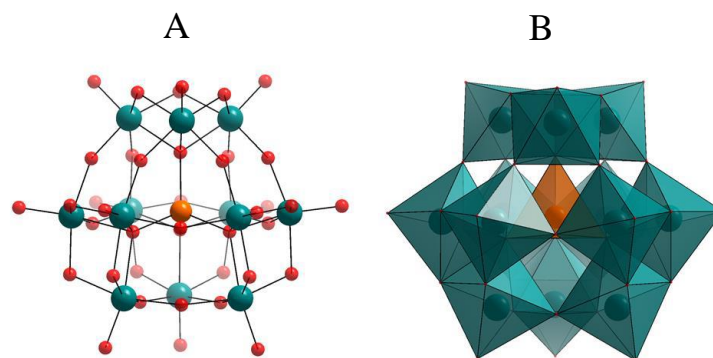


**Figure 3.** A) Ball and stick and polyhedral, B) representation of the Keggin polyoxometalate  $(\text{XM}_{12}\text{O}_{40})^5$

For some structures, primarily the Keggin and Dawson anions, pH-controlled hydrolysis of the cluster allows for the controlled removal of one or more of the addenda atoms. "lacunary" polyoxometalates are the name given to the resulting species, the term "lacuna" refers to a gap or unfilled space. The several lacunary structures of the Keggin and Dawson clusters constitute the richest and most thoroughly investigated set of lacunary polyanions<sup>28</sup>, due to their potential as platforms for the synthesis of organic-inorganic hybrid compounds with a variety of organofunctionalisations.<sup>29</sup> Mono-,  $\{\text{XM}_{11}\}$ , di-,  $\{\text{XM}_{10}\}$  and tri-,  $\{\text{XM}_9\}$ , lacunary structures based on the Keggin cluster are recognised, most often produced from the Si and P templated cluster types, of which the tungstosilicates are typically more stable (**Figure 4**). Multiple isomeric versions of the mono- and tri- lacunary structures are available depending on the isomer of the plenary Keggin anion from which they have generated structurally and the places from which the addenda are removed. Di- lacunary  $\{\text{W}_{10}\}$  structures exist for both phospho- and silico-tungstate Keggin anions. However, the synthesis and isolation of the stable Si analogue is more straightforward and more accessible to obtain in a single isomeric form ( $\gamma$ ).<sup>30</sup>

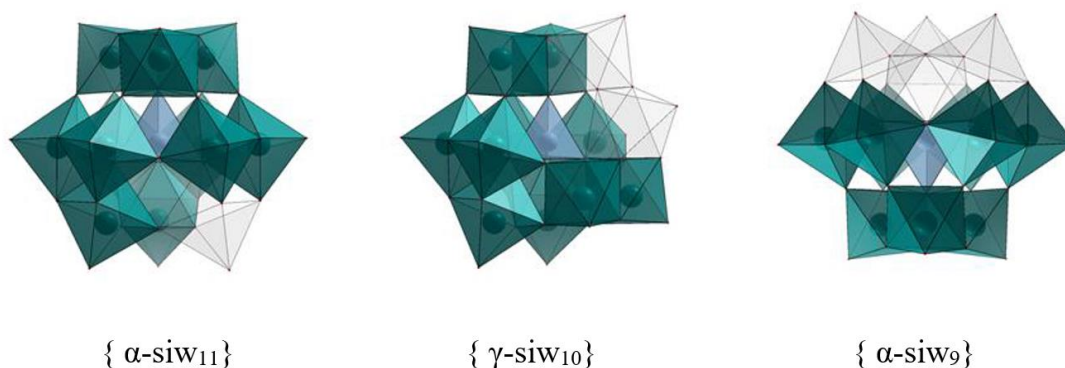


**Figure 4.** Based on the Si-templated Keggin anion, polyhedral representations of a few isomers of mono, di, and tri lacunary structures.

A potassium salt was found to be the initial phosphotungstate Wells-Dawson cluster in 1953. Since then, this heteropolyanion has received considerable attention.<sup>31,32</sup> Heteropolyanion clusters are widely investigated because of their inherent higher stability to isopolyanions. For example, the redox characteristics of Wells-Dawson  $[\text{X}_2\text{M}_{18}\text{O}_{62}]^{n-}$  and Keggin  $[\text{XM}_{12}\text{O}_{40}]^{n-}$  clusters, have been extensively studied as well as their application in catalysis.<sup>33</sup> Phospho-molybdate and tungstate structures are the most common of the Dawson and Keggin assemblies.

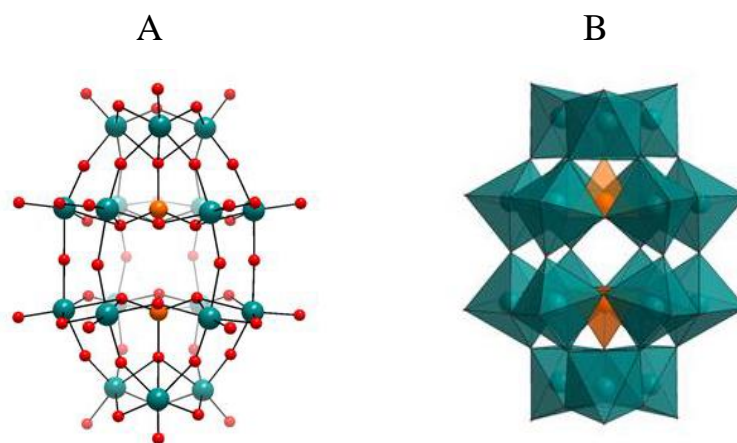


**Figure 5.** A) Ball and stick and polyhedral. B) representation of the Wells-Dawson polyoxometalate ( $\text{X}_2\text{M}_{18}\text{O}_{62}$ )

Since the Wells-Dawson cluster appears to be two fused tri-lacunary  $\{XM_9\}$  Keggin fragments, it is closely related to the Keggin structure. The structure has three bimetallic units made from two condensed octahedra,  $\{M_2O_{10}\}$  and two internal heteroanion centers, typically tetrahedral linked to one  $\{M_3O_{13}\}$  unit each. The Dawson cluster (**Figure 5**), composes the trimetallic capping units while the dimetallic units form the belt of the cluster (**Figure 6**). The capping polyhedra comprise six terminal oxygen atoms, while on the belt regions comprise twelve. Interestingly, The chemical characteristics of the Dawson cluster are substantially influenced by the discrepancy between the "cap" and "belt" locations, where the electron transport qualities are different.<sup>34</sup>

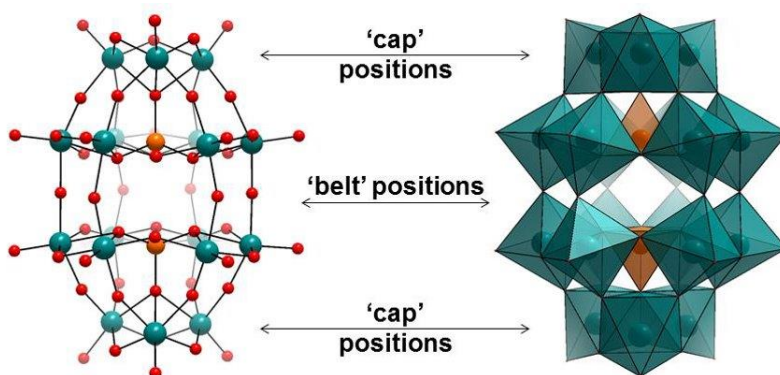


**Figure 6.** Schematic illustrating the two polyhedral environments of the Dawson structure.

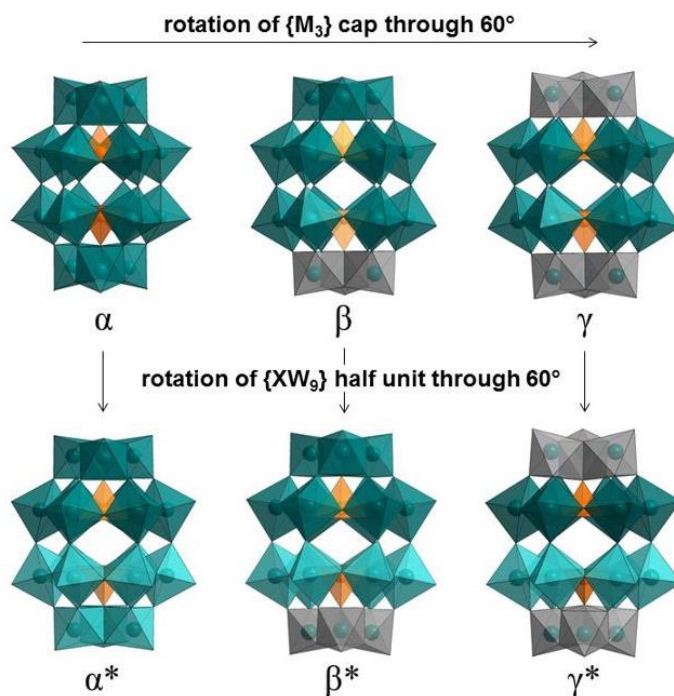


**Figure 7.** The six rotational isomers of Wells-Dawson structure.<sup>35</sup>

Similar to the Keggin, the Dawson anion has symmetry components that lead to the occurrence of several structural isomers.<sup>21</sup> The primary  $\alpha$ - isomer is the most stable, and is used as the starting structure to create the  $\beta$ - and  $\gamma$ - isomers by rotating one or both of the  $\{M_3O_{13}\}$  caps  $60^\circ$  around the  $C_3$  axis (**Figure 7**). Three different isomers,  $\alpha^*$ ,  $\beta^*$ , and  $\gamma^*$ , are created when one of the  $\{XW_9\}$  halves is rotated by  $60^\circ$ , however, only the  $\gamma^*$ - variant has been observed experimentally.<sup>36,37</sup>

The Keggin and Dawson heteropolyanion structures have significant variability in the central heteroanion and addenda components. The tungstate (VI), molybdate (VI), and vanadate (V) structures are the most studied. However, many reported structures either fully swap out addenda for more typically metallic elements or contain the metals as mixed addenda. The most prevalent group heteroatoms are P and Si, followed by S and As, while non-tetrahedral anions have also been observed in a few non-classical forms.<sup>15,38</sup>

In the Dawson cluster, fewer lacunary structures may be accessed and isolated without base degradation of the entire structure occurring. Only the  $\alpha$ - $\{X_2W_{18}\}$  isomer can produce a stable lacunary species. These structures are created by removing a single metal from either one of the two belt locations or one of the cap positions, hence mono-lacunary structures can display positional isomerism. Additionally, it is possible to remove either the six addenda of the more prominent "face" type unit  $\{M_6O_{14}\}$  or the three addenda of the entire  $\{M_3O_{13}\}$  cap to produce the less typical  $\{X_2M_{15}\}$  tri-lacunary and  $\{X_2M_{12}\}$  hexalacunary structures.

### 1.1.3 Properties of POMs

POMs are of particular interest due to their wide range of properties, including high solubility, tuneability and interesting redox properties. These clusters are also referred to as soluble metal oxides, due to their ability to form a wide range of interactions, including hydrogen bonds, electrostatic interactions, non-covalent interactions, and covalent interactions, resulting in high solubility in a variety of polar solvent media. The tuneable nature of POMs composition, structure, charge, and size has sparked significant interest for use in various applications, such as catalysis and versatile building blocks for the construction of larger materials.<sup>39,40</sup> It is also possible to incorporate into materials such as composites, polymers, and films.<sup>8,41</sup> POMs can also interact

with biomolecules,<sup>42,43</sup> and numerous studies have demonstrated their biological activity. As a result, new applications in biotechnology and pharmaceuticals are being explored.<sup>44,45</sup>

According to their acid-base characteristics and interesting redox behaviour, heteropoly acids, particularly those based on the Keggin and Dawson clusters, are most frequently utilised in catalysis.<sup>4</sup> This is one of the most extensively researched areas and very common application of POM chemistry. The protonated species acts as a powerful proton donor, hence, acid catalyst for a wide range of processes, including esterification and hydrolysis.<sup>46</sup> Additionally, the base-catalyzed processes often exploit the electron-rich surface oxygen atoms on polyanions as primary sites to attack electrophiles or remove protons. This is especially true for highly charged lacunary structures.<sup>47</sup>

POMs now attract a lot of attention as catalysts in the production of green energy, such as water oxidation and CO<sub>2</sub> reduction,<sup>48</sup> due to the increasing urgency to address environmental problems in more recent years.<sup>48,49</sup>

The rich electrochemistry displayed by many POMs plays an important role in their catalytic behaviour and reactivity. The charge density, geometry, and type of the counter-cations all have an impact on the electrochemistry of POMs in addition to the redox-active metals present in the POM framework. They have a remarkable ability to store and transfer multiple electrons because their framework is composed of highly, sometimes completely (d<sup>0</sup>), oxidised transition metal ions. Many can also undergo rapid multi-electron redox processes while maintaining structural stability, in particular the Dawson and Keggin clusters.

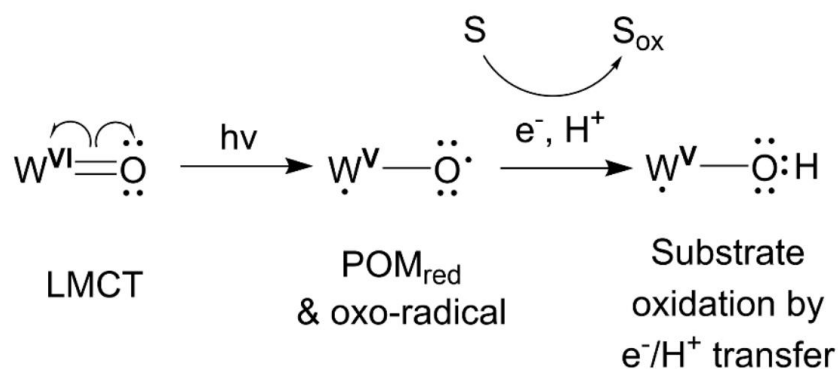


**Figure 8.** The photoreduction of excitation of the LMCT band and the subsequent oxidation of a substrate.<sup>50</sup>

In addition to their rich reversible redox chemistry, POMs are recognised for their inherent photochemistry, which makes them desirable photocatalysts.<sup>51,52</sup> They exhibit distinct UV absorption bands due mainly to O–M ligand-to-metal-charge transfer (LMCT) bands. A radical centred on the oxo-ligand is produced when an electron is promoted from a doubly occupied bonding orbital (the HOMO) of terminal oxygen to an unoccupied antibonding d-orbital (the LUMO) on the metal (**Figure 8**). The photocatalytic activity of POM is based on this photo-excited species, which entails a brief triplet state that is more reactive in both oxidised and reduced form than when in the ground state. The so-called "heteropoly blues" are mixed-valence species marked by a distinctive blue colour due to a newly formed intervalence charge-transfer (IVCT) absorption band at about 700 nm. Electron transfer (or proton-coupled electron transfer) from a suitable substrate can trap  $d^1$  electrons on the metal centres.

## 1.2 Organofunctionalisation of POMs

Organofunctionalisation is a direct and highly controllable method for modifying the electronic structure and physical characteristics of a POM cluster by introducing organic groups, typically silicon or phosphorous-containing species. This allows the nature of the non-covalent interactions can be tuned accordingly to access desired characteristics, creating an organic-inorganic hybrid material. The term "hybrid material" is defined as a composite comprising of organic and inorganic

components combined on a molecular level.<sup>53</sup> Combining each constituent material's physical and chemical features, organic-inorganic hybrid chemistry is drawing considerable attention as a way of creating new functional materials in nanoscience and nanotechnology.<sup>54</sup> Characteristics can be modified in both the organic and inorganic component's intended structure and composition, as well as in how they are integrated into a hybrid material. Synergistic effects can improve the inherent properties of the final materials' molecular or nano building blocks.

### 1.2.1 Introduction to Hybrid POMs

The enormous structural diversity of hybrid POM clusters and the excellent control possible at the molecular level, there is the opportunity to diversify and optimise POM clusters for specific applications. Here, with a focus on covalent organofunctionalisation, a brief summary of the synthetic methods used for fusing organic moieties with POMs to create organic-inorganic hybrid POM molecules (or "hybrid POMs") is provided.

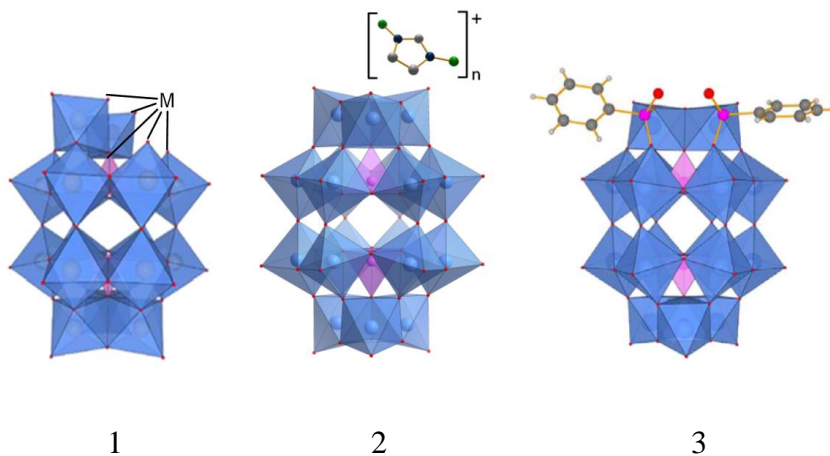


**Figure 9.** Schematic of three representations of POM functionalisation approaches.<sup>55</sup>

- 1) the replacement of addenda atoms in lacunary POMs with transition metals, lanthanides, or main-group elements.
- 2) non-covalent interaction of cationic inorganic or organic complexes and molecules with POM.
- 3) the covalent grafting of organic or organometallic species through substituted addenda atoms in lacunary structures or to terminal oxygen atoms.

Three basic methods are used to functionalise POMs (**Figure 9**). The first is the placement of transition metals, lanthanides, or main-group elements in place of addenda atoms in the lacunary structure. The second, cationic inorganic or organic molecules and complexes interact non-covalently with the POM. Third, the covalent attachment of organic or organometallic species, whether through substituted addenda atoms in the open positions of lacunary structures or to terminal oxygen atoms.

The interactions between the POM and its other constituents determine the two types of organic-inorganic hybrid POM. Hydrogen bonds, van der Waals interactions, and electrostatic interactions are examples of weak non-bonding interactions that can occur in class I hybrids. As a matter of fact, the electrostatic interactions of common organic counter cations, like tetra alkyl ammoniums with POMs, mainly correspond to a simple class I hybrid. However, numerous studies have shown that much more complex cationic species, the same as organometallic complexes, photosensitisers, and ionic liquids, can also be used.<sup>56,57</sup> Although the materials properties are largely driven by the cation and aren't easily controlled by specific interactions, these materials can be susceptible to changes in the solution, such polarity, ionic strength, pH, temperature and other variables.<sup>58,59</sup>

Class II hybrids are far more resilient than class I hybrids due to the strong covalent bonding between the organic moieties and the POM, despite being generally more challenging to synthesise. Covalent functionalisation allows for the fine-tuning of a wide variety of characteristics, allowing for a more efficient strategy in the creation of functional materials. The tunability provides a far great scope enables a more varied design strategy, hence, different structures with highly tailored properties for functional materials.<sup>60,61</sup> Class II organic-inorganic hybrid POMs will be the main focus of the work in this thesis.

## **1.2.2 Covalent Organofunctionalisation**

The covalent organofunctionalisation of POMs involves the integration of organic moieties into these clusters. Covalent organofunctionalisation has been used to both control and enhance their redox properties for a variety of applications, including energy storage, molecular magnetism and catalysis. Dolbecq,<sup>62</sup> Proust,<sup>63</sup> and Parac-Vogt<sup>64</sup> have all published comprehensive reviews on the wide range of synthetic techniques for the covalent organofunctionalisation of POMs. The covalent approach, involved in class II hybrid preparation, offers significant control over the species

physicochemical properties as the intrinsic properties of the resulting hybrid materials can be tuned through the design of the individual components. Subsequently, this allows the hybrids to exhibit more diverse and precise functionality. Typically, organic ligands are linked by the cluster's oxo-anions, primarily in lacunary structures, to p-block components such as N, Si, P, Ge, and Sn which are connected to an organic group. Alternatively, d- and f-block components are similarly bound to the cluster surface or inserted into a vacancy and can have organic groups coordinated. However, this method of covalent functionalisation will not be further described.

Isopolyoxometalates are primarily organofunctionalised by nitrogen-based bridging groups that are directly attached to metal addenda in place of oxo ligands. However, organo-azido, -hydrazido, and -diazenido bridges are also frequently used. Organoimido groups are the most prevalent. In contrast, the Keggin and Dawson clusters, which have been described for the functionalisation of the heteropolyoxometalates, are markedly more diverse. Here, we provide a quick summary of the heteropolyoxometalate covalent organofunctionalisation mechanisms. Alkoxide functional groups are one of the most frequently used in covalent functionalisation. The use of triols, especially those based on tris(hydroxymethyl)alkanes, are by far the most widespread.

The triols are frequently linked to the Anderson cluster, notably polyoxomolybdates  $[\text{XM}_6\text{O}_{18}\{(\text{OCH}_2)_3\text{CR}\}_2]^{n-}$  ( $\text{X} = \text{Mn}^{\text{III}}, \text{Al}^{\text{III}}, \text{Cr}^{\text{III}}, \text{Fe}^{\text{III}}, \text{Co}^{\text{III}}$ ),<sup>65</sup> despite having been utilised to functionalise a variety of POM clusters, including mixed-addenda Dawson structures ( $[\text{P}_2\text{W}_{15}\text{V}_3\text{O}_{62}]^{9-}$ ).<sup>5</sup> Condensation or esterification of hydroxy or alkoxo groups with the bridging oxo ligands of the central heteroanion  $\{\text{XO}_6\}$  results in the formation of tris(hydroxymethyl)alkane Anderson hybrids. These typically form a bifunctionalised structure by capping both faces of the cluster (**Figure 10**). When the structure terminated by a reactive group that can be employed in subsequent reactions, the tris(hydroxymethyl)methane group  $-(\text{OCH}_2)_3\text{C}-$ , TRIS, has frequently been used as a post-functionalisation platform.<sup>64</sup>

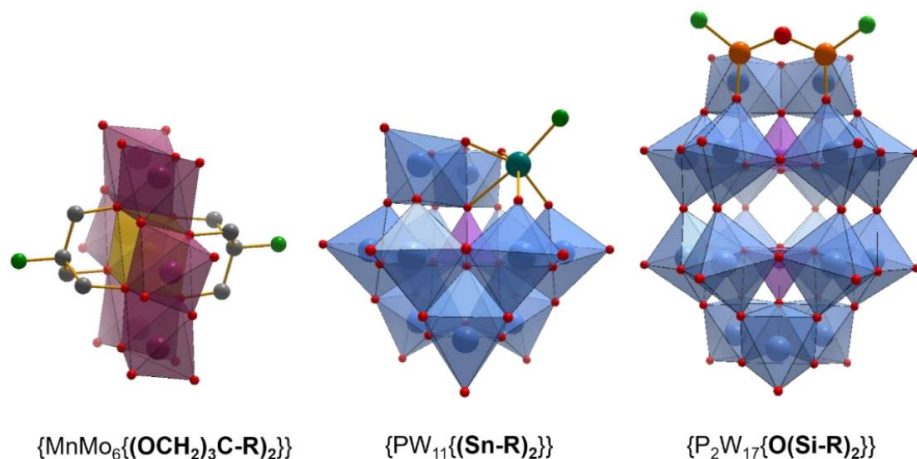


**Figure 10.** Hybrid heteropolyxometalates are represented as polyhedra and ligands represented as balls and sticks, with illustrations of three typical organofunctionalisation techniques. Plum polyhedra represent  $\{\text{MoO}_6\}$ , magenta polyhedra represent  $\{\text{PO}_4\}$ , yellow polyhedra represent  $\{\text{MnO}_6\}$ , and blue polyhedra represent  $\{\text{WO}_6\}$ . Red spheres represent Oxygen, grey spheres represent carbon, orange spheres represent silicon; teal spheres represent tin and green spheres represent the R group.<sup>55</sup>

Given the rarity of molybdate and vanadate lacunary structures, functionalisation of Keggin and Dawson species is typically undertaken via the tungstate lacunary structure. This procedure involves the removal of one  $\{\text{MO}\}$  or multiple  $\{\text{M}_x\text{O}_{2x}\}$  units from the cluster via pH-controlled breakdown. Due to their higher nucleophilicity and proximity to the cavity's surface, or "lacuna" the unshared oxygen atoms are more reactive to electrophilic groups. One such class of substances that can be inserted into the lacuna site(s) are organotin compounds. Organostannyl hybrids are some of the most developed. When utilised as an electrophilic reagent, organotin trihalides typically bond to four lacuna oxo groups and one heteroanion oxo group to insert a single tin centre with a pendant R-group into a lacunary site (**Figure 10**).<sup>66</sup> While the principle of organogermanium functionalisation is quite similar to that of organotin analogues, far fewer instances have been documented.<sup>67</sup>

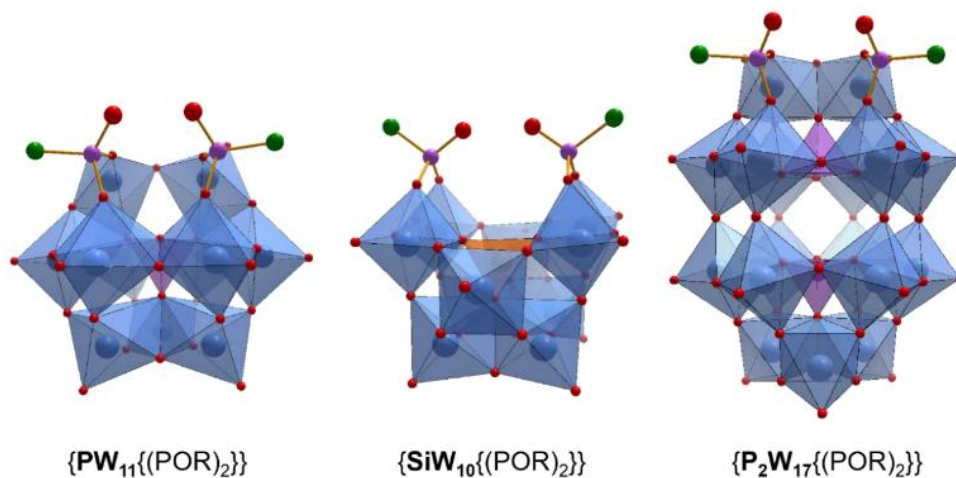


**Figure 11.** Schematic illustrating the Keggin and Dawson clusters of hybrid organophosphonates in polyhedral, with ball and stick ligand representation. Red spheres represent oxygen atoms; magenta spheres represent phosphorus atoms; green spheres represent the R group. Blue polyhedra represent  $\{WO_6\}$  units; magenta polyhedra represent  $\{PO_4\}$  units; orange polyhedra represent  $\{SiO_4\}$  units.<sup>55</sup>

Organosilicates, modified by hydrolyzing Si-Cl or Si-OR bonds using trichlorosilanes or trialkoxysilanes as reagents, is another frequently used organic group to modify lacunary Keggin and Dawson clusters. When using the mono-, di-, and tri-lacunary structures of the Keggin POM, which allow for the incorporation of various numbers of silicon centres, many organosilyl hybrids have been produced.<sup>68,69</sup> However, only functionalised monolacunary structures have been described for the Dawson structure. Each silicon centre is grafted onto one pair of the lacuna oxo-groups to form two organosilyl groups, which are then connected by a siloxane bridge (-Si-O-Si-) across the empty site. **(Figure 10)**<sup>70,71</sup>

Organophosphonate and organoarsenate derivatives are the final ones to be discussed. Although there are very few recorded instances of the latter, they are similar in reactivity and bonding.<sup>72</sup> Only two phosphonate groups inhabit unoccupied sites on a single cluster, unlike the organosilyl derivatives, regardless of whether that be mono-, di-, or tri-lacunary Keggin clusters and mono-lacunary Dawson clusters. **(Figure 11)**<sup>72-75</sup>

Thus, phosphonic dichloride ( $RPOCl_2$ ) or phosphonic acid ( $RPO(OH)_2$ ) groups react with pairs of nucleophilic oxoanions to form phosphonic acid, and the latter requires additional stoichiometric

acid as a catalyst for the condensation reaction, thereby introducing two organophosphonate ligands into a free site. The interest in the strong electronic conjugation between the organic component and the POM cluster via the phosphonate linker, which is covered in more detail below, has led to an increase in reports of organophosphonate hybrids in past years.<sup>55</sup>

### 1.3 Asymmetric Hybrid POMs: Synergistic Function

The majority of reported bi-functionalised hybrid POMs are symmetric systems, where both organic moieties bound to the cluster core are identical. Asymmetric POM synthesis involves the controlled addition of two distinctly different organic groups to create an asymmetric hybrid species. Access to these cluster types are of great interest as it has the potential to create new molecular nanomaterials with multiple or modular functionality and allowing them to be tailored for other highly specific or advanced applications. Several asymmetric hybrid POM systems have been described,<sup>76,77</sup> showing encouraging improvements in function over their unmodified POM clusters and their symmetric hybrid POM counterparts. Oms & Saad et al.<sup>77</sup> used post-functionalisation techniques to produce unique photochromic chemicals from asymmetric spiropyran (SP)-functionalised hybrid clusters. This asymmetric TRIS-NH<sub>2</sub>/TRIS-SP hybrid product, [MnMo<sub>6</sub>O<sub>18</sub>{(OCH<sub>2</sub>)<sub>3</sub>CNH<sub>2</sub>} {(OCH<sub>2</sub>)<sub>3</sub>CNHC<sub>21</sub>H<sub>19</sub>N<sub>2</sub>O<sub>4</sub>}], was obtained through gradual crystallisation from a pre-made symmetric TRIS-NH<sub>2</sub>/TRIS-NH<sub>2</sub> Mn-Anderson, [MnMo<sub>6</sub>O<sub>18</sub>{(OCH<sub>2</sub>)<sub>3</sub>CNH<sub>2</sub>}<sub>2</sub>], and <1 eq. of a carboxylic acid -terminated spiropyran.<sup>76</sup> In contrast to the symmetric TRIS-SP/TRIS-SP counterpart, the TRIS-NH<sub>2</sub>/TRIS-SP cluster displayed solid-state photochromic characteristics at room temperature and light intensity.

By combining a second functional moiety, an optically-active spironaphthoxazine (SN), and a fluorescent boron dipyrromethene, shows that this molecule has the potential to be further developed by post-functionalisation at the free amine position (BODIPY).<sup>77,78</sup> In addition, the photochromic and/or fluorescence behaviours of the two asymmetric systems differed from those of their symmetric counterparts, revealing significant synergistic effects between the two moieties and the POM centres in the asymmetric structure. The most striking finding was that activating the photochromism of the SP moiety with UV or yellow light irradiation allowed for fine-tuning of the BODIPY fluorescence in the TRIS-SP/TRIS-BODIPY (SP-POM-BODIPY) system (**Figure 12**).



**Figure 12.** The photoswitchable fluorescence of an asymmetric Anderson hybrid cluster functionalised with photochromic spirocyan (SP) and luminescent boron-dipyrromethene (BODIPY) moieties.<sup>77</sup>

The photoswitchable fluorescence cycled effectively twenty times, demonstrating that the hybrid POM triad is an efficient molecular switch with superior resistance to photofatigue compared to organic SP-BODIPY devices. Similarly, Boulmier *et al.*<sup>79</sup> isolated a new tetrathiafulvalene (TTF) functionalised asymmetric Mn- Anderson cluster, TRIS-TTF/TRIS-SP, which exhibited optical characteristics peculiar to POM materials by postfunctionalising the TRIS-NH<sub>2</sub>/TRIS-SP asymmetric system.<sup>79</sup>

## 1.4 Synthetic Methods for Asymmetric Functionalisation

The development of synthetic methods for hybrid materials with the best control over incorporating various groups and modifying and tuning their characteristics is an ongoing challenge. In most cases, the reported bi-functionalised hybrid POMs are symmetric structures with two identical organic groups attached to the inorganic core. Hybrid POM structures can be further complicated by the controlled addition of two different organic and inorganic groups to create an asymmetric hybrid system, which in turn provides more opportunities for fine control over physicochemical properties and function, enhancement of synergistic effects between the various components, and management of self-assembling behaviours. Few asymmetric functionalised hybrid POMs have been reported due to the enormous challenge of overcoming their difficult synthesis and purification years. The following section highlights and describes hybrid synthetic approaches and the functional groups responsible for their key characteristics that make.

### 1.4.1 Stepwise Approach

#### 1.4.1.1 Singly- organofunctionalised hybrid POMs

Recently, isolated single-sided hybrid clusters have attracted attention as synthesis platforms for asymmetrically bi-functionalised hybrid clusters. Wu et al. reported the first synthesis of a single-TRIS-NH<sub>2</sub> functionalised Anderson-type POM by esterification of the cluster [CrMo<sub>6</sub>O<sub>18</sub>(OH)<sub>6</sub>]<sup>3-</sup> with pentaerythritol.<sup>80</sup> This achieved asymmetric functionalisation in two steps without the need for an initial double TRIS-modified POM and its subsequent post functionalisation and purification steps. The protonated structure of the Cr-Anderson-type cluster is not readily grafted on both sides at once, in contrast to the Mn-Anderson cluster that is frequently chosen for triol modification. The stability of the other three hydroxy groups on the opposite face of the cluster is increased when the three from a TRIS-based ligand are substituted for the three on the face of the cluster. This considerably reduces the reactivity towards a second ligand under the same conditions. As a result, the group used three hybrid POMs with single triol functionalisation's as precursors in a subsequent investigation to produce a series of double-sided asymmetric derivatives, [ $\{C_2H_5C(CH_2O)_3\}MMO_6O_{18}\{(OCH_2)_3CNH_2\}$ ] (M= Cr, Al, Mn). Notably, the

prevention of the symmetric side product formation allowed for a simple separation, resulting in a high yields.<sup>81</sup> It's interesting to note that both two-step techniques carried out on either single-sided hybrid precursor can give substantial yields of asymmetric result (**Figure 13**).

Most examples of asymmetric POM hybrids that have been described are based on the Anderson cluster, which the authors frequently attribute to the simple adaptable TRIS-based ligand procedure. Micoine *et al.* excellent preparation of several organotin Dawson POM hybrids stands out as an outlier.<sup>82</sup>

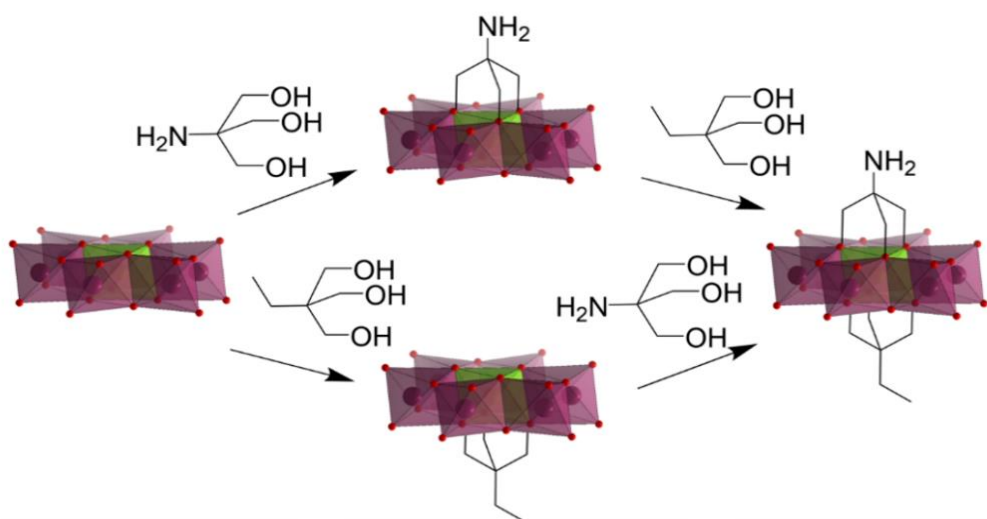


**Figure 13.** Schematic illustrating the two synthesis pathways for the asymmetric hybrid Anderson-type POM  $[C_2H_5C(CH_2O)_3]$  showing both possible orders of the two-step procedure.<sup>81</sup>

They used a novel synthetic method to produce a series of bi-functionalised hybrids,  $[P_2W_{17}O_{61}\{(SnR)(CONHAr)\}]^{6-}$ , which demonstrated that both the R and Ar organic moieties could be changed. They did this by reacting aromatic isocyanates ( $ArNCO$ ) with organotin hybrid POMs,  $[P_2W_{17}O_{61}\{SnR\}]^{7-}$  (**Figure 14a**). They had previously observed that the nearby bridging oxo sites become more nucleophilic and reactive towards electrophilic reagents when a low oxidation state metal centre is incorporated into the lacunary site.<sup>83</sup> Subsequently, they used their discovery of oxo-site activation to investigate the addition of a second, distinct organic moiety in order to create a number of new asymmetrically functionalised Dawson hybrids. The breadth of the reaction was illustrated by grafting a succession of nine electrophilic aryl-isocyanates onto one

organostannane modified Dawson (R = butyl), and phenyl-isocyanate onto two additional variants. This was done in order to show that the reaction could produce the desired products. The extent of the reaction was shown (**Figure 14b**). Sadly, they discovered that the hydrolytic instability of the doubly functionalised products led them back to the Sn-hybrid starting materials quickly after handling them in the air. Nevertheless, the method used in this work to create new bi-functionalised Dawson POM hybrids with unique, organic moieties appears promising.

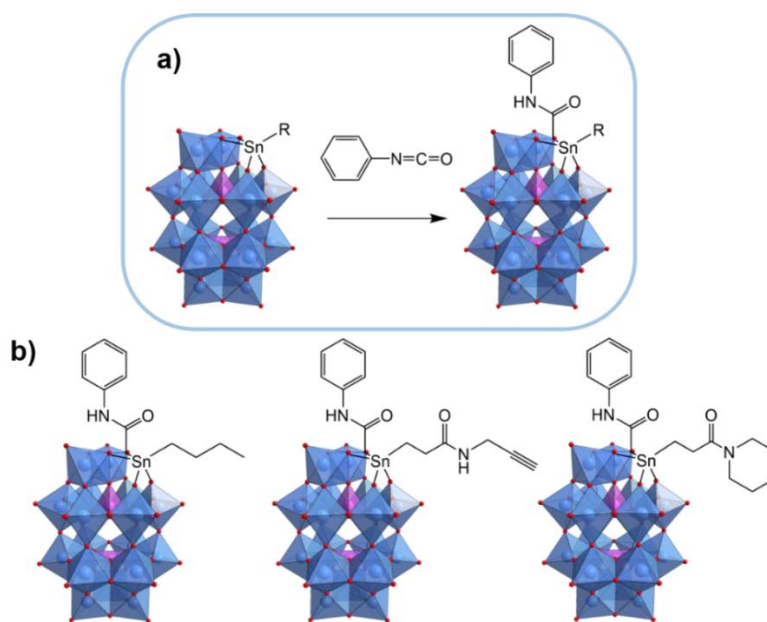


**Figure 14.** a) The overall synthesis scheme for the reaction of aromatic isocyanates with the organotin hybrid,  $[P_2W_{17}O_{61}\{SnR\}]$ , b) three instances of doubly-functionalised asymmetric hybrid POM products.<sup>82</sup>

### 1.4.2 The Post-functionalisation of Hybrid POMs

Post-functionalisation involves the covalent linking of multi-electron redox responsive POM cores with almost any organic molecule or metal cation. Direct covalent attachment of organic functional groups, for which various organofunctionalisation techniques are available, can be used to modify the intrinsic physical, chemical, and electrical properties of POMs, therefore, generating a huge range of species with highly tailored properties.<sup>62</sup> When reactive sites are present on the organic

moieties of hybrid POMs, this enables subsequent modification of the hybrid structure through covalent bonding to other organic molecules or through the coordination of metallic ion species. According to a recent summary by Anyushin et al.,<sup>64</sup> numerous hybrid POMs have undergone a variety of post-functionalisation techniques, such as amide and ester bond formations, metal-catalysed coupling reactions, and polymerisations. This illustrates the enormous scope available for POM functionalisation.

As a result, it has been possible to covalently link a variety of functional chemical components to POMs, including organometallic complexes,<sup>84</sup> dyes,<sup>77,85</sup> and biomolecules.<sup>86,87</sup> Furthermore, POMs have been designed to undergo self-assembly, extended coordination, surface immobilisation, polymerisation, and biological inclusion into novel materials and devices by combining with the appropriate organic groups.<sup>63,88</sup> As a result, covalent hybridisation offers significant potential for material properties to be regulated and tailored to the intended application. Several noteworthy documented instances of functional hybrid POM systems are discussed below.

#### 1.4.2.1 Controlled Post-functionalisation of Hybrid POMs

A Fmoc-TRIS/TRIS-NH<sub>2</sub> Mn-Anderson [MnM<sub>6</sub>O<sub>18</sub>(OCH<sub>2</sub>)<sub>3</sub>CNH-Fmoc(OCH<sub>2</sub>)<sub>3</sub>CNH<sub>2</sub>] "universal" precursor hybrid was isolated using the aforementioned RP-HPLC approach created by Yvon *et al.* This was employed for post-functionalisation at the TRIS-NH<sub>2</sub> amine (Fmoc= 9 fluorenylmethyloxycarbonyl) (**Figure 15a**).<sup>89</sup> After that, the second amine may be deprotected at the Fmoc group, enabling yet another modification (**Figure 15b**). The "universal" precursor approach should enable controlled stepwise reactions at both TRIS-based moieties, as well as in the preparation of hybrid POMs that may not be so easily distinguished from symmetric hybrid side-products. This could be due to their similar hydrophobicity/hydrophilicity and poor retention on the stationary phase. The team employed the precursor in a later investigation to build step-by-step, a unique hybrid peptide chains.<sup>90</sup>

Amino acids could be linked one at a time via peptide coupling reactions to the other side of the POM cluster before being released from the resin, after they had been attached to a pre-made amino acid chain supported by resin and the Fmoc group had been subsequently deprotected.

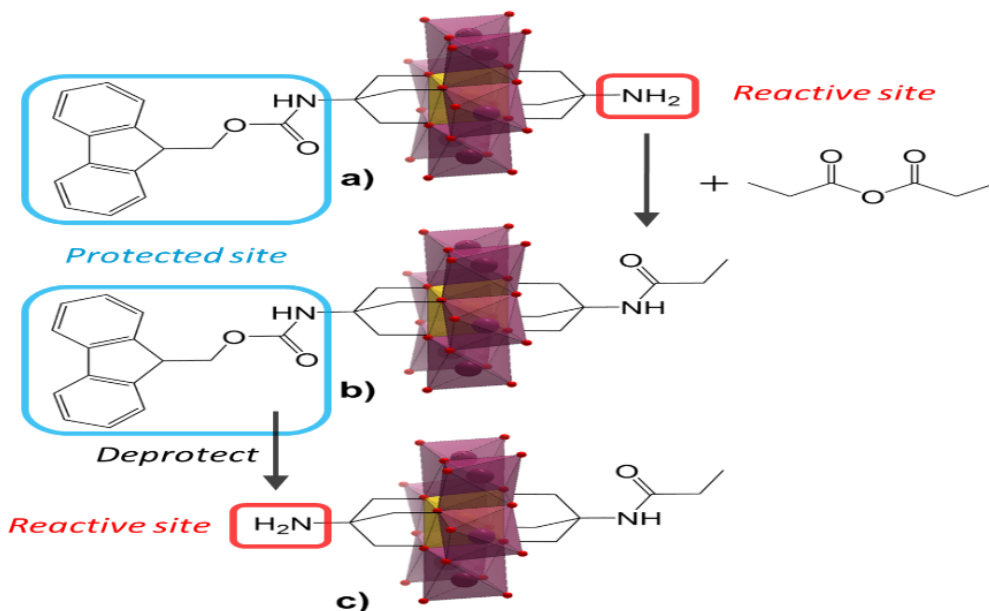


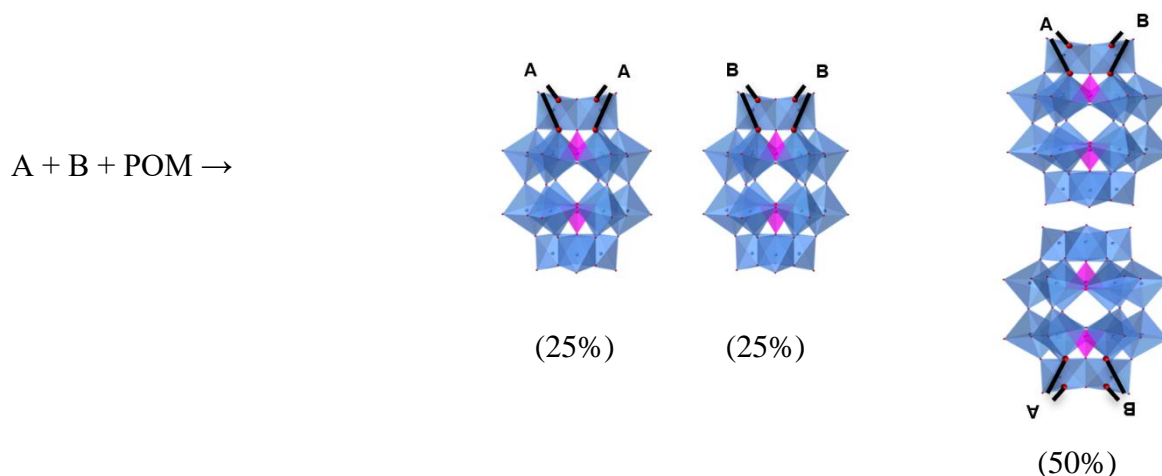
**Figure 15.** a) Fmoc–TRIS/TRIS-NH<sub>2</sub> Mn–Anderson [MnMo<sub>6</sub>O<sub>18</sub>{(OCH<sub>2</sub>)<sub>3</sub>CNH-Fmoc}{(OCH<sub>2</sub>)<sub>3</sub>CNH<sub>2</sub>}], the “universal” precursor asymmetric POM. b) An asymmetric Fmoc–TRIS/TRIS-propylamine Mn– Anderson intermediate. c) The “universal” precursor of an asymmetric TRIS-NH<sub>2</sub>/TRIS-propylamine Mn–Anderson synthesised by the post-functionalisation.<sup>89,91</sup>

Using a similar approach, successive controllable assembly of POM hybrid oligomers was achieved using Cu-catalysed alkyne-azide cycloadditions, also known as click processes.<sup>92</sup> The universal precursor was first post-functionalised to create the asymmetric TRIS-NH<sub>2</sub>/TRIS-azide or TRIS-NH<sub>2</sub>/TRIS-alkyne POM synthons, which were then separated from one-pot reaction mixtures using RP-HPLC. The TRIS-NH<sub>2</sub> moieties at the oligomer ends could then be selectively activated through coupling processes to reintroduce terminal alkynes ready for the next click addition. They could then click together like building blocks in a modular fashion. While utilising symmetric synthons would lead to uncontrolled polymerisation and polydisperse chains, using an asymmetric synthon ensures that reactions can only take place independently/individually and restrict chain growth.

These studies highlight the breadth of asymmetric POM structure research and the ability to design bespoke hybrid systems. The structure and content of the hybrid material can be carefully designed and controlled by enabling step-by-step post-functionalisation at specific sites.

### 1.4.3 Purification from Symmetric Side-Products

Reacting stoichiometric amounts of the two organic linker groups (A and B) with the POM and isolating the asymmetric product from the hybrid mixture is a straightforward method for creating a bi-functionalised, asymmetric hybrid POM. Yields as high as 50% can be anticipated, provided that the reaction runs to completion.



The relative driving force for the organic linkers A and B binding to the POM can fluctuate due to variations in their chemical structures. This is controlled by characteristics, such as size, hydrophilicity, and the inductive effects of functional groups which may impact the second lacunary sites reactivity to the other linker. As result, separating the three products from the mixture can be easier because the relative solubilities of the organic linkers their corresponding symmetric hybrid POMs may significantly vary from one another.

The first reported asymmetric hybrid POM,  $[\text{MnMo}_6\text{O}_{18}\{(\text{OCH}_2)_3\text{CNO}_2\}\{(\text{OCH}_2)_3\text{CNH}_2\}]$ , was isolated using slow fractional crystallisation. Song et al. reported the single-pot process in which a Mn Anderson cluster was simultaneously reacted with two different TRIS  $(-\text{(OCH}_2)_3\text{C}-)$  capping groups, resulting in amino and nitro functional groups (**Figure 16a**).<sup>93</sup> Every few hours, precipitates crystallised from the mother liquor were filtered and analysed using electrospray

ionisation mass spectrometry (ESI-MS). Recrystallisation of the particular batch that was determined to possess the appropriate amount of molecular weight was necessary in order to achieve the goal of isolating the desired asymmetric product.

The researchers then used the unique asymmetric hybrid structure to react with various aromatic aldehydes, creating several new asymmetric compounds containing imine moieties from the terminal amine (**Figure 16b**). This innovative work demonstrated the flexibility and control that asymmetric hybrid structures could offer in terms of molecular design and tuneability by further exploiting organofunctionalisation. It is beneficial to create synthesis and purification procedures that are applicable to a wide range of processes because batch analysis and slow crystallisation are labour-intensive, complicated processes that are unlikely to perform effectively for all POM hybrid combinations.

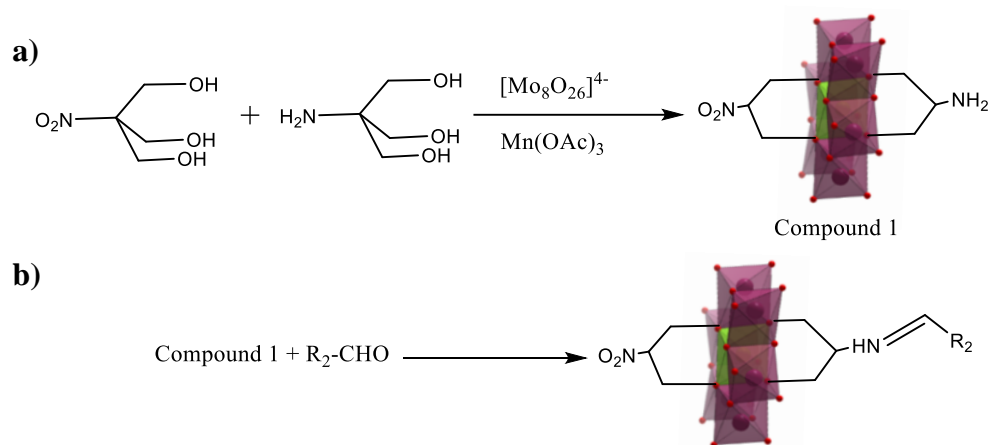


**Figure 16.** Schematic illustrating two different reaction pathways to synthesise asymmetric Anderson hybrids: a)  $[\text{MnMo}_6\text{O}_{18}\{(\text{OCH}_2)_3\text{CNO}_2\}\{(\text{OCH}_2)_3\text{CNH}_2\}]$  via capping an Mn-Anderson cluster, b)  $[\text{MnMo}_6\text{O}_{18}\{(\text{OCH}_2)_3\text{CNO}_2\}\{(\text{OCH}_2)_3\text{CN}=\text{CH}(\text{C}_5\text{H}_4\text{N})\}]$  synthesised by reacting (a) with 4-pyridylcarboxylaldehyde<sup>93</sup>.

Alternative methods, such as silica or alumina column chromatography, exist. However, these are typically avoided for purifying POM-based compounds due to their incompatible anionic nature, which runs the risk of significant adsorption, cation alteration, and, consequently, low yields.<sup>94</sup> The isolation of one asymmetric hybrid Anderson was created by attaching 3,5-bis(tetradecyloxy)benzoic acid to a precursor of the symmetric TRIS-NH<sub>2</sub>/TRIS-NH<sub>2</sub> hybrid

[MnMo<sub>6</sub>O<sub>18</sub>{(OCH<sub>2</sub>)<sub>3</sub>CNH<sub>2</sub>}<sub>2</sub>].<sup>95</sup> This is one instance where this method has been employed successfully.<sup>96,97</sup> Asymmetric functionalisation has the potential to be employed in the specific design of self-assembling materials because it has been used to produce amphiphilic molecules. This allowed the production of stable Langmuir-Blodgett films.

Yvon *et al.* created a special reverse-phase (RP)-HPLC approach for purifying POM hybrid mixtures that was intended to work flexibly with an extensive range of POM and ligand combinations.<sup>89</sup> According to the approach, the ligands and their corresponding POM hybrid affinities for RP media must be notably different, with the asymmetric hybrid showing a moderate affinity for the symmetric forms.

Several asymmetric Mn-Anderson hybrids were isolated from the mother liquors of one-pot reactions involving either Mn or Anderson. Two separate tris-alkoxo ligands containing a Mn-Anderson cluster, or, in a post-functionalisation process, a pre-made TRIS-NH<sub>2</sub>/TRIS-NH<sub>2</sub> hybrid POM [MnMo<sub>6</sub>O<sub>18</sub>{(OCH<sub>2</sub>)<sub>3</sub>CNH<sub>2</sub>}<sub>2</sub> with two unique anhydride and/or acyl chloride reagents.

## 2 Aims

Herein, this project aims to tackle issues of synthesising and purifying asymmetric POMs comprising different organic ligands, including amine and carboxylic groups and provide potential alternative synthetic pathways. In order to achieve asymmetric Amine-Carboxylic Acid Organic-Inorganic Hybrid Wells Dawson Polyoxometalates (POMs) synthesis, the key goal is the optimisation of the low-cost and high-yielding one-pot synthesis methods for the production of symmetric hybrid POMs based on the Wells–Dawson anion  $[\text{P}_2\text{W}_{17}\text{O}_{57}(\text{PPA})_2]$  and  $[\text{P}_2\text{W}_{17}\text{O}_{57}(\text{AEP})_2]$ .

The overall aim is to develop a reliable and efficient synthetic method for creating organic–inorganic asymmetrically organofunctionalised hybrid POMs based on the Wells-Dawson anion  $[\text{P}_2\text{W}_{17}\text{O}_{57}(\text{AEP})(\text{PPA})]$  procedure and isolation of the hybrid POM from the crude and characterise the resulting products using a variety of analytical techniques, including nuclear magnetic resonance (NMR) spectroscopy, infrared (IR), and mass spectrometry (MS), the molecular structure and properties of such species increases our understanding of how the various components influence the functional characteristics of the asymmetric hybrid POMs. Identifying features such as, ligands, metal centres and structural geometry that directly influence the characteristics of the structures heightens the understanding of how these individually alter the clusters electronic and physical properties. A greater knowledge of asymmetric hybrid POMs will also enable more precise tuning of the structures in order to probe the most desirable characteristics and will allow the bespoke development of a new generation of materials for applications in energy storage, catalysis and molecular magnetism.

Employing UV-Vis spectroscopy for the purpose of electronic characterisation of the symmetric hybrid POMs  $[\text{P}_2\text{W}_{17}\text{O}_{57}\{(\text{PPA})_2\}]$ ,  $[\text{P}_2\text{W}_{17}\text{O}_{57}\{(\text{AEP})_2\}]$  and asymmetric hybrid POM  $[\text{P}_2\text{W}_{17}\text{O}_{57}\{(\text{PPA})(\text{AEP})\}]$  and cyclic voltammetry was applied in order to research the molecular electrochemistry.

## 3 Results and Discussion

### Asymmetric Amine-Carboxylic Acid Hybrid Wells Dawson Polyoxometalates

The robotic synthesis of functional molecules and assemblies is becoming an increasingly significant tool to help explore the chemical and biochemical space in a way that is both repeatable and scalable.<sup>98–104</sup>

Since anionic peptides are crucial protein components for interacting with inorganic surfaces,<sup>105,106</sup> and functioning as antimicrobial agents against bacteria and fungus, they have received a great deal of attention, and they may have a significant part to play in preventing neurodegenerative disorders like Alzheimer's and Parkinson's.<sup>107</sup> However, there currently needs to be more general approaches to automatically insert anionic inorganic amino acid residues into a peptide chain under robotic control,<sup>90,108</sup> owing to the complexity of synthesis procedures for inorganic amino acids, which are confined to particular amino acids. In order to accomplish this, we opted to use polyoxometalates (POMs), a large class of clusters constructed from multiple transition metal ions linked by shared oxo or hydroxo anions,<sup>109</sup>. Due to their molecular nature, POMs introduce higher charge densities,<sup>110</sup> redox activity<sup>111,112</sup> and additional coordination/catalytic sites into the peptide chain,<sup>113</sup> opening up novel possibilities for protein biochemistry and inorganic medicinal chemistry.

#### 3.1 Synthesis and Characterisation of Symmetric Hybrid POMs

##### **[P<sub>2</sub>W<sub>17</sub>O<sub>57</sub>{(PPA)<sub>2</sub>}] (1) and [P<sub>2</sub>W<sub>17</sub>O<sub>57</sub>{(AEP)<sub>2</sub>}] (2)**

The [P<sub>2</sub>W<sub>17</sub>O<sub>57</sub>{(PPA)<sub>2</sub>}] (1) and [P<sub>2</sub>W<sub>17</sub>O<sub>57</sub>(AEP)<sub>2</sub>] (2) are symmetric hybrids are side products of the “one-pot” reaction to prepare the asymmetric hybrid [P<sub>2</sub>W<sub>17</sub>O<sub>57</sub>(AEP)(PPA)] (3). Many examples exist in the literature showing that amines react with carboxylic acid functionalised POM hybrids.<sup>114–116</sup> The purification of the required asymmetric hybrid POM from the symmetric hybrid POM by-products is the primary challenge with this method, as addressed by Cronin and co-workers in a couple of studies.<sup>89,93</sup>

The two symmetric hybrid POMs  $[P_2W_{17}O_{57}\{(PPA)_2\}]$  (1) and  $[P_2W_{17}O_{57}(AEP)_2]$  (2) were separately synthesised in order to facilitate research on the chemicals in their purest form. By drawing comparisons to their structures and behaviours, they were used to assist in the characterisation of the chemical for the  $[P_2W_{17}O_{57}(AEP)(PPA)]$  (3).

### 3.1.1 $[P_2W_{17}O_{57}\{(PPA)_2\}]$ (1)

The synthetic approach for producing the hybrid species required the preparation of a separate Wells Dawson POM  $[P_2W_{17}O_{61}]^{10-}$  this compound will be referred to as (W<sub>17</sub>) from this point forward. (**Figure 17**). A simple two-step process produced good yields, according to the literature reports.<sup>117,118</sup>

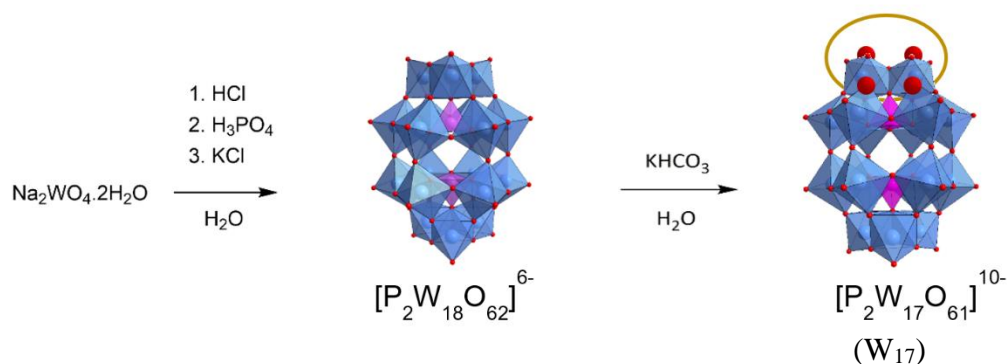


**Figure 17.** scheme showing the synthesis of the POM  $[P_2W_{17}O_{61}]^{10-}$ . Colour code: blue polyhedra =  $\{WO_6\}$ ; magenta polyhedra =  $\{PO_4\}$ .

In the acid catalysed reaction, two molar equivalents of (PPA) were reacted with one equivalent of  $K_{10}[P_2W_{17}O_{61}]$  (W<sub>17</sub>) in DMF stirring overnight at (85°C) (**Figure 18**). Ether was added in excess to the reaction mixture, and centrifuged to give a blue oily layer. Dissolve it in water, and add an excess of dioxane to precipitate a blue solid after centrifuging it.



(pink) from -14.36 ppm to -12.98 ppm.<sup>122</sup> In the (1) <sup>31</sup>P spectrum, the positive region has a single peak at 27.49 ppm (**Figure 20**).

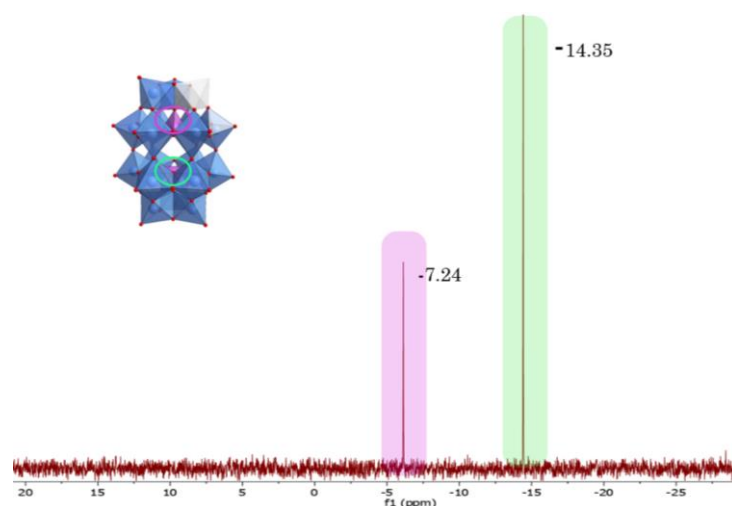


**Figure 19.** <sup>31</sup>P (162 MHz) NMR spectrum of (W<sub>17</sub>)

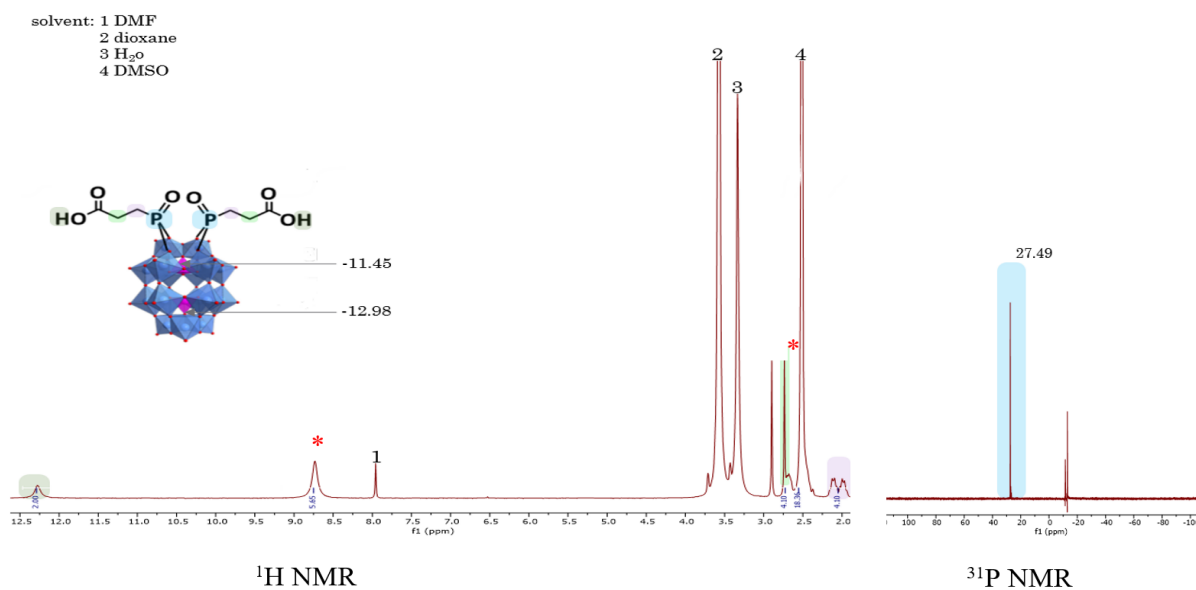


**Figure 20.** <sup>1</sup>H NMR (500 MHz) and <sup>31</sup>P NMR (202 MHz) of [P<sub>2</sub>W<sub>17</sub>O<sub>57</sub>]{(PPA)<sub>2</sub>} in DMSO-d<sub>6</sub> shows the peaks assignment to each proton, (\*) indicate DMA cation signals, solvent (1= DMF, 2= dioxane, 3= H<sub>2</sub>O, 4=DMSO)

Mass spectrometry was also used to confirm the structure of the hybrid POM. Since the Dawson POM was synthesised as a potassium salt, it is not strange that ESI techniques would detect proton and sodium ions as counterions.<sup>123</sup> Due to their anionic composition, POM clusters are particularly prone to this free exchange of cations during analysis.<sup>124</sup> The  $m/z$  values to which assignments are made are those of the peak that is most central within the broad bell-shaped peak that results from the different relatively abundant isotopes of tungsten. These are the values to which assignments are made.

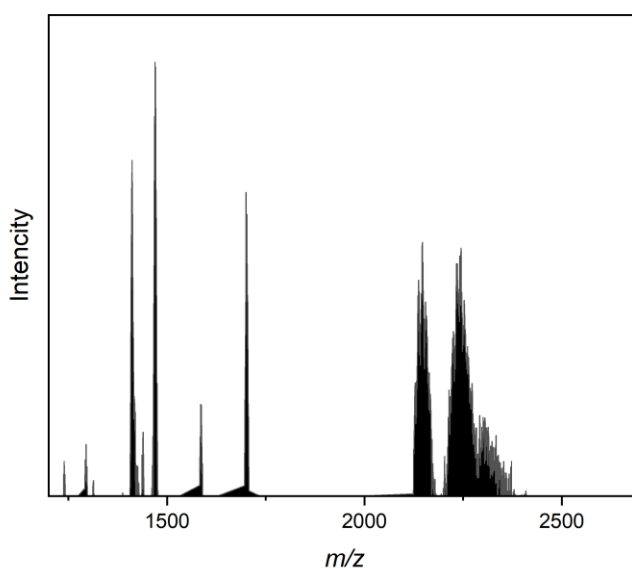


**Figure 21.** Negative mode ESI mass spectrum of **1** in acetonitrile.

Assignment	Z	m/z (obs)	m/z (calc)
$\text{H}_4[\text{P}_2\text{W}_{17}\text{O}_{57}\{(\text{PO}_5\text{C}_9\text{H}_{29}\text{O}_2\text{N}_3)_2\}]$	2-	2203.37891	2203.4096
$\text{H}_3\text{Na}[\text{P}_2\text{W}_{17}\text{O}_{57}(\text{PO}_3\text{C}_3\text{H}_5\text{O}_3)_2]$	2-	2214.36988	2214.4283
$\text{H}_2\text{Na}_2[\text{P}_2\text{W}_{17}\text{O}_{57}(\text{PO}_3\text{C}_3\text{H}_5\text{O}_3)_2]$	2-	2225.36086	2224.4211
$\text{HNa}_3[\text{P}_2\text{W}_{17}\text{O}_{57}(\text{PO}_3\text{C}_3\text{H}_5\text{O}_3)_2]$	2-	2236.35183	2236.4152
$\text{Na}_4[\text{P}_2\text{W}_{17}\text{O}_{57}(\text{PO}_3\text{C}_3\text{H}_5\text{O}_3)_2]$	2-	2247.3428	2247.3966

**Table 1.** ESI-MS peak assignments for **1**.

Infrared spectroscopy was applied to characterise the new hybrid compounds (**Figure 22**). The peaks observed at 2587- 3250  $\text{cm}^{-1}$  were assigned to the O-H, the C=O in carboxyl observed at 1723  $\text{cm}^{-1}$ . The peak identified at 1461  $\text{cm}^{-1}$  is bending mode of C-H bonds. POM and linker-specific bands appear in the fingerprint area. The P-O and P=O stretch associated with the linker and POM phosphate is observed at 1087  $\text{cm}^{-1}$  and 1133  $\text{cm}^{-1}$  respectively. The W-O-W bending mode of the bridging oxygens appears as a broad band between 526 and 721  $\text{cm}^{-1}$ , while the W=O stretching modes correspond to the bands at 908 and 951  $\text{cm}^{-1}$ .

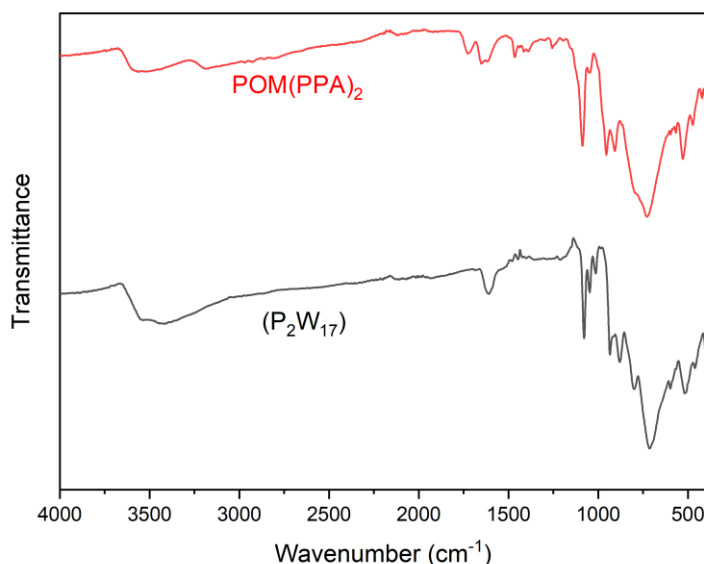


**Figure 22.** Stacked IR (ATR) spectra of symmetric hybrid  $[\text{POM(PPA)}_2]$  (red line), lacunary Dawson  $\text{K}_{10}\text{-}[\text{P}_2\text{W}_{17}\text{O}_{61}]$  ( $\text{P}_2\text{W}_{17}$ ) (black line).

In addition to this, UV-vis spectroscopy was used in order to investigate the hybrid-POMs absorption characteristics. POMs, as a whole, display powerful and broad UV absorption bands, which may be linked to ligand to metal charge transfer (LMCT)  $\text{O} \rightarrow \text{W}$ .<sup>125,126</sup> (UV-Vis) absorption spectra of (1) in  $\text{H}_2\text{O}$  exhibit absorption features characteristic of the Dawson anion  $[\text{P}_2\text{W}_{18}\text{O}_{62}]^{6-}$  ( $\text{P}_2\text{W}_{18}$ ), with a broad ligand-to-metal charge-transfer (LMCT)  $\text{O} \rightarrow \text{W}$  band centred at around 300 nm (**Figure 23**).

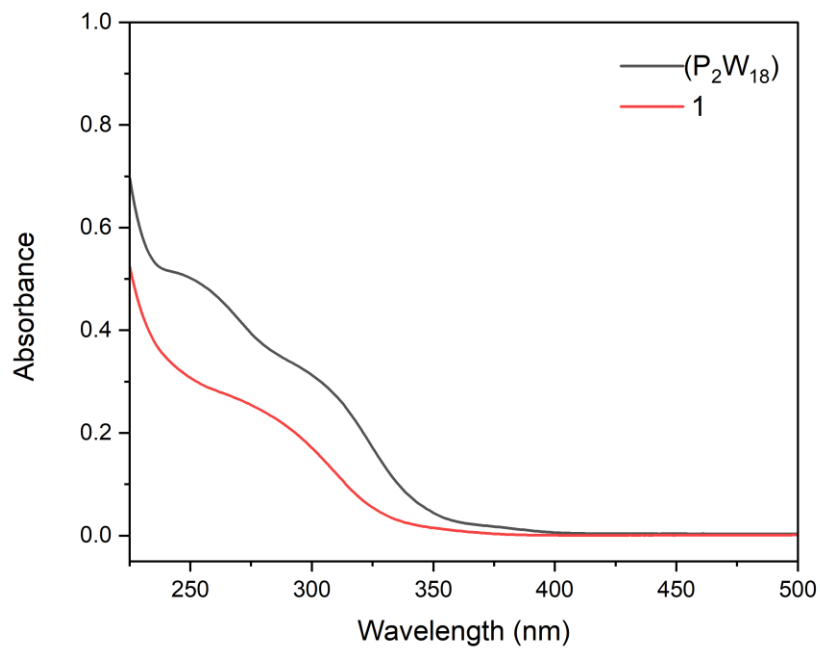


**Figure 23.** Overlaid UV-Vis absorbance spectra of symmetric hybrid [POM(PPA)<sub>2</sub>] (red), Dawson K<sub>6</sub>[P<sub>2</sub>W<sub>18</sub>O<sub>62</sub>] (black).

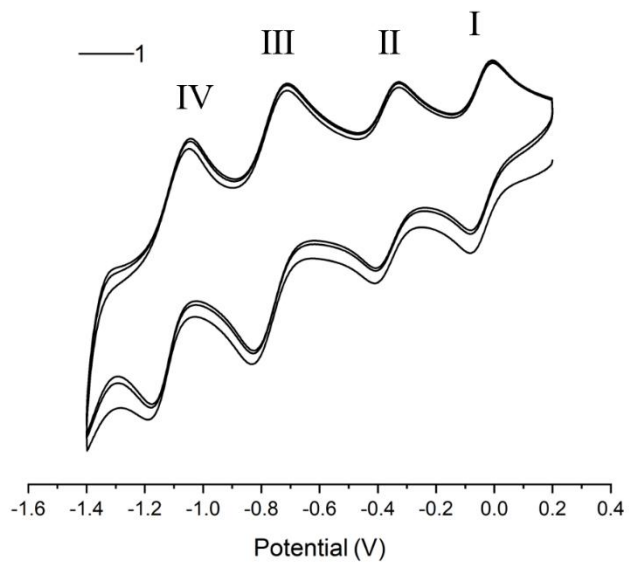


**Figure 24.** Cyclic voltammograms of [POM(PPA)<sub>2</sub>] (0.5 mM) in DMF, with 0.1M TBAPF<sub>6</sub> as electrolyte at a glassy carbon working electrode. Scan rate: 100 mV s<sup>-1</sup>.

Redox potential vs. Fc/Fc <sup>+</sup> (V)	I	II	III	IV
E <sub>red</sub>	-0.088	-0.420	-0.838	-1.188
E <sub>ox</sub>	-0.024	-0.350	-0.758	-1.120
E <sub>1/2</sub>	-0.056	-0.385	-0.798	-1.154

**Table 2.** Redox potentials of **1** in DMF.

As a typical species, the cyclic voltammetry (CV) of (**1**) was first analysed in DMF (thereby conserving its molecular nature) using 0.1 M tetrabutylammonium hexafluorophosphate ([TBA][PF<sub>6</sub>]) as the supporting electrolyte, in the potential range of 0.4 to -1.6 V vs. Fc/Fc<sup>+</sup> were observed (**Figure 24, Table.2**). The given CVs suggest that the POMs feature at least quasi-reversible redox processes in the relevant areas. The term "quasi-reversible" is used to describe a process that, despite visual appearances to the contrary, in fact technically irreversible since the peak-to-peak voltage difference is more than 57 mV.<sup>127</sup> Electrochemically irreversible is a process in which electron transfer at the electrode surface is slow relative to mass transport. Because of the slower kinetics at the electrodes, far more significant negative applied potentials are required for meaningful current to flow. Thus, the peak-to-peak separation is larger than the 57 mV expected for an electrochemically reversible one-electron redox pair.

### 3.1.2 [P<sub>2</sub>W<sub>17</sub>O<sub>57</sub>(AEP)<sub>2</sub>] (**2**)

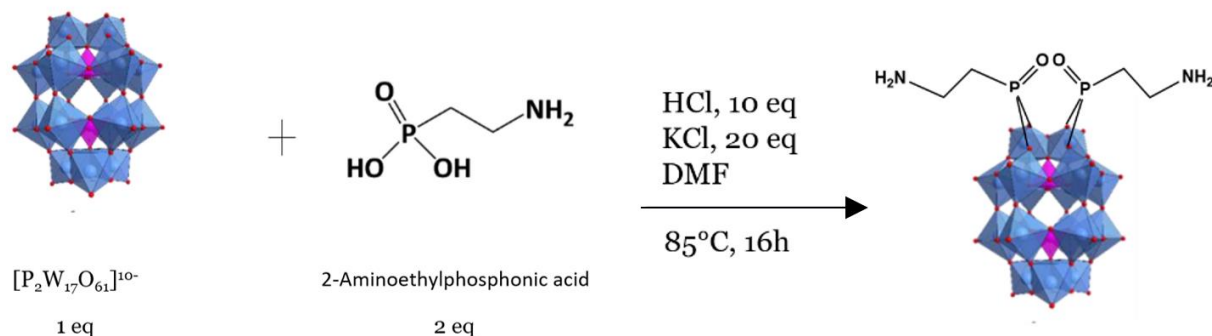


**Figure 25.** Hybridisation scheme showing the synthesis of the hybrid-POM (**2**).

The synthetic technique requires the production of a separate Wells-Dawson POM ( $W_{17}$ ) in order to produce the hybrid species. According to the literature,<sup>117,118</sup> a straightforward two-step procedure provided high yields.

Two molar equivalents of (AEP) were reacted with one molar equivalent of  $K_{10}[P_2W_{17}O_{61}]$  ( $W_{17}$ ) in DMF and stirred overnight at (85°C) (**Figure 25**). The reaction mixture was saturated with ether, and centrifuged to produce a blue oily layer. After centrifuging, the oily layer was dissolved in water and dioxane was added in excess to precipitate a blue solid.

Due to the existence of distinct phosphorus environments,  $^{31}P$  NMR proved to be an effective technique for characterising the components of the hybrids. Furthermore, because of the POM's electronic nature, we can use  $^{31}P$  NMR to track the success of the hybridisation. The positive area of the (2)  $^{31}P$  spectra contains a single peak at 22.96 ppm (**Figure 26**). This compound has also been characterised using ESI mass spectrometry, a crucial tool for macromolecule characterisation. The POMs ESI mass spectra confirm the synthesis of the compounds.

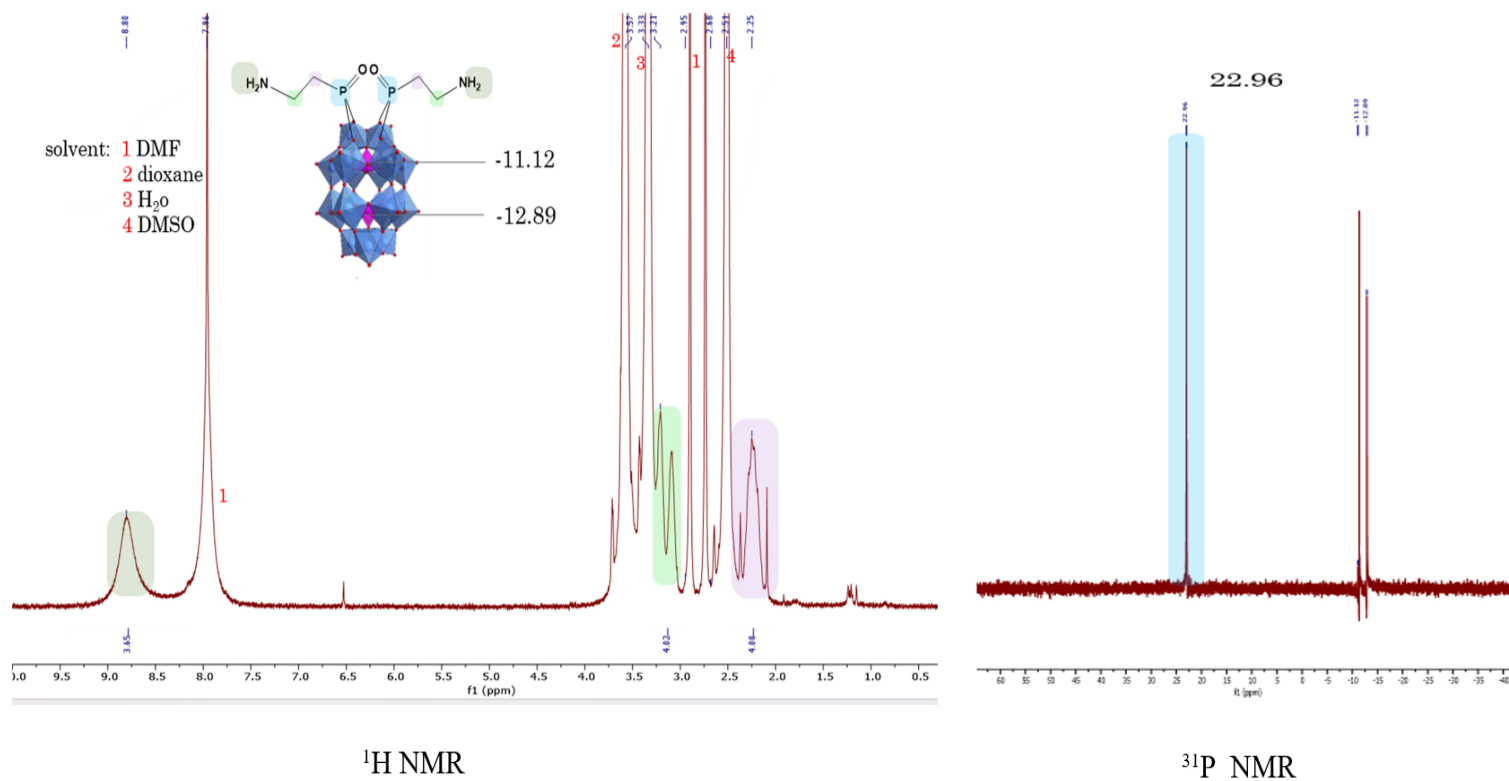


**Figure 26.**  $^1H$  NMR (500 MHz) and  $^{31}P$  (202 MHz) NMR of  $[P_2W_{17}O_{57}\{(AEP)_2\}]$  in  $DMSO-d_6$  shows the peaks assignment to each proton.

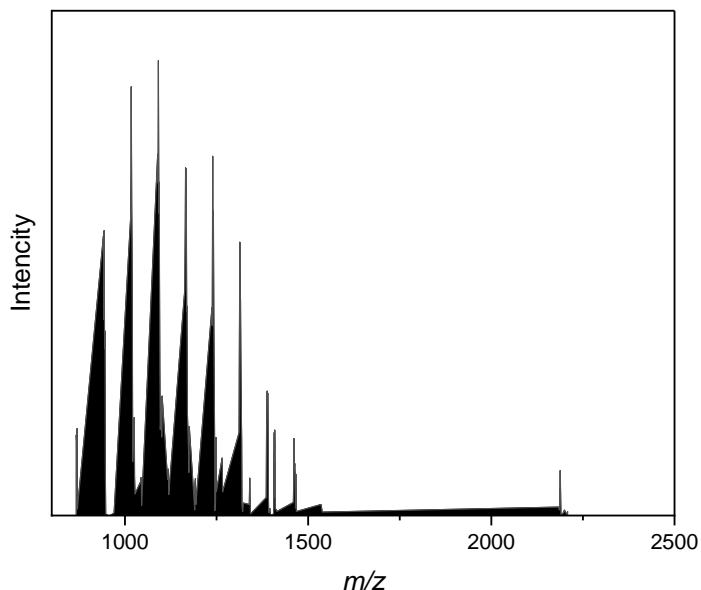


**Figure 27.** ESI mass spectrum of  $[P_2W_{17}O_{57}\{(AEP)_2\}]$ .

Assignment	Z	m/z (obs)	m/z (calc)
$Na_3[P_2W_{17}O_{57}\{(PO_3C_3H_8N_4H_2)_2\}]$	3-	1535.22565	1535.362

**Table 3.** ESI-MS peak assignments for **2**.

Infrared spectroscopy was used to more efficiently identify hybrid molecules (**Figure 28**). The peaks observed at 2854- 2961  $cm^{-1}$  were assigned to the N-H. The peak identified at 1451  $cm^{-1}$  is bending mode of C-H bonds. POM and linker-specific bands are located farther inside the fingerprint area. The P-O and P=O stretch associated with the linker and POM phosphate is observed at 1081  $cm^{-1}$  and 1133  $cm^{-1}$  respectively. The W-O-W bending mode of the bridging oxygens appears as a broad band between 528 and 735  $cm^{-1}$ , while the W=O stretching modes correspond to the bands at 908 and 954  $cm^{-1}$ .

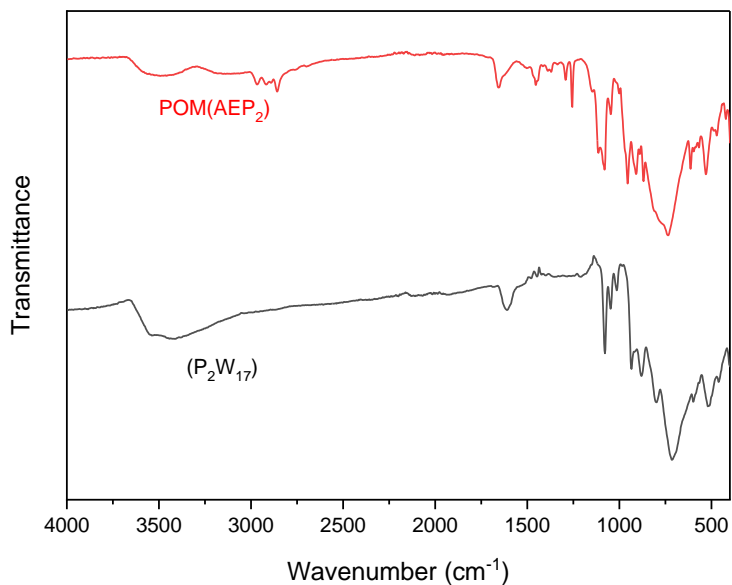


**Figure 28.** IR spectrum comparing  $[P_2W_{17}O_{57}(AEP)_2]$  (red) to  $(W_{17})$  (black).

UV-vis spectroscopy was also used to investigate the hybrid-POM absorption characteristics. The intense and wide UV absorbance bands of POMs are connected with the ligand-to-metal charge transfer (LMCT)  $O \rightarrow W$  band at around 290 nm (**Figure 29**).

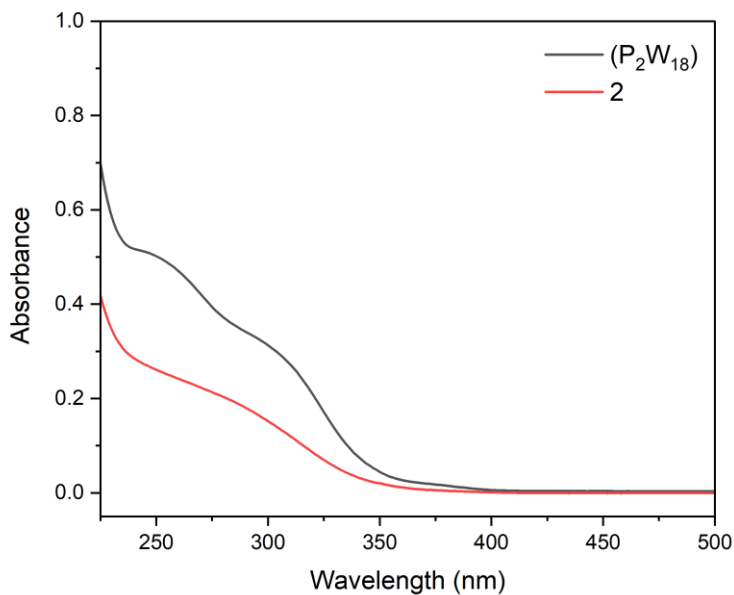


**Figure 29.** UV-Vis absorbance spectra of symmetric hybrid  $[POM(AEP)_2]$  (red), Dawson  $K_6[P_2W_{18}O_{62}]$  (black)

Cyclic voltammetry was used to carry out the electrochemical characterisation that needed to be done on the molecular assemblies. CV examined compound (**2**) in a DMF solution with 0.1M [TBA][PF<sub>6</sub>] as an electrolyte,<sup>128</sup> which was observed between 0.2 and -1.6 V vs. Fc/Fc<sup>+</sup> (**Figure 30, Table 4**).

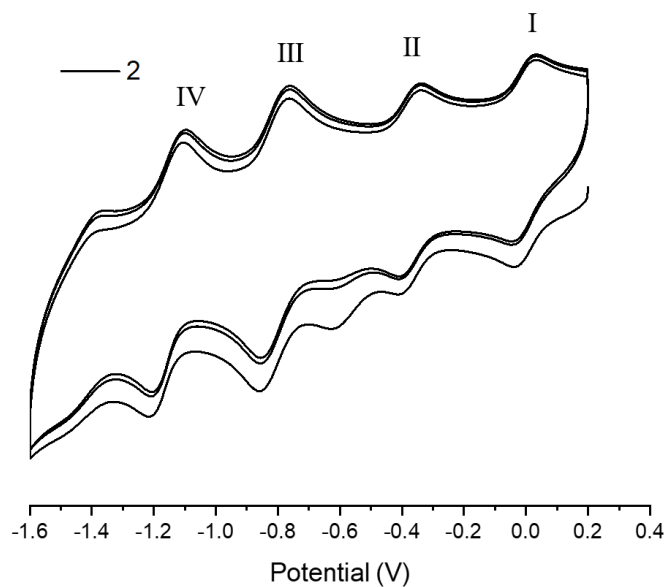


**Figure 30.** Overlaid cyclic voltammograms of [POM(AEP)<sub>2</sub>] (0.5 mM) in DMF, with 0.1M TBAPF<sub>6</sub> as electrolyte at a glassy carbon working electrode. Scan rate: 100 mVs<sup>-1</sup>.

Redox potential vs. Fc/Fc <sup>+</sup> (V)	I	II	III	IV
E <sub>red</sub>	-0.040	-0.410	-0.856	-1.208
E <sub>ox</sub>	-0.024	-0.346	-0.788	-1.152
E <sub>1/2</sub>	-0.032	-0.378	-0.822	-1.18

**Table 4.** Redox potentials of **2** in DMF.

## 3.2 Attempt Synthesis and Characterisation of Asymmetric Hybrid POM [P<sub>2</sub>W<sub>17</sub>O<sub>57</sub>{(PPA)(AEP)}] (3)

Three species were initially suspected to be present in the crude product mixture once the reaction was complete. These were identified by <sup>31</sup>P NMR spectroscopy as the asymmetric hybrid POM [P<sub>2</sub>W<sub>17</sub>O<sub>57</sub>{(PPA)(AEP)}] (3), the symmetric hybrid [P<sub>2</sub>W<sub>17</sub>O<sub>57</sub>{(PPA)<sub>2</sub>}] (1) (see Part 3.1.1), and the symmetric hybrid [P<sub>2</sub>W<sub>17</sub>O<sub>57</sub>{(AEP)<sub>2</sub>}] (2) (see part 3.1.2).

A one-pot synthesis of the asymmetric organic-inorganic hybrid Wells-Dawson phosphotungstates bearing amino and carboxylate moieties was investigated. An acid mediated condensation of 3-phosphonopropionic acid (PPA) and 2-aminoethylphosphonic acid (AEP) with the mono-lacunary Dawson-type anion K<sub>10</sub>[P<sub>2</sub>W<sub>17</sub>O<sub>61</sub>] (W<sub>17</sub>) was conducted with a molar ratio of 1:1:1 (**Figure 31**). Based on previous work within the Newton group, a mixed condensation process to access asymmetric hybrid POMs generally results in three POM clusters.<sup>129</sup> Following work-up, analysis of the crude mixture by <sup>31</sup>P NMR spectroscopy suggested three species were present. These were identified as the asymmetric hybrid POM [P<sub>2</sub>W<sub>17</sub>O<sub>57</sub>{(PPA)(AEP)}] (3), the symmetric hybrid [P<sub>2</sub>W<sub>17</sub>O<sub>57</sub>{(PPA)<sub>2</sub>}] (1) (see Part 3.1.1), and the symmetric hybrid [P<sub>2</sub>W<sub>17</sub>O<sub>57</sub>{(AEP)<sub>2</sub>}] (2) (see part 3.1.2). To get the exact ratio for compounds (1), (2), and (3), prepare an NMR sample with (10 mg) of the crude POM (3) in DMSO-d<sub>6</sub> (0.75 mL). Using an experiment with 128 scans and a d1 set to 10 on Bruker Ascend™ 400MHz.

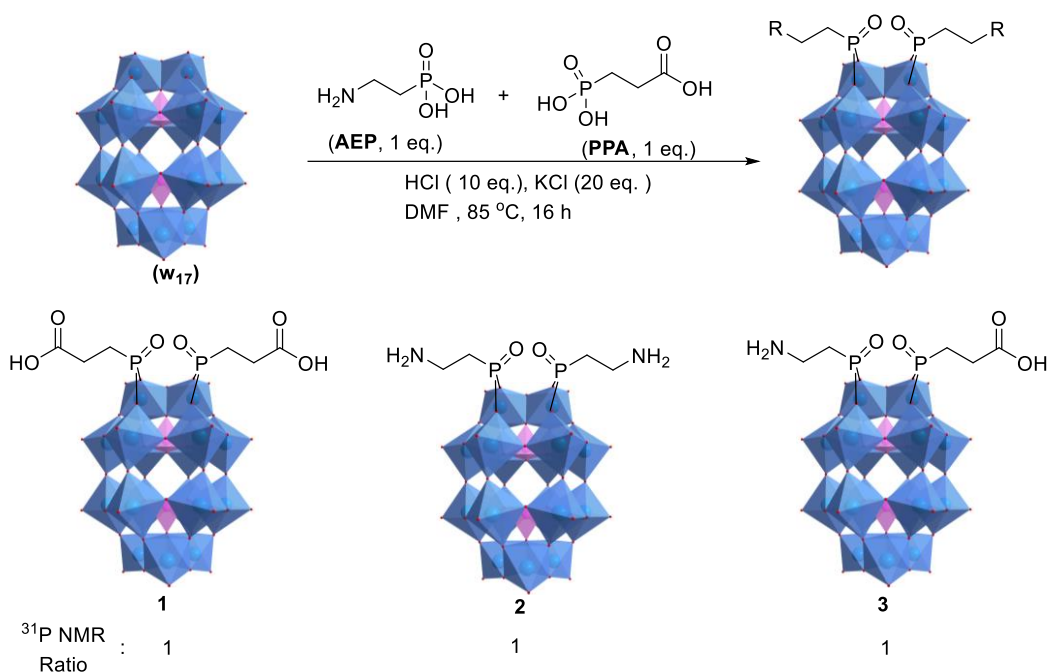


**Figure 31.** Hybridisation scheme showing the synthesis of the hybrid-POM (3),  $^{31}\text{P}$  NMR Ratio.

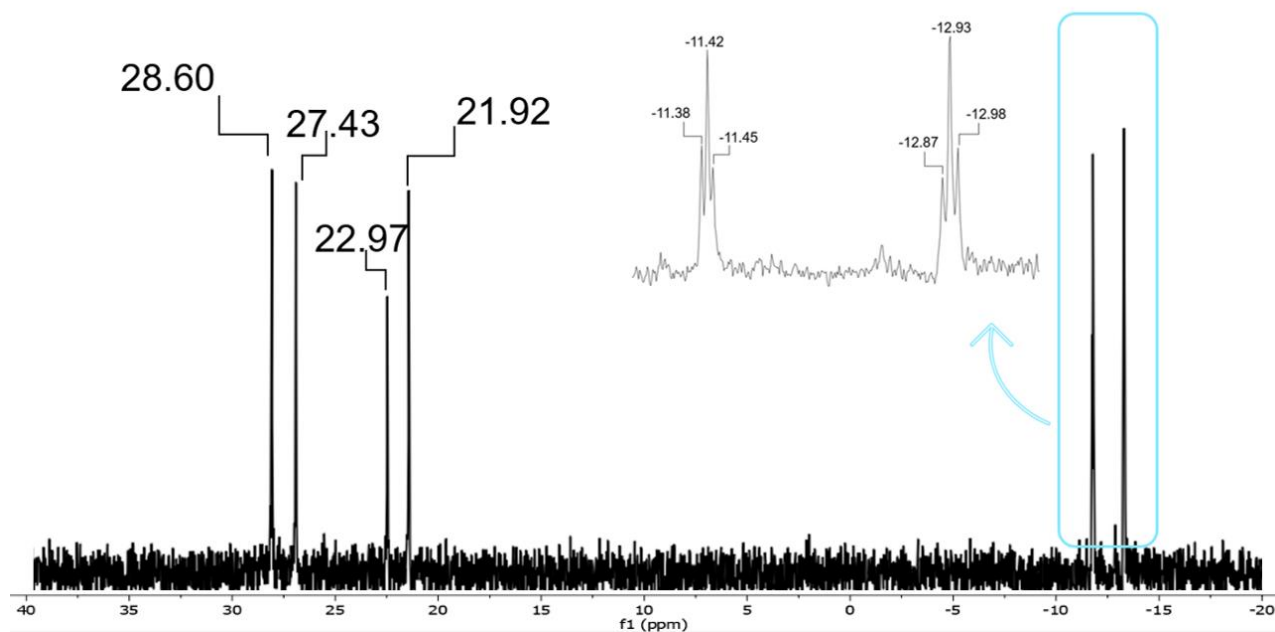


**Figure 32.**  $^{31}\text{P}$  NMR (162 MHz) in  $\text{DMSO-d}_6$  of the crude mixture of hybrid POM products produced during the synthesis of **3**. The inset depicts an enlargement of the negative spectral region's peaks.

The  $^{31}\text{P}$  NMR spectra of the crude mixture show four resonances in the expected region for the ligand. Unbound PPA and AEP are present at 28.60 and 21.92 ppm, respectively, which are not observed, suggesting only hybridised ligand is present. This is further supported by three pairs of signals are also seen in the negative region corresponding to the pairings of phosphate centres in the POM core of each of the three hybrids (**Figure 32**), while the bound ligand peaks for symmetric structures (**1**) and (**2**) are detected at 27.43 and 22.97 ppm.

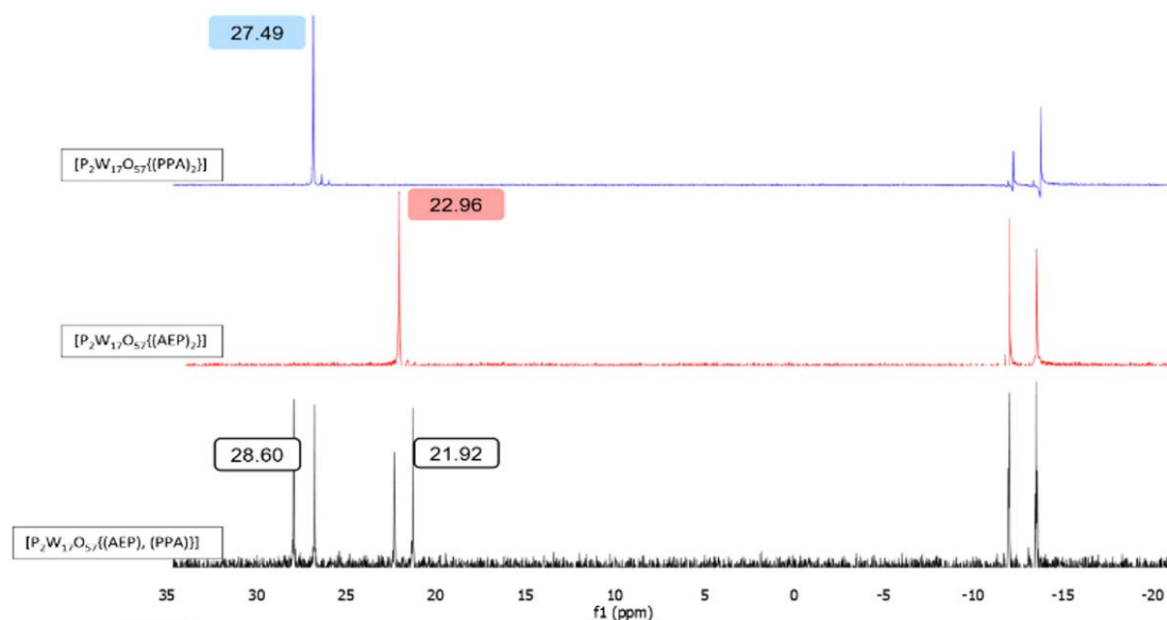


**Figure 33.**  $^{31}\text{P}$  NMR (**1**), (**2**) (202 MHz), (**3**) (162 MHz) in  $\text{DMSO-d}_6$ .

Getting the required asymmetric hybrid product (**3**) isolated is challenging. Unfortunately, after trying some strategies, the purification of the asymmetric hybrid POM did not work well. A few ways to purify the asymmetric hybrid POM are discussed in the following points.

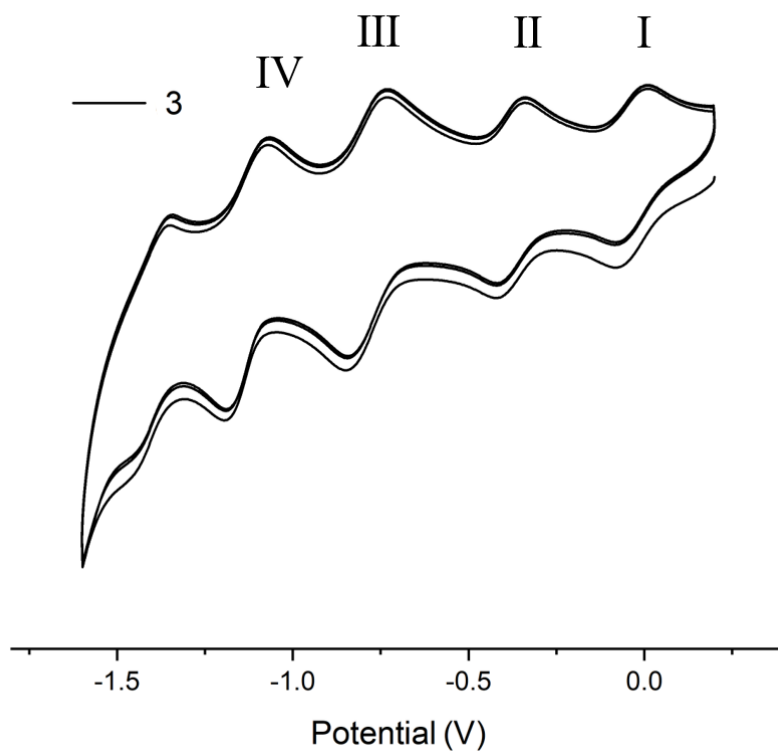


**Figure 34.** Overlaid cyclic voltammograms of crude mixture hybrid POM (**3**) (0.5 mM) in DMF, with 0.1M TBAPF<sub>6</sub> as electrolyte at a glassy carbon working electrode. Scan rate: 100 mVs<sup>-1</sup>.

Redox potential vs. Fc/Fc <sup>+</sup> (V)	I	II	III	IV
E <sub>red</sub>	-0.084	-0.420	-0.846	-1.192
E <sub>ox</sub>	0.006	-0.348	-0.762	-1.130
E <sub>1/2</sub>	-0.039	-0.384	-0.804	-1.161

**Table 5.** Redox potentials of **2** in DMF.

### 3.3 Purification of Asymmetric Hybrid POM

#### $[P_2W_{17}O_{57}\{(TPY)(C_{18})\}]$

Synthesis and purification of asymmetric hybrid POM  $[P_2W_{17}O_{57}\{(TPY)(C_{18})\}]$ , which is discussed and reported in the paper “Asymmetric Hybrid Polyoxometalates: A Platform for Multifunctional Redox-Active Nanomaterials”<sup>129</sup> is repeated here.

A 1:1 acidified solvent combination of DMF and acetonitrile was used in a one-pot acid-catalysed condensation reaction between one molar equivalent of the phosphonic acid ligands TPY and C<sub>18</sub> and one molar equivalent of the potassium salt of the mono-lacunary Dawson-type anion K<sub>10</sub>- $[P_2W_{17}O_{61}]$  (Figure 35).

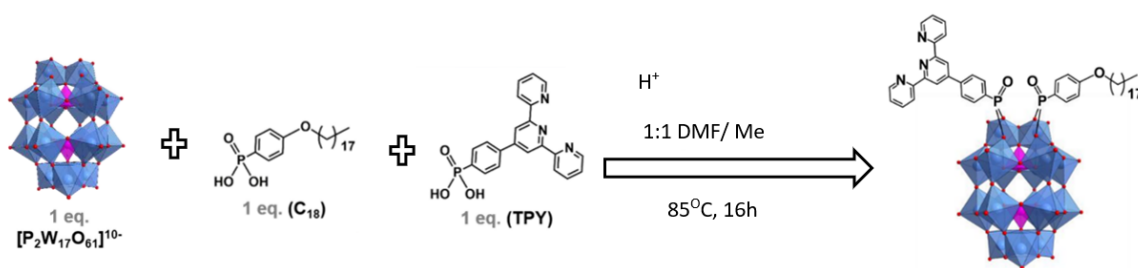


**Figure 35.** Synthesis of the asymmetric hybrid POM,  $[P_2W_{17}O_{57}\{(TPY)(C_{18})\}]$ .

Based on <sup>31</sup>P NMR spectroscopy there are three species present in the resulting mixture; they are the asymmetric hybrid  $[POM\{(TPY)(C_{18})\}]$  the symmetric TPY hybrid  $[P_2W_{17}O_{57}(TPY)_2]$ , and the symmetric C<sub>18</sub> hybrid  $[P_2W_{17}O_{57}(C_{18})_2]$ . Covalently bound ligand <sup>31</sup>P signals for TPY and C<sub>18</sub> are seen at 13.40 and 16.72 ppm, whereas bound ligand peaks for symmetric structures  $[P_2W_{17}O_{57}(TPY)_2]$  and  $[P_2W_{17}O_{57}(C_{18})_2]$  are observed at 14.18 and 15.97 ppm, respectively. Furthermore, signals in the range of -11.33 - -12.95 correspond to the three pairs of phosphorus centres in the POM cores.

The following solvent extraction steps were used to isolate the target asymmetric hybrid product,  $[POM\{(TPY)(C_{18})\}]$ . The mixture resulted from adding an excessive amount of ether to the

orange-yellow reaction mixture. After centrifuging, the orange-brown and green solids were separated from the yellow supernatant. The solvent was removed under reduced pressure to give a crystalline orange-brown solid, assigned as [POM(C<sub>18</sub>)<sub>2</sub>] using <sup>31</sup>P NMR spectroscopy. Separation of [POM(TPY)<sub>2</sub>] by centrifugation from the residual crude solid, which was a combination of [POM(TPY)<sub>2</sub>], [POM{(TPY)(C<sub>18</sub>)}], and trace [POM(C<sub>18</sub>)<sub>2</sub>], was achieved by re-dissolving in minimum acetonitrile, in which [POM(TPY)<sub>2</sub>] is sparingly soluble. The next step was re-precipitating [POM{(TPY)(C<sub>18</sub>)}] from the acetonitrile using an excess of ether while leaving any remaining residues of [POM(C<sub>18</sub>)<sub>2</sub>] in the solution. It is important to repeat the steps of dissolving in minimal acetonitrile to remove any insoluble [POM(TPY)<sub>2</sub>]. Then re-precipitating [POM{(TPY)(C<sub>18</sub>)}] from the supernatant with ether until no signals corresponding to [POM(TPY)<sub>2</sub>] or [POM(C<sub>18</sub>)<sub>2</sub>] are detectable by <sup>31</sup>P or <sup>1</sup>H NMR spectroscopy. Multiple batches of the asymmetric hybrid [POM{(TPY)(C<sub>18</sub>)}] were successfully synthesised using this method, in 10 – 25% yield.<sup>129</sup>

### 3.3.1 Attempt Purification by Solvent Test

In an effort to isolate asymmetric hybrid POM **1** without the use of costly or time-consuming, and complicated purification procedures, solvent extraction purification processes were examined. Investigation by <sup>31</sup>P NMR spectroscopy revealed that the crude hybrid mixtures comprised the three predicted hybrids: the asymmetric hybrid **1** and two symmetric hybrid side-products **2** and **3**. Purification of this crude hybrid mixture using the solvent extraction method as described above was attempted for both the asymmetric procedure as well as the individual synthesis of symmetric hybrids **2** and **3**. However, the results were found to be varied and poorly reproducible across for all ligand procedures, which is attributed to poor solubility of clusters **1** - **3**.

In an attempt to isolate the symmetric from the asymmetric ones, symmetric compounds were dissolved in 5 different solvents. The five solvents are, MeCN, Acetone, MeOH, MeNO<sub>2</sub>, and IPA. (**Figure 38**).

Dissolving (20 mg) of the POMs (**1**), (**2**), and (**3**) in (500 μL) of the solvent to determine their solubility. The method involves sonicating the POMs in the five solvents, centrifuging and decanting the solvent, and then running <sup>31</sup>P NMR on the precipitate.

Amides are derivatives of carboxylic acids in which the OH group of the carboxylic acid has been replaced by the NH<sub>2</sub>, NHR, or NR<sub>2</sub> of an amine. The formation of an amide from a carboxylic acid and an amine is a condensation reaction since it also results in the release of water.<sup>130</sup>

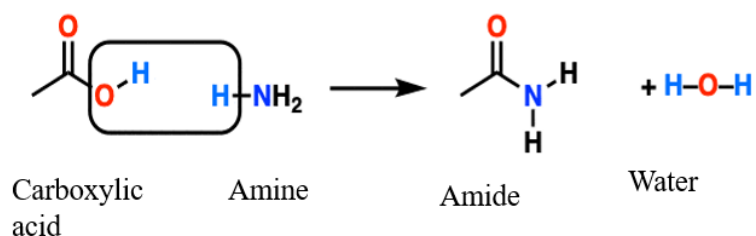


**Figure 36.** Amides are the product of a net “condensation” reaction between a carboxylic acid and an amine.

In reverse here, hydrolysis, in the strictest sense, is any reaction involving water. The acid speeds up the amide-water reaction.<sup>131</sup>

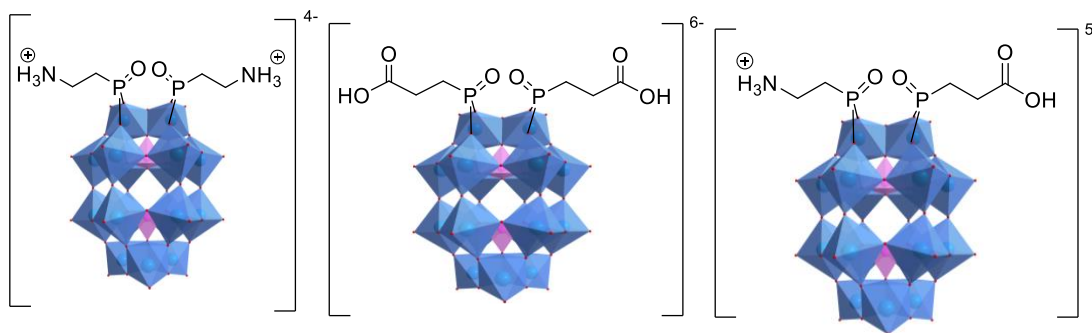
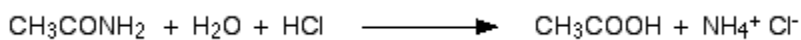


**Figure 37.** The total formal charge of the cluster changed with the addition of acid.

Unfortunately, the symmetric and asymmetric hybrid products that resulted from any and all reactions could not be readily distinguished by their respective exclusive solubilities in any solvent. Sadly, the majority of solvent extraction efforts failed with both, resulting in isolated solids containing varying proportions of two or all three hybrids, preventing the achievement of repeatability in the purifying step.

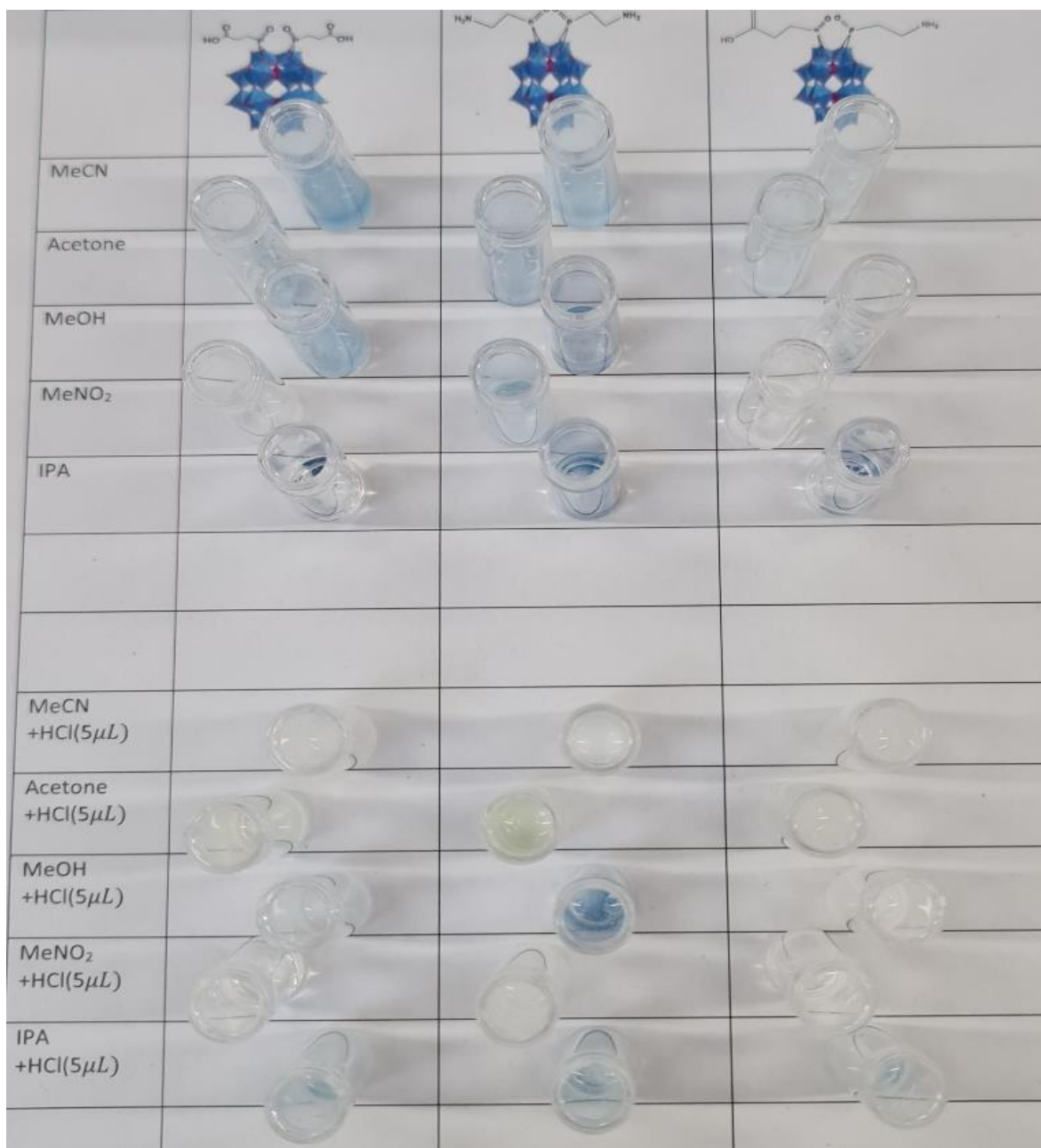


**Figure 38.** The POMs (1),(2), and (3) in the solvents (MeCN, Acetone, MeOH, MeNO<sub>2</sub>, and IPA), then in the solvents + (5 μL) HCl.



equivalent of the potassium salt of the mono-lacunary Dawson-type anion  $K_{10}[P_2W_{17}O_{61}]$  ( $W_{17}$ ) dissolved in DMF in an acid-catalysed one-pot condensation process (**Figure 41**).

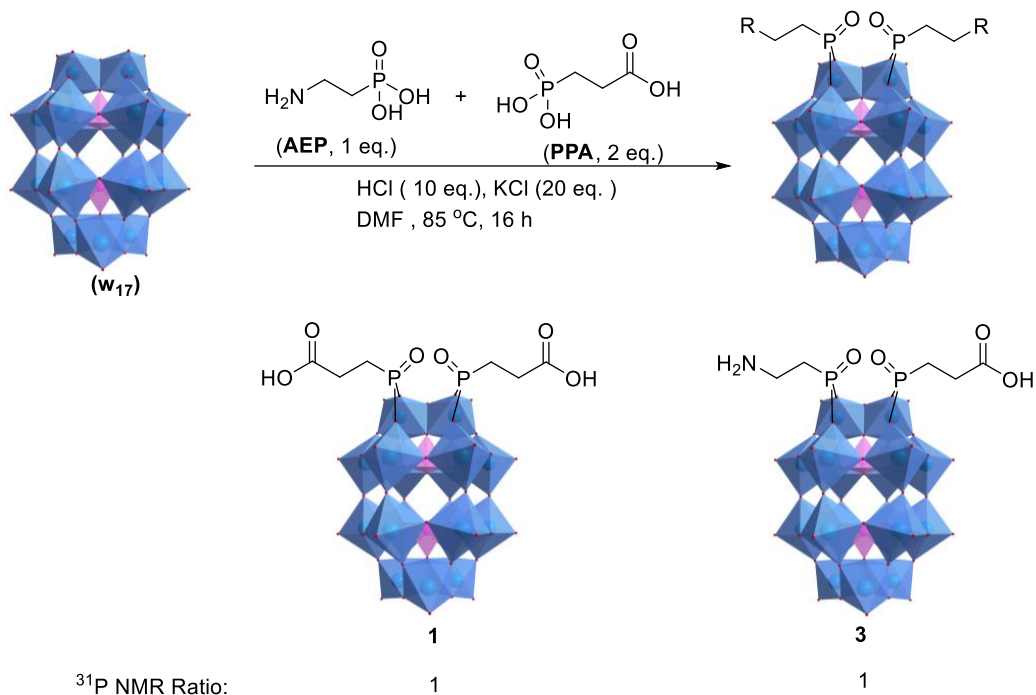


**Figure 41.** Hybridisation scheme showing the synthesis of the asymmetric hybrid-POM  $[P_2W_{17}O_{57}(\text{AEP}, 1\text{eq.}), (\text{PPA}, 2\text{eq.})]$ .

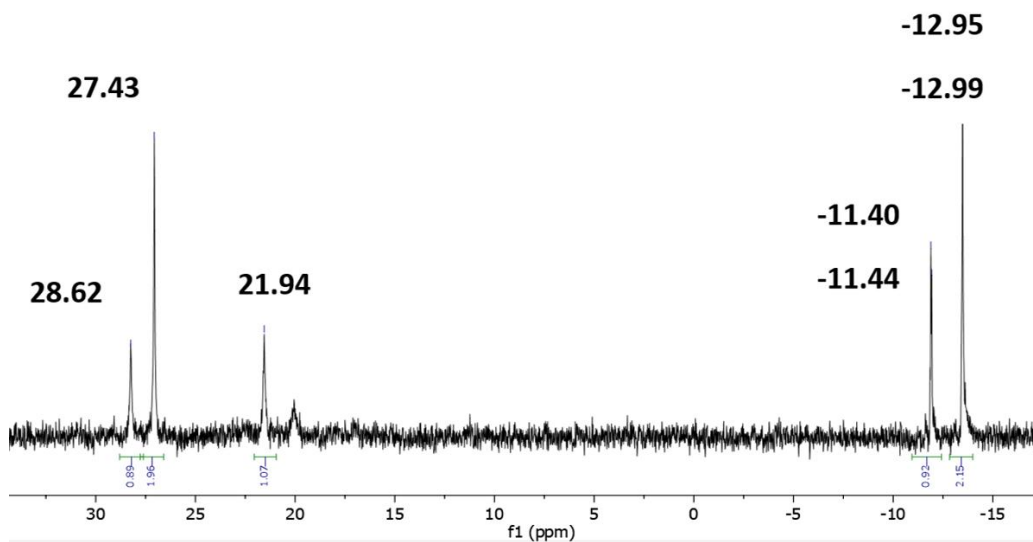


**Figure 42.** <sup>31</sup>P NMR (162 MHz) in DMSO-d<sub>6</sub> of the crude mixture of hybrid POM products produced during the synthesis of  $[P_2W_{17}O_{57}(\text{AEP}, 1\text{eq.}), (\text{PPA}, 2\text{eq.})]$ .

On Bruker Ascend™ 400 MHz spectrometers to acquire  $^{31}\text{P}$  NMR, using an experiment with 128 scans and a d1 set to 10, be allowed to know the exact ratio of each compound. Changing the started material equivalent led to different results. Two molecular equivalents of 3-phosphonopropionic acid (PPA) reacts faster with the  $\text{K}_{10}[\text{P}_2\text{W}_{17}\text{O}_{61}]$  ( $\text{W}_{17}$ ) than one molecular equivalents of 2-aminoethylphosphonic acid (AEP), which causes only one ratio of **(1)** and one ratio of asymmetric hybrid POM  $[\text{P}_2\text{W}_{17}\text{O}_{57}\{(\text{PPA})(\text{AEP})\}]$ . This reaction helped to purify the crude POM **(3)** from the symmetric hybrid  $[\text{P}_2\text{W}_{17}\text{O}_{57}\{(\text{AEP})_2\}]$  **(2)**.

Conversely, when One molar equivalent of the mono-lacunary Dawson-type anion  $\text{K}_{10}\text{-}[\text{P}_2\text{W}_{17}\text{O}_{61}]$  ( $\text{W}_{17}$ ) is reacted with two molars equivalent 2-aminoethylphosphonic acid (AEP) and one molar equivalent of 3-phosphonopropionic acid (PPA), its synthesis the three POMs (**Figure 43**)

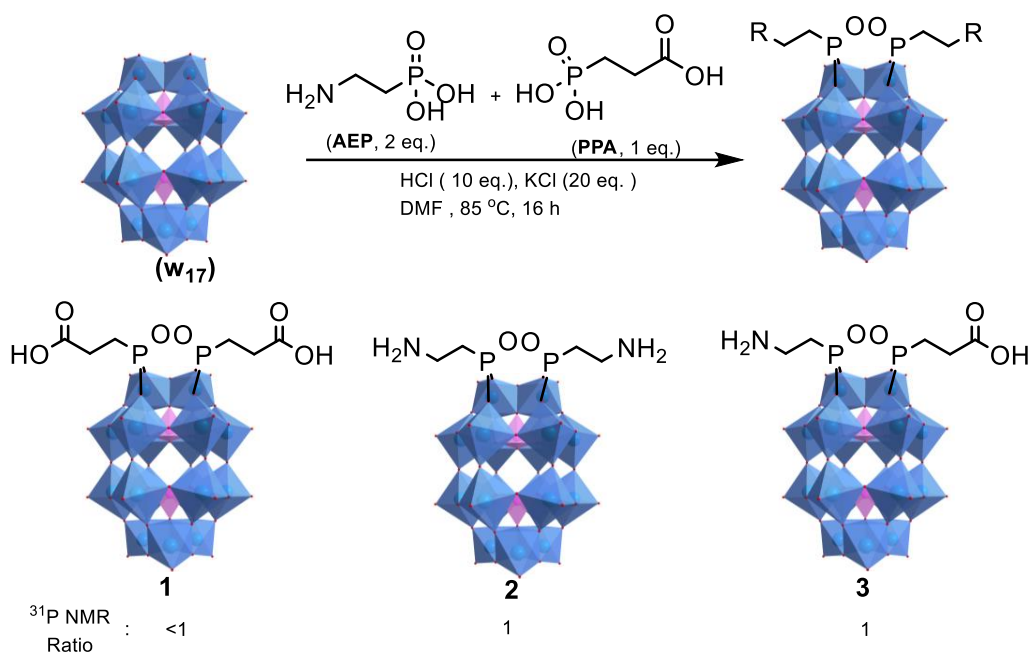


**Figure 43.** Hybridisation scheme showing the synthesis of the asymmetric hybrid-POM  $[\text{P}_2\text{W}_{17}\text{O}_{57}(\text{AEP}, 2\text{eq.}), (\text{PPA}, 1\text{eq.})]$ .

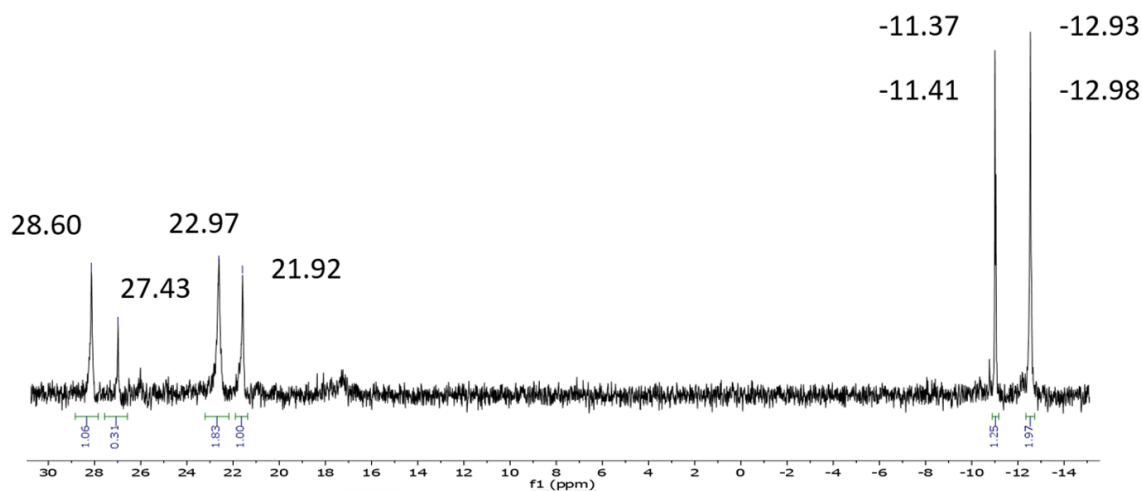


**Figure 44.**  $^{31}\text{P}$  NMR (162 MHz) in  $\text{DMSO-d}_6$  of the crude mixture of hybrid POM products produced during the synthesis of  $[\text{P}_2\text{W}_{17}\text{O}_{57}(\text{AEP}, 2\text{eq.}), (\text{PPA}, 1\text{eq.})]$ .

The  $^{31}\text{P}$  NMR confirms the presence of the three POMs. The  $[\text{P}_2\text{W}_{17}\text{O}_{57}\{(\text{PPA})_2\}]$  (**1**) ratio is lower than the POMs (**2**) and (**3**), suggesting that substituting a different equivalent of the starting material might improve outcomes. The dissipation of (**2**) in a 2 eq. of (PPA) and 1 eq. of (AEP) reaction, whereas (**1**) persisted in a 2 eq. of (AEP) and 1 eq. of (PPA) reaction, may provide insight into the relative rates at which these POMs are generated.

### 3.4 Exploring Photo-/Electro-Chemical Properties

UV-vis spectroscopy was applied in order to examine the hybrid POMs' absorption characteristics. POMs, as a whole, have strong and wide UV absorption bands, and these bands are related with ligand to metal charge transfer (LMCT)  $\text{O} \rightarrow \text{W}$ .<sup>132</sup>

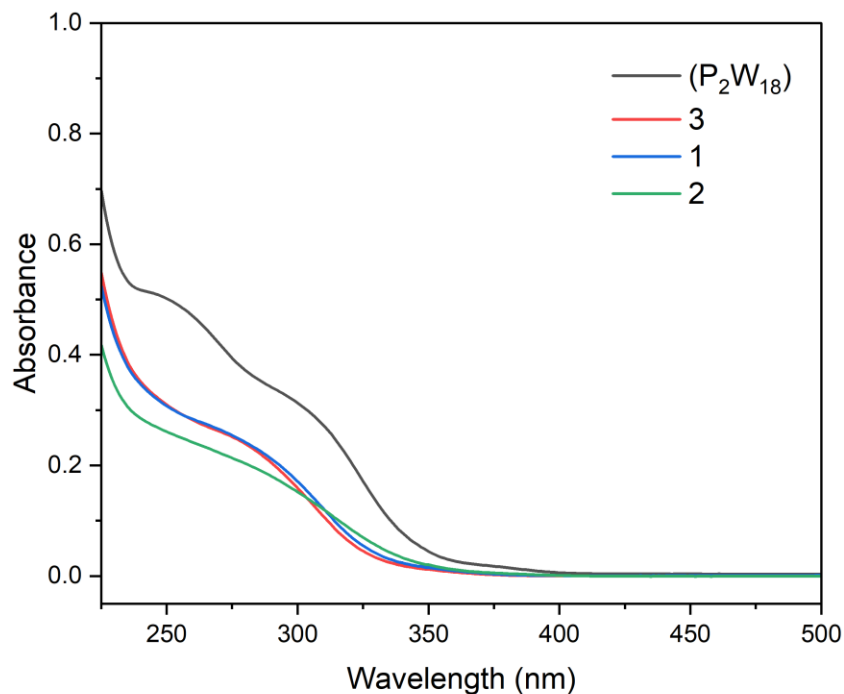


**Figure 45.** Overlay of the UV-vis spectra of **(3)** (red), **(1)** (blue) and **(2)** (green) compared with  $(P_2W_{18})$  (black).

POMs display various photochemical features, which may be induced by the activation of the O→M charge transfer (LMCT) band. Excitation of the OM charge transfer (LMCT) band elicits photochemically active POMs with a wealth of photochemical characteristics.<sup>125</sup> An electron is stimulated from a spin-paired, doubly occupied bonding orbital (HOMO) to an empty antibonding orbital, resulting in the development of a short-lived charge separated state (LUMO); this leads to the creation of an oxo-radical centred at the oxo-ligand that may participate in a variety of oxidation and hydrogen abstraction processes.<sup>133,134</sup> In most cases, just the spectrum's ultraviolet (UV) region is used for this photo-activation. The organo-functionalisation of POMs has also shown to be a helpful technique for modulating the HOMO-LUMO levels of the molecule and directing this excitation towards visible wavelengths. When comparing the two hybrid POMs **(1)**, **(2)** with crude poms **(3)**, we find only slight differences.

The following technique that was used to investigate the redox state of the material was cyclic voltammetry. It was anticipated that this method would be especially revealing due to the fact that both the cation and the anion are anticipated to be redox active. The relative reduction potentials were determined using cyclic voltammetry (CV). Under an argon environment, CV was done on all hybrid POMs in anhydrous DMF with 0.1 M [TBA][PF<sub>6</sub>] as the supporting electrolyte. The relative reduction potentials were determined using cyclic voltammetry (CV). Under an argon environment, CV was done on all hybrid POMs in anhydrous DMF with 0.1 M [TBA][PF<sub>6</sub>] as the supporting electrolyte. A glassy carbon (d = 3 mm) working electrode, Pt wire as the counter electrode, Ag wire as a pseudo-reference, and Ferrocene/Ferrocenium (Fc<sup>+</sup>/Fc) redox couple as the external reference was used in a three-electrode arrangement.

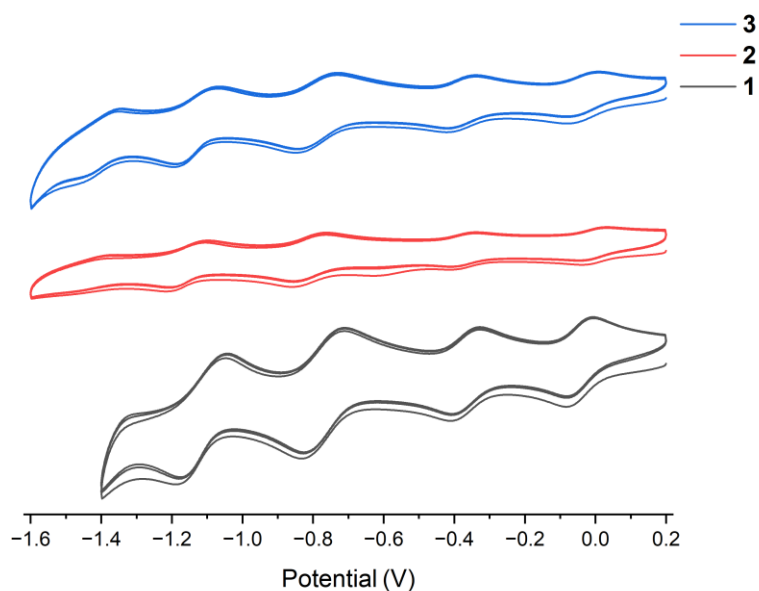


**Figure 46.** Cyclic voltammograms of POMs (1) (black), and (2) (red) compared to crude POM (3) (blue).

## 3.5 Experimental

### 3.5.1 Methods

We used Bruker Ascend™ 400 MHz and 500MHz spectrometers to acquire  $^1\text{H}$  NMR,  $^{31}\text{P}$  NMR, and  $^{13}\text{C}$  NMR spectra.

In negative mode, Bruker MicroTOF and Impact II spectrometers were used to record electrospray ionisation mass spectrometry (ESI-MS). To introduce the samples to the spectrometer, a volume of 20  $\mu\text{L}$  of acetonitrile solution (ca. 0.1 mg  $\text{mL}^{-1}$ ) was injected into a flow of 70:30 v/v MeOH/ $\text{H}_2\text{O}$  using an autosampler. Bruker's Compass Data Analysis software was performed to process the collected information.

The Infra-red IR spectrum was measured using a Bruker Alpha FTIR spectrometer equipped with a platinum ATR module.

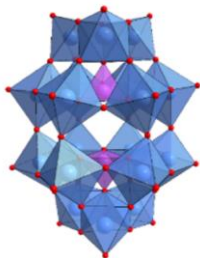
The Cary 5000 UV/VIS NIR spectrophotometer was employed to conduct the UV/Visible absorption spectroscopy.

Non-aqueous cyclic voltammetry (CV) tests were conducted using a working electrode (glassy carbon,  $d=3\text{mm}$ ), a reference electrode (Ag wire), and a counter electrode (Pt wire). The experiments were carried out in dry DMF with TBA.PF<sub>6</sub> (0.1 M) as the supporting electrolyte. All ferrocene-referenced potentials are expressed in the  $E_{1/2}$  of the ferrocene/ferrocenium redox pair. Under aqueous circumstances, three electrodes were used: a working electrode (glassy carbon,  $d=3\text{mm}$ ), a reference electrode (Ag/AgCl), and a counter electrode (Pt wire). Throughout the experiment, all solutions were held for 10 mins and remained under a positive pressure of nitrogen. A scan rate of 100  $\text{mVs}^{-1}$  was used for all experiments. The CHI600e was used for the electrochemical measurement (CH Instruments) workstation.

## 3.5.2 Syntheses

All reagents and solvents were obtained from commercial sources and used without additional purification unless otherwise noted.

### 3.5.2.1 $\text{K}_6[\text{P}_2\text{W}_{18}\text{O}_{62}]$

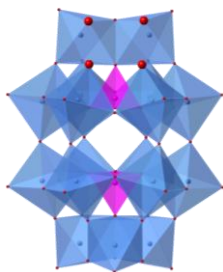


$\text{Na}_2\text{WO}_4 \cdot 2\text{H}_2\text{O}$  (100 g, 0.3 moles) was dissolved in water (116.6 mL). Drop by drop, (84 mL) of HCl (4 M) was added. After the addition was finished, a white precipitate was produced and then dissolved. Then, add dropwise (84 mL) of  $\text{H}_3\text{PO}_4$  (4 M). The end product, a yellow solution, was refluxed at 110 °C for 24 hours. The clear yellow solution was allowed to cool to room temperature when the reaction was finished. A yellow precipitate was created in the solution after (50 g, 0.67 moles) of KCl was added. After filtering, a pale-yellow solid was produced, and it was left to air dry overnight. After being dissolved in water (216 mL), heated to remove any remaining solvent, and allowed to cool overnight, the yellow solid produced a yellow precipitate. This precipitate was then washed with cold water ( $2 \times 10$  mL), yielding a yellow crystalline solid (69.56 g, 85%).<sup>117</sup>

$^{31}\text{P}$  NMR (202 MHz,  $\text{D}_2\text{O}$ )  $\delta = -13.02$ .

**IR** (neat,  $\text{cm}^{-1}$ ) 3564, 3471, 1605, 1080, 1020, 957, 901.44, 716, 592, 516, 473. Data in good agreement with the literature.<sup>117</sup>

### 3.5.2.2 $K_{10}[P_2W_{17}O_{57}]$



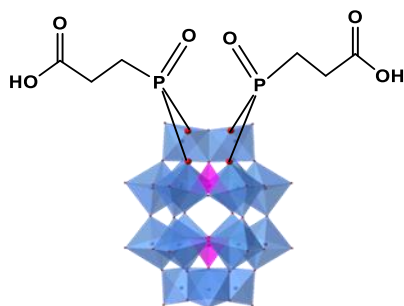
$K_6[P_2W_{18}O_{62}]$  (64.57 g, 11.5 mmol) was dissolved in  $H_2O$  (160 mL). The reaction liquid was then mixed with solution of  $KHCO_3$  (16.14 g, 0.2 mol) in (160 ml) and stirred overnight to produce a milky white precipitate. The precipitate was filtered, then washed with acetone and water.  $K_{10}[P_2W_{17}O_{61}]$  (45.13 g, 68%) as white powder crystals were produced from the crude by recrystallising it from a small amount of heated  $H_2O$ .<sup>118</sup>

$^{31}P$  NMR (162 MHz,  $D_2O$ )  $\delta$ =-7.24, -14.35.

IR (neat,  $cm^{-1}$ ) 3533, 3422 (O-H, b), 1076, 1045, 1014, 934, 884.97, 796.47, 716.22. Data in good agreement with the literature.<sup>118</sup>

### 3.5.2.3 $[P_2W_{17}O_{57}\{(PPA)_2\}]$

$K_3(C_2H_8N)_3[P_2W_{17}O_{57}\{(PO_3C_2H_4COOH)_2\}]$



3-Phosphonophosphonic acid (101 mg, 0.33 mmol, 1eq.),  $K_{10}[P_2W_{17}O_{61}]$  (1.5 g, 0.33 mmol, 1eq.), and KCl (0.49 g, 6.57 mmol) were suspended in DMF (30 mL). Add dropwise of 12M HCl (275 L, 3.3 mmol) while stirring, and the mixture was then heated (85 °C) for 16 h. Before adding ether

(120 mL) to the reaction mixture to precipitate a dark blue greasy coating, it was allowed to cool. After centrifuging the mixture, separate the oily layer from the supernatant. Add the smallest amount of water (10 mL) to dissolve the dark blue oil, and an excess of dioxane (80 mL) was then added to cause it to precipitate. A light blue solid was obtained after centrifuging the mixture and collecting the supernatant. The solid was then vacuum-dried until it resembled a solid blue powder (1.3 g, 88%)

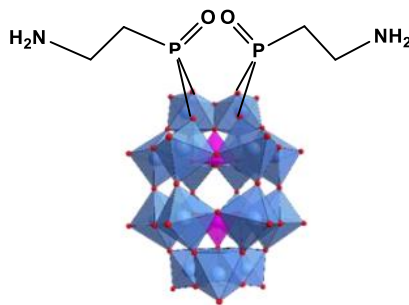
**$^1\text{H}$  NMR** (500 MHz, DMSO- $d_6$ )  $\delta$ =12.28 (br.s, 2H, -COOH), 8.73 (br.s, 6H,  $\text{NH}_2(\text{CH}_3)_2^+$ ), 2.74 (m, 4H,  $\text{HOOC-CH}_2^-$ ), 2.52 (br.s,  $J=18\text{H}$ ,  $\text{NH}_2(\text{CH}_3)_2^+$ ), 2.15 –1.95 (m, 4H,  $\text{PO-CH}_2^-$ ).

**$^{31}\text{P}$  NMR** (202 MHz, DMSO- $d_6$ )  $\delta$  27.49, -11.19, -12.98.

**IR** (neat,  $\text{cm}^{-1}$ ) 422 (s), 471 (s), 526 (vs), 721 (br, vs), 908 (s), 951 (s), 1087 (s), 1389 (w), 1414 (w), 1461 (m), 1615 (w), 1651 (m), 1723 (m, C=O), 2925 (w, C-H), 2966 (w, C-H), 2587- 3250 (m, br, O-H).

#### 3.5.2.4 [ $\text{P}_2\text{W}_{17}\text{O}_{57}\{(\text{AEP})_2\}$ ]

$\text{K}_3(\text{C}_2\text{H}_8\text{N})_3[\text{P}_2\text{W}_{17}\text{O}_{57}\{(\text{PO}_3\text{C}_2\text{H}_4\text{NH}_2)_2\}]$



Three substances were suspended in DMF:  $\text{K}_{10}\text{-}[\text{P}_2\text{W}_{17}\text{O}_{61}]$  (1.5 g, 0.33 mmol, 1eq.), 2-Aminoethylphosphonic acid (82 mg, 0.33 mmol, 1eq.), and KCl (0.49 g, 6.57 mmol) (30 mL). Stirred as 12M HCl (275 L, 3.3 mmol) was added dropwise, and the mixture was then heated (85 °C) for 16 h. Before adding a large excess ether(100 mL) to precipitate a dark blue oily coating, the reaction liquid was allowed to cool. Centrifuged the mixture and separated the oily layer from the supernatant. With the addition of excess dioxane (90 mL), the dark blue oil precipitated after being dissolved in the least amount of water (7 mL). After centrifuging the mixture, a light blue

solid was obtained by decanting the supernatant. The solid was then vacuum-dried until it became dry blue powder (1.4g, 93%)

**<sup>1</sup>H NMR** (500 MHz, DMSO-*d*<sub>6</sub>)  $\delta$ =16.08 (br.s, 4H), 8.80 (br.s, 6H), 2.74 (s, 4H), 2.50 (br.s, 18H), 2.25 (m, 4H).

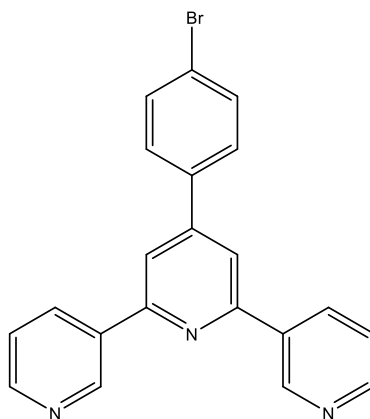
**<sup>31</sup>P NMR** (202 MHz, DMSO-*d*<sub>6</sub>)  $\delta$ =22.97, -11.46, -12.89.

**IR** (neat,  $\text{cm}^{-1}$ ) 421 (s), 470 (s), 528 (vs), 735 (vs), 908 (s), 954 (s), 1081 (s), 1377 (w), 1414 (w), 1451 (m), 1558 (w), 1656 (m), 2857 (br, C-H), 2964 (w, C-H).

### 3.5.2.5 TPY

TPY was synthesised using a method developed by Elizabeth Hampson<sup>129</sup>

#### Synthesis of BrPhTPY

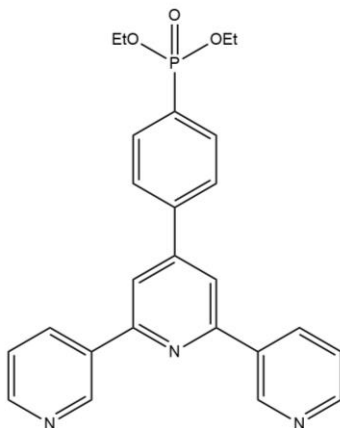


4-Bromobenzaldehyde (5 g, 27.0 mmol, 1eq.), KOH (4.54 g, 81 mmol, 3eq.) and 2-Acetylpyridine (6.06 mL, 54 mmol, 2eq.) were dissolved in ethanol (300 mL). 35% Ammonium hydroxide solution (62 mL) was added to the magnetically stirring mixture which was then heated at reflux (75°C) for 24 hours. The resulting suspension was filtered, washed with ethanol (2 × 5mL), and the filter cake was left to dry in open air for 2 hours. The crude powder was refined by trituration from hot chloroform (50 mL) using cold ethanol (100 mL) to give a white powder which was collected by vacuum filtration. A second crop of material was isolated from the filtrate, the solids were combined, and vacuum-dried to yield BrPhTPY (2.39 g, 23%) as a white powder.<sup>135,136</sup>

**<sup>1</sup>H NMR** (400 MHz, CDCl<sub>3</sub>) δ=8.76 (ddd, *J*=4.8, 1.9, 0.9 Hz, 2H), 8.73 (br.s, 2H), 8.70 (dt, *J*=7.9, 1.1 Hz, 2H), 7.91 (td, *J*=7.7, 1.8 Hz, 6H), 7.85 – 7.77 (m, 2H), 7.75 – 7.63 (m, 2H), 7.39 (ddd, *J*=7.5, 4.8, 1.2 Hz, 2H).<sup>137</sup>

**MS (ESI):** Calc for [C<sub>21</sub>H<sub>14</sub>N<sub>3</sub>Br<sub>1</sub>+H]<sup>+</sup>, 390.0426. Found 390.0413.

### Synthesis of PO(OEt)<sub>2</sub>PhTPY



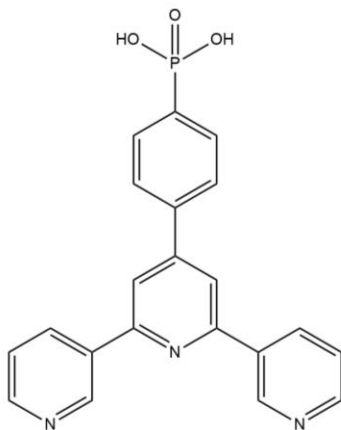
BrPhTPY (2 g, 5.12 mmol), PPh<sub>3</sub> (405 mg, 1.52 mmol), and Pd(OAc)<sub>2</sub> (116 mg, 0.52 mmol), were under argon, then added Ethanol (64 mL), Diethylphosphite (2.6 mL, 20.64 mmol) and Triethylamine (2.15 mL, 15.44 mmol), the mixture was heated at reflux (75 °C) while stirring for 22 hours. Before filtering, the solution was allowed to cool to room temperature, and the solvent was then removed in a vacuo. The yellow precipitate had to be recrystallised twice from hot CH<sub>3</sub>CN. In order to produce PO(OEt)<sub>2</sub>PhTPY, an off-white crystalline solid (1.44 g, 61%).<sup>138,139</sup>

**<sup>1</sup>H NMR** (400 MHz, CDCl<sub>3</sub>) δ=8.84 (br.s, 2H), 8.79-8.75 (ddd, *J*= 8.0, 4.9 Hz, 2H), 8.06-8.10 (dd, *J*= 8.4, 3.9 Hz, 2H), 8.04 – 7.97 (m, 4H), 7.97 (s, 2H), 7.45 (s, 2H), 4.29 – 4.08 (m, 4H), 1.38 (t, *J*= 7.1 Hz, 6H).

**<sup>31</sup>P NMR** (162 MHz, CDCl<sub>3</sub>) δ=18.61.

**MS (ESI):** Calc for [C<sub>25</sub>H<sub>24</sub>N<sub>3</sub>O<sub>3</sub>P<sub>1</sub>+H]<sup>+</sup>, 446.1628. Found 446.1618.

### Synthesis of TPY, PO(OH)<sub>2</sub>PhTPY – C<sub>21</sub>H<sub>16</sub>N<sub>3</sub>PO<sub>3</sub>



PO(OEt)<sub>2</sub>PhTPY (333 mg, 0.73 mmol) was dissolved in dry DCM (9 mL), and Bromotrimethylsilane (0.3 mL, 2.16 mmol) was added under argon before the mixture was stirred at RT for 16 h. The solvent was removed in vacuo before adding a methanol-DCM mixture (7 mL, 1:1 v/v), and the solution was stirred at RT for 3 h. The cloudy purple mixture was filtered to yield the crude product as a lilac powder. The crude was washed with hot CH<sub>3</sub>CN and then ether to give TPY as an off-white powder (299 mg, 89%).

**<sup>1</sup>H NMR** (400 MHz, DMSO-d<sub>6</sub>) δ=8.88-8.87 (ddd, *J*=1.9 Hz, 2H), 8.86 (br.s, 2H), 8.85-8.84 (d, *J*=4.4 Hz 2H), 8.28-8.23 (td, *J*=7.8, 1.8 Hz, 2H), 8.12-8.09 (m, 2H), 7.94-7.89 (m, 2H), 7.73-7.70 (dd, *J*=7.5, 5.1 Hz, 2H).

**<sup>31</sup>P NMR** (162 MHz, DMSO-d<sub>6</sub>) δ=11.93.

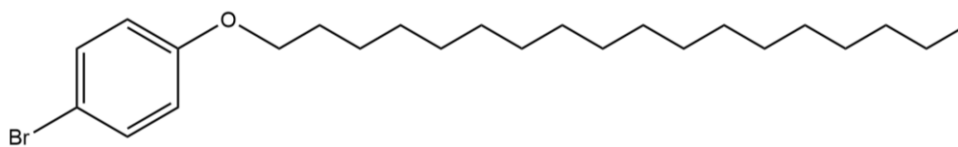
**MS (ESI)** Calc for [C<sub>21</sub>H<sub>16</sub>N<sub>3</sub>O<sub>3</sub>P1+H]<sup>+</sup> 390.1002, Found: 390.1003

**IR (neat, cm<sup>-1</sup>)** 665, 781, 894, 1071, 1133, 1241, 1288, 1393, 1424, 1527, 1595.

### 3.5.2.6 C<sub>18</sub>

C<sub>18</sub> was synthesised using a method developed by Sharad Amin.<sup>140</sup>

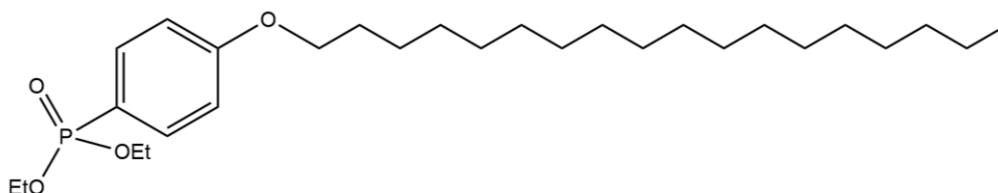
#### Synthesis of BrPhOC<sub>18</sub>



Bromooctadecane (1g, 3.00 mmol) and 4-Bromophenol (623 mg, 3.6 mmol) were dissolved in DMF (14 mL). The reaction mixture was heated (80°C) for 20 hours after  $K_2CO_3$  (1.66 g, 12.0 mmol) and KI (87 mg, 0.523 mmol) were added to this solution. The solvent was subsequently removed in vacuo once the reaction had been cooled to room temperature. Diethyl ether (34 mL) was used to dissolve the solid product, followed by washes ( $2 \times 50$  mL) 2M NaOH and brine (50 mL). Orange oil was produced when the organic fraction was dried over  $MgSO_4$ , and the solvent was removed in vacuo. The next step was recrystallising the crude product using only a minimal amount of heated ethanol (15 mL) to produce  $BrPhOC_{18}$  as a white solid (606 mg, 47%).<sup>141</sup>

$^1H$  NMR (400 MHz,  $CDCl_3$ )  $\delta$ =7.42 – 7.33 (m, 2H), 6.83 – 6.75 (m, 2H), 3.93 (t,  $J$ = 6.6 Hz, 2H,  $CH_2$ ), 1.84 – 1.73 (m, 2H,  $CH_2$ ), 1.46 – 1.23 (m, 30H,  $-CH_2-$ ), 0.90 (t,  $J$ = 6.7 Hz, 3H,  $CH_3$ ).

### Synthesis of $PO(OEt)_2PhOC_{18}$



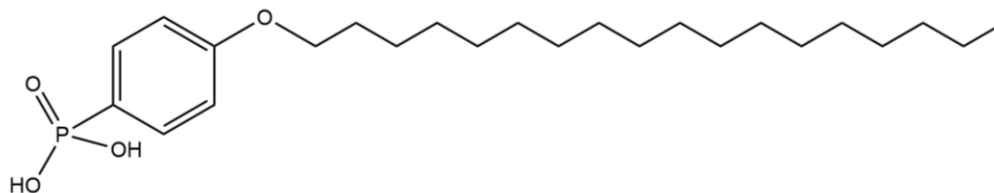
$BrPhOC_{18}$  (2.5 g, 5.87 mmol),  $PPh_3$  ( 507 mg, 1.9 mmol), and  $Pd(OAc)_2$  (145 mg, 0.65 mmol), were under argon, then added Ethanol (80 mL), Diethylphosphite (3.32 mL, 25.8 mmol) and Triethylamine (2.69 mL, 19.3 mmol), the mixture was under argon heated at reflux (75 °C) while stirring for 22 hours. Before filtering, the solution was allowed to cool to room temperature, and the solvent was then removed in a vacuo. The yellow precipitate had to be recrystallised twice from hot  $CH_3CN$ . In order to produce  $PO(OEt)_2PhOC_{18}$ , an off-white crystalline solid (1.63 g, 57%).<sup>142</sup>

**<sup>1</sup>H NMR** (400 MHz, CDCl<sub>3</sub>) δ=7.81- 7.65 (m, 2H), 7.01- 6.92 (m, 2H), 4.21 – 3.98 (m, 6H, O-CH<sub>2</sub>), 1.89- 1.74 (m, 2H, CH<sub>2</sub>), 1.46- 1.28 (m, 30H, CH<sub>2</sub>), 0.90 (t, *J* = 6.8 Hz, 3H, CH<sub>3</sub>).

**<sup>31</sup>P NMR** (162 MHz, CDCl<sub>3</sub>) δ= 19.86.

**MS (ESI)** Calc for [C<sub>28</sub>H<sub>51</sub>O<sub>4</sub> P+H]<sup>+</sup> : 483.36, Found: 483.36

### Synthesis of C<sub>18</sub>, PO(OH)<sub>2</sub>PhOC<sub>18</sub> – C<sub>24</sub>H<sub>43</sub>O<sub>4</sub> P



Dry PO(OEt)<sub>2</sub>PhOC<sub>18</sub> (1.015g, 2.11 mmol) was dissolved in dry DCM (10 mL). Then, Bromotrimethylsilane (TMSBr) (0.97 mL, 7.35 mmol) was added under argon to form a pale yellow solution. The mixture was then stirred for 20 h at RT. A yellow oil was produced after the solvent and extra TMSBr were evaporated in vacuo. A 10 mL mixture of methanol and water (80:20 v/v) was added to the flask and stirred for 3 hours to produce a white suspension. After centrifuging the mixture, the solvent was separated from the white precipitate. To produce the crude as an off-white solid, the solid was vacuum-dried. The unfinished product was next washed with diethyl ether (2 × 25 mL). Then stirred with (25 mL) of heated acetonitrile and finally filtered. C<sub>18</sub> was obtained as a white powder (525 mg, 59%) by washing the solid with ether (25 mL) once more and allowing it to dry in the air.

**<sup>1</sup>H NMR** (400 MHz, Methanol-d<sub>4</sub>) δ=7.78- 7.68 (m, 2H), 7.03- 6.99 (m, 2H), 4.04 (t, *J*= 6.4 Hz, 2H, O-CH<sub>2</sub>), 1.82- 1.77 (m, 2H, CH<sub>2</sub>), 1.49- 1.20 (m, 30H, -CH<sub>2</sub>), 0.92 (t, *J*= 6.8 Hz, 3H, CH<sub>3</sub>).

**<sup>31</sup>P NMR** (162 MHz, Methanol-d<sub>4</sub>) δ=17.25.

**MS (ESI)** Calc for [C<sub>24</sub>H<sub>43</sub>O<sub>4</sub> P-H]<sup>-</sup> : 425.29, Found: 425.28.

**IR (neat, cm<sup>-1</sup>)** 828 (s), 945 (vs), 1008 (br, vs), 1142 (vs), 1254 (s), 1292 (w), 1461 (m), 1474 (m), 1503 (w), 1525 (w), 1570 (w), 1598 (s), 2847 (vs), 2915 (vs).

### 3.5.2.7 [P<sub>2</sub>W<sub>17</sub>O<sub>57</sub>{(TPY)(C<sub>18</sub>)}]

[P<sub>2</sub>W<sub>17</sub>O<sub>57</sub>{(TPY)(C<sub>18</sub>)}] was synthesised using a method developed by Elizabeth Hampson<sup>129</sup>



DMF-CH<sub>3</sub>CN (50 mL, 1:1 v/v) was used to suspend and stir K<sub>10</sub>-[P<sub>2</sub>W<sub>17</sub>O<sub>61</sub>] (1.6 g, 0.35 mmol, 1eq.), TPY (0.14 g, 0.35 mmol, 1eq.), C<sub>18</sub> (0.15 g, 0.35 mmol, 1eq.), and KCl (0.52 g, 6.98 mmol). Dropwise additions of 12M HCl (290 μL, 3.5 mmol) were added while stirring the solution, and the mixture was then heated to 85°C for 16 hours. Before filtration, the mixture was allowed to cool to RT. The milky solution was given a high excess of ether (120 mL) before centrifuging it to produce a dark orange-brown precipitate in a yellow supernatant. After removing the solvent, the precipitate was sonicated in ether, centrifuged, and decanted once more until it resembled a free-flowing green-brown powder. The solid was centrifuged after being sonicated in acetonitrile (10–15 mL) to separate an insoluble pale green-blue solid. Ether (25 mL) was added to the yellow supernatant after it had been decanted to precipitate a dark orange-brown solid and produce a pale yellow supernatant. Centrifugation was used to collect the solid, which was then sonicated in ether and dried in the air with low heat. Until no [POM(TPY)<sub>2</sub>] or [POM(C<sub>18</sub>)<sub>2</sub>] could be seen in the <sup>31</sup>P and <sup>1</sup>H NMR, the following steps were repeated: re-dissolving in acetonitrile, centrifuging to remove any insoluble [POM(TPY)<sub>2</sub>], then re-precipitating [POM{(TPY)(C<sub>18</sub>)}], from the supernatant with ether. In order to remove any insoluble material, the dry solid was eventually dissolved in a little amount of acetone and centrifuged. Following the removal of the solvent in vacuo, [POM{(TPY)(C<sub>18</sub>)}], was obtained as a dark orange crystalline solid (280 mg, 31%, assuming a maximum statistical recovery of 50% for an asymmetric product).

<sup>1</sup>H NMR (400 MHz, DMSO-d<sub>6</sub>) δ = 8.81-8.78 (m, 6H, Ar-H), 8.72-8.70 (td, 2H, Ar-H), 8.26-8.02 (4H, NH<sub>2</sub>(CH<sub>3</sub>)<sub>2</sub><sup>+</sup>), 8.22-8.20 (m, 2H, Ar-H), 8.07-8.02 (m, 2H, Ar-H), 7.56- 7.53 (m, 2H, Ar-H),

7.03-7.00 (dd, 2H, Ar-H), 4.04 (t, 2H, O-CH<sub>2</sub>), 2.57 (t, 12H, NH<sub>2</sub>(CH<sub>3</sub>)<sub>2</sub><sup>+</sup>), 1.75 (2H, CH<sub>2</sub>), 1.42-1.18 (m, 30H, -CH<sub>2</sub>-), 0.86 (t, 3H, CH<sub>3</sub>).

<sup>31</sup>P NMR (162 MHz, DMSO-d<sub>6</sub>) δ= 16.72, 13.41, -11.28, -12.95.

**IR (neat, cm<sup>-1</sup>)** 424 (s), 471 (s), 525 (s), 566 (s), 592 (s), 667 (s), 716 (br, vs, W-O-W), 800 (br, vs, W-O-W), 906 (s, W-O-W), 955 (s, W=O), 962 (s, W=O), 1082 (s, P-O), 1133 (w, P=O), 1254 (w), 1295 (w), 1388 (w), 1414 (w), 1462 (m), 1503 (w), 1531 (w), 1569-1595 (m), 1651 (w), 2850 (m, C-H), 2919 (m, C-H).<sup>129</sup>

## 4 Preparation of Symmetric Hybrid POM

### [P<sub>2</sub>W<sub>17</sub>O<sub>57</sub>{(RuTPY)<sub>2</sub>}

Numerous research studies used POMs with ruthenium polypyridyl complexes, albeit often used as photoactive cations. However, because of the difficulty in synthesising a sufficient covalent coupling, reports of ruthenium complexes in hybrid POMs covalently bound are rarer.<sup>143,144</sup> In the design of efficient charge-transfer materials, structural stability is essential, yet, covalent interactions allow for more flexibility in the configuration of the hybrid system and tuneability in its electronic structure.

### 4.1 Synthesis of RuTPY Ligand

The preparation of the ligand complex, RuTPY, followed the plan shown in (**Figure 46**). The ruthenium trichloride complex Ru<sup>III</sup>-PO(OEt)<sub>2</sub>TPY was first created by reacting ruthenium (III) chloride with the substituted-terpyridine phosphonate ester PO(OEt)<sub>2</sub>TPY. A method modified from the literature was then used to coordinate the Ru<sup>III</sup> centre to 4,4'-dimethyl 2,2'-bipyridine (dmbpy) under reductive conditions.<sup>145-147</sup> In order to create the phosphonic acid ligand RuTPY, the phosphonate ester Ru-Cl(dmbpy)PO(OEt)<sub>2</sub>TPY was hydrolyzed by protection with TMSBr, similar to how TPY was.

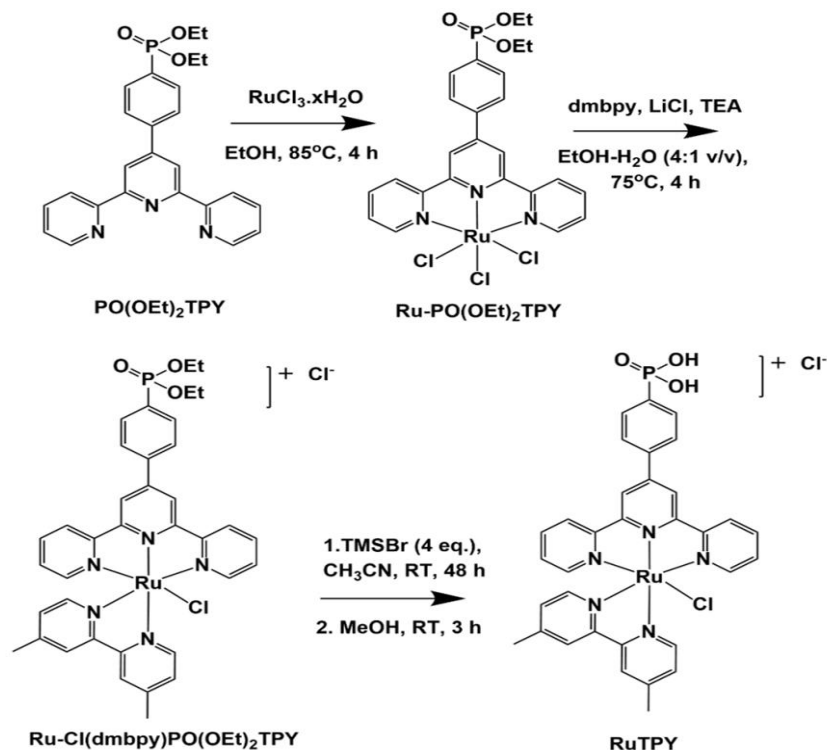


**Figure 47.** Synthesis of the RuTPY ligand.

### [P<sub>2</sub>W<sub>17</sub>O<sub>57</sub>{(RuTPY)<sub>2</sub>}

In her doctoral thesis, Elizabeth Hampson discovered a technique to synthesise [P<sub>2</sub>W<sub>17</sub>O<sub>57</sub>{(RuTPY)<sub>2</sub>}] This approach was used in the following part.

In **(Figure 48)**, we see the synthetic route that will lead us to the desired hybrid species. The anionic and cationic components were prepared as their respective simple alkali metal and halide salts. According to the literature report, the compound K<sub>10</sub>·[P<sub>2</sub>W<sub>17</sub>O<sub>61</sub>] (W<sub>17</sub>) was produced in high yields by following a process that included a divergent two-step synthesis.<sup>117,118</sup>

[P<sub>2</sub>W<sub>17</sub>O<sub>57</sub>{(RuTPY)<sub>2</sub>}] was prepared in a one-pot hybridisation reaction using the similar conditions as for the symmetric POM hybrid **1** and **2**; one equivalent of (W<sub>17</sub>), and two equivalent of RuTPY in a DMF were refluxed for 19h in an acid-catalysed condensation reaction.

The  $^{31}\text{P}$  NMR in  $\text{DMSO-d}_6$  shows a single peak on 14.35 ppm, which is diagnostic for the  $[\text{P}_2\text{W}_{17}\text{O}_{57}\{(\text{RuTPY})_2\}]$  and has shifted downfield compared to the starting material RuTPY. The  $^1\text{H}$  NMR for the hybrids displays several peaks corresponding to the various aromatic environments on the molecule's core and different environments (**Figure 49**).

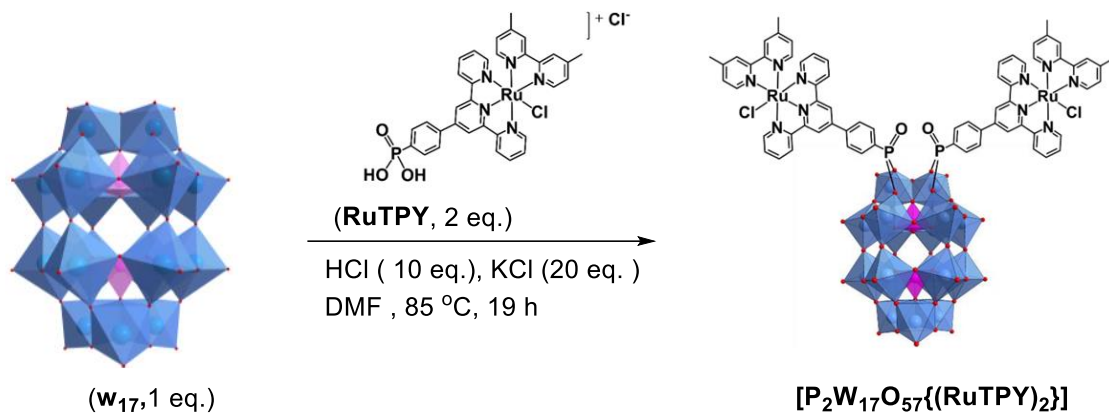


**Figure 48.** Hybridisation scheme showing the synthesis of the hybrid-POM  $[\text{P}_2\text{W}_{17}\text{O}_{57}\{(\text{RuTPY})_2\}]$ .

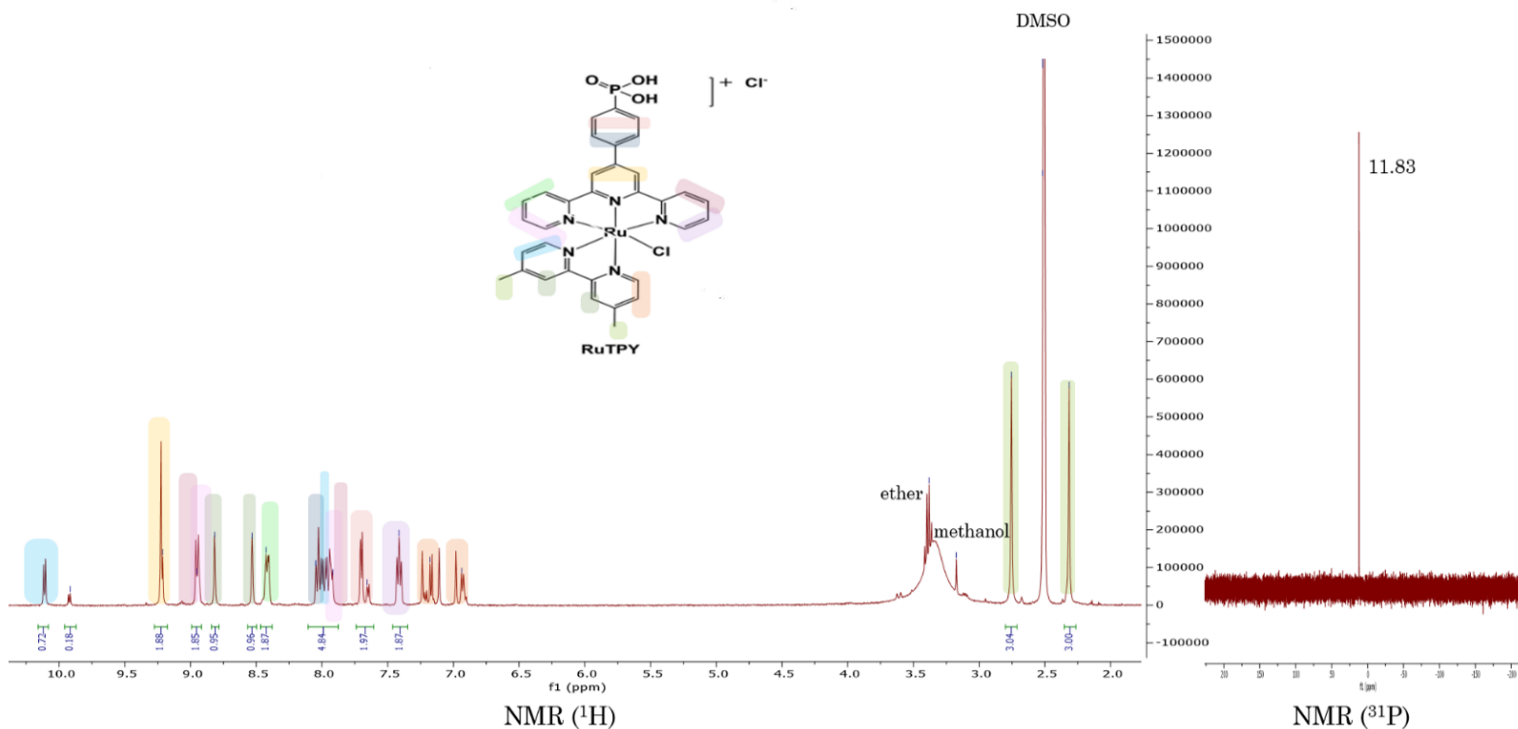


**Figure 49.**  $^1\text{H}$  NMR (400 MHz) and  $^{31}\text{P}$  NMR (162 MHz) of the ligand (RuTPY) in DMSO- $d_6$ .

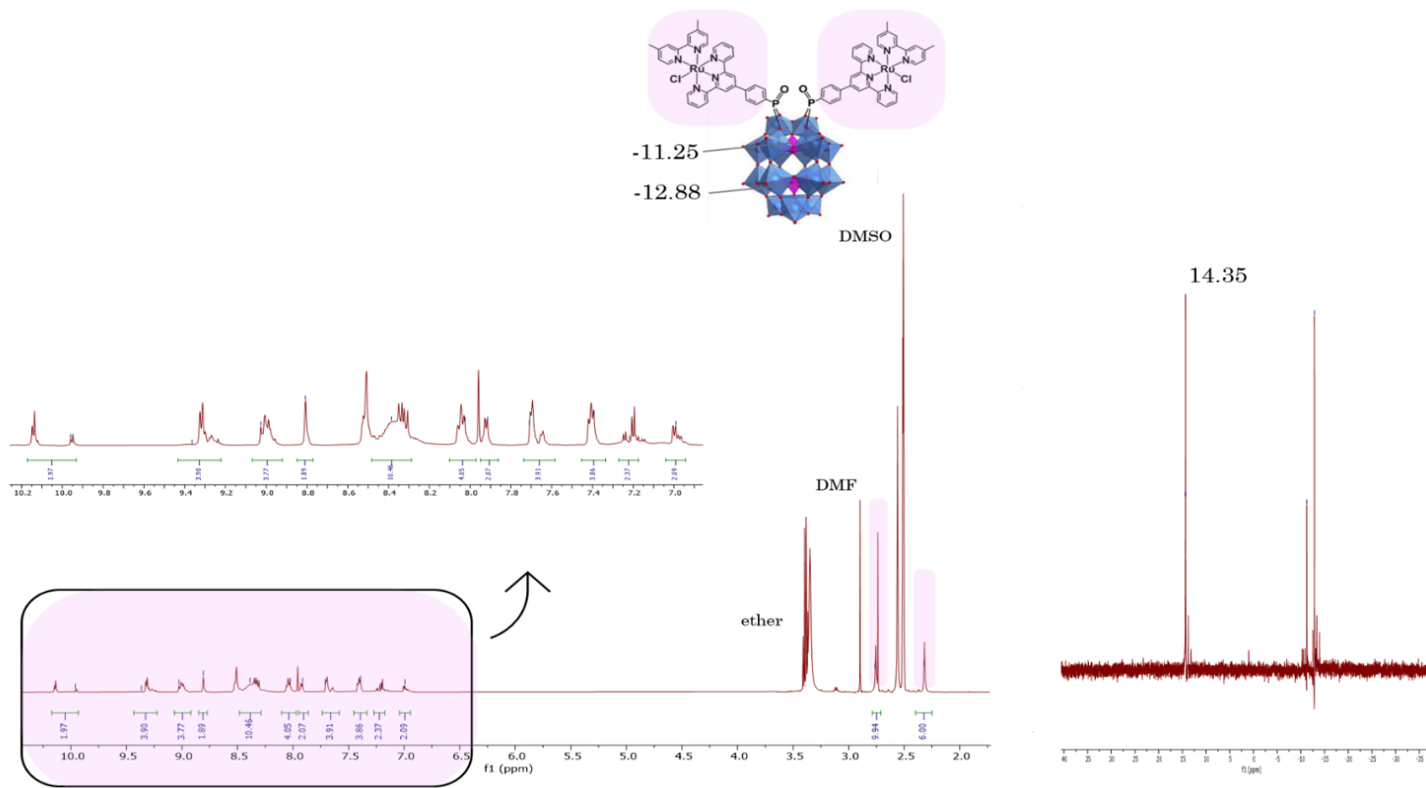


**Figure 50.**  $^1\text{H}$  NMR (500 MHz) and  $^{31}\text{P}$  NMR (202 MHz) of  $[\text{P}_2\text{W}_{17}\text{O}_{57}\{(\text{RuTPY})_2\}]$  in DMSO- $d_6$ .

The structure of the hybrid POM  $[P_2W_{17}O_{57}\{(RuTPY)_2\}]$  anion with an overall charge has been confirmed by the ESI mass spectrum.

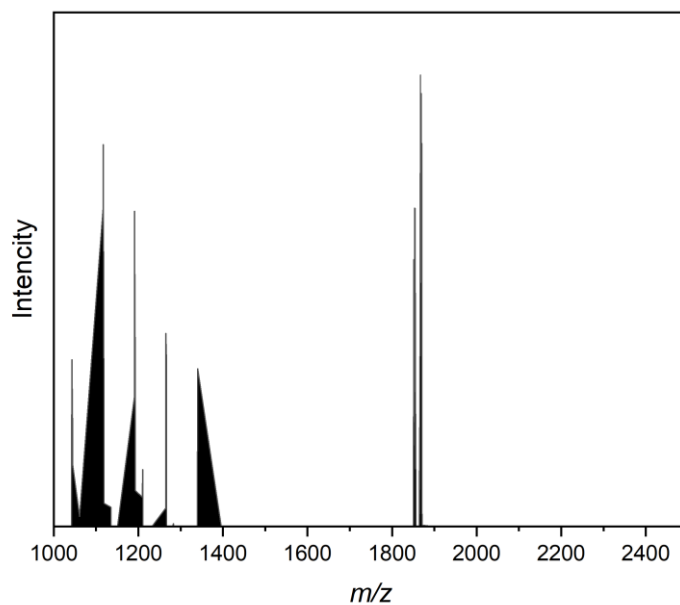


**Figure 51.** ESI mass spectrum of  $[P_2W_{17}O_{57}\{(RuTPY)_2\}]$ .

Assignment	Z	m/z (obs)	m/z (calc)
$H[P_2W_{17}O_{57}\{(PO_3C_{33}H_{26}N_5RuCl)_2\}]$	3-	1838.9905	1838.6223
$HNa[P_2W_{17}O_{57}\{(PO_3C_{33}H_{26}N_5RuCl)_2\}]$	2-	2793.9835	2768.9245

**Table 6.** ESI-MS peak assignments for  $[P_2W_{17}O_{57}\{(TPY)_2\}]$ .

IR spectroscopy validated the structural characteristics of the symmetric hybrid POM.<sup>148</sup>

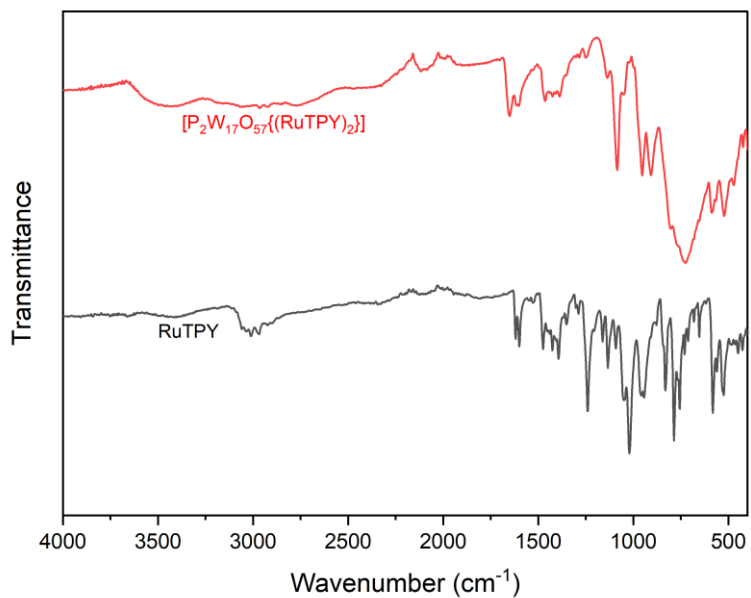


**Figure 52.** ATR-IR spectrum of  $[P_2W_{17}O_{57}\{(RuTPY)_2\}]$  (red), comparing with the ligand RuTPY (black).

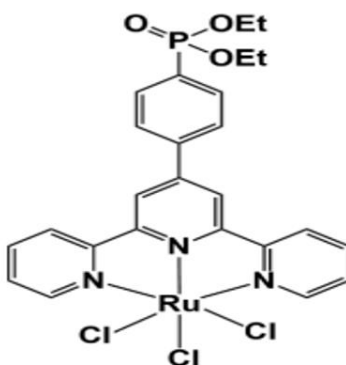
## 4.2 Experimental

### 4.2.1 Syntheses

All reagents and solvents were obtained from commercial sources and used without additional purification unless otherwise noted.

#### 4.2.1.1 RuTPY

##### Synthesis of Ru-PO(OEt)<sub>2</sub>TPY

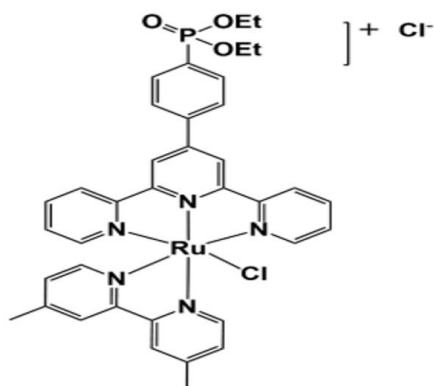


In 60 mL of ethanol, RuCl<sub>3</sub> (109 mg, 0.52 mmol) and PO(OEt)<sub>2</sub>TPY (200 mg, 0.52 mmol) were dissolved, then the mixture was heated at reflux (85°C) with stirring for 4 h. Before centrifuging, the mixture was allowed to cool to room temperature. After removing the dark red supernatant, the brown solid was centrifuged, sonicated, and then washed with ethanol (3 × 20 mL) before being separated from the solvent. The solvent was relatively light in colour after three repetitions of this operation. After drying in the air, being washed with ether (3 × 20 mL), and then dried under vacuum, the solid produced Ru-PO(OEt)<sub>2</sub>TPY as a reddish-brown solid (236 mg, 68%).

<sup>1</sup>H NMR (400 MHz, DMSO-d<sub>6</sub>) δ=9.74 (dd, *J*= 6.5, 12.8 Hz, 2H), 6.97 (br.s, 2H), 3.89-3.39 (m, 4H; -OCH<sub>2</sub>-), 1.16 (t, *J*= 7.1 Hz, 6H; -CH<sub>3</sub>), -0.11 (br.s, 2H), -2.94 (br.s, 2H). (In this spectral region, additional δ -peaks were not visible).<sup>149</sup>

<sup>31</sup>P NMR (162 MHz, DMSO-d<sub>6</sub>) δ= -11.02.

##### Synthesis of Ru-Cl(dmbpy)PO(OEt)<sub>2</sub>TPY



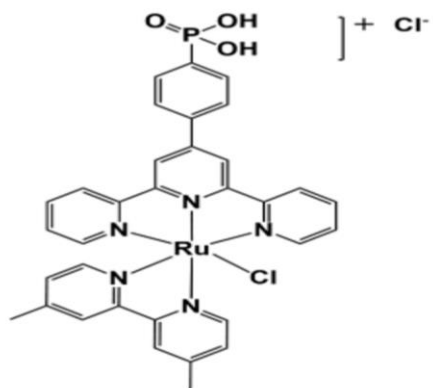
In 95 mL of ethanol-H<sub>2</sub>O (4:1 v/v), Ru-PO(OEt)<sub>2</sub>TPY (1.03 g, 1.58 mmol), 4,4'-dimethyl 2,2'-dipyridyl (349 mg, 1.89 mmol) and (200 mg, 4.73 mmol) of LiCl were suspended. Triethylamine (0.53 mL, 3.80 mmol) was added to the mixture while it was stirred. During a 4h stirring period, the mixture was heated to reflux (90°C). The solvent was then extracted in a vacuum after the mixture had been heated through filtering. After centrifuging, sonicating, and removing the orange-brown supernatant from the solid, the brown solid was washed with HCl (2 M) (3 × 20 mL). After three iterations of this procedure, the solvent's colour had become incredibly pale. Three further ether (20 mL) washes were performed on the solid in the same manner. prior to drying under vacuum to produce the dark brown-red solid Ru-Cl(dmbpy)PO(OEt)<sub>2</sub>TPY (1.10 g, 87%).<sup>150,151</sup>

**<sup>1</sup>H NMR** (400 MHz, DMSO-d<sub>6</sub>) δ= 9.93 (d, *J*= 5.7 Hz, 1H), 9.23 (s, 2H), 8.95 (d, *J*= 8.1 Hz, 2H), 8.83 (s, 1H), 8.54 (s, 1H), 8.48 (dd, *J*= 3.5, 8.2 Hz, 2H), 8.07– 7.97 (m, 4H), 7.97 (d, *J*=6.0 Hz, 1H), 7.65 (d, *J*= 5.5 Hz, 2H), 7.42 (ddd, *J*= 6.6, 5.5, 1.2 Hz, 2H), 7.18 (d, *J*= 5.9 Hz, 1H), 6.94 (d, 1H), 4.20 – 4.06 (m, 4H; -OCH<sub>2</sub>-), 2.76 (s, 3H; bpy-CH<sub>3</sub>), 2.32 (s, 3H; bpy-CH<sub>3</sub>), 1.32 (t, *J*= 7.0 Hz, 6H; CH<sub>3</sub>).

**<sup>31</sup>P NMR** (162 MHz, DMSO-d<sub>6</sub>) δ= 17.21.

**MS (ESI)** Calc for [C<sub>37</sub>H<sub>36</sub>N<sub>5</sub>O<sub>3</sub>P<sub>1</sub>Ru<sub>1</sub>C<sub>11</sub>]<sup>+</sup>, 766.1289. Found 766.1288.

### Synthesis of RuTPY



Ru-Cl(dmbpy)PO(OEt)<sub>2</sub>TPY (1.19 g, 1.55 mmol) was combined with dry acetonitrile (50 mL), stirred under argon, Bromotrimethylsilane (0.90 mL, 6.53 mmol) was then added to the mixture and then allowed to stand for 40 hours. After that, the solution received 50 mL of methanol and was stirred continuously for a further 3 hours at RT in the air. Before centrifuging, the solid was suspended in about 20 mL of methanol after the solvent was extracted in a vacuo. By repeatedly repeating the steps of centrifugation, sonication, and decanting the solvent from the solid until the solvent was colourless, the dark reddish-brown supernatant was separated from the solid and washed with ether (15 mL) three times. In order to produce. Lastly, the solid was allowed to dry in the air while being gently heated for ~30 min to produce RuTPY as a dark red solid (1.01 g, 92%).

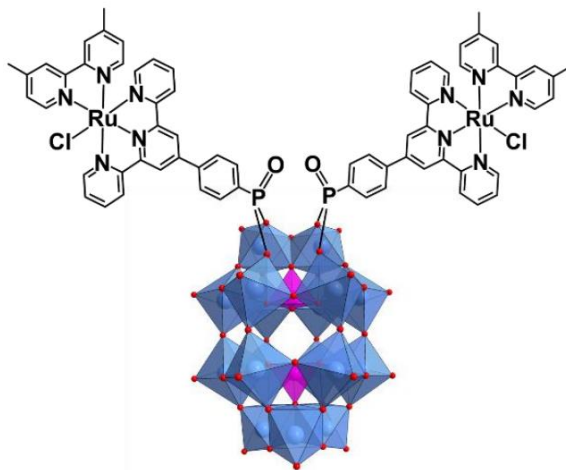
**<sup>1</sup>H NMR** (400 MHz, DMSO-d<sub>6</sub>) δ=10.11 (d, *J*= 5.8 Hz, 1H), 9.22 (s, 2H), 8.95 (d, *J*= 8.3 Hz, 2H), 8.82 (s, 1H), 8.53 (s, 1H), 8.42 (td, *J*= 3.1, 8.4, 9.0 Hz, 2H), 8.07– 7.89 (m, 5H), 7.67 (d, *J*= 5.7 Hz, 2H), 7.41 (t, *J*= 6.6 Hz, 2H), 7.13 (t, *J*= 5.8 Hz, 1H), 6.90 (d, *J*= 6.3 Hz, 1H; Ar-H), 3.39 (q, *J*= 7.0 Hz, 1H), 2.75 (s, 3H; bpyCH<sub>3</sub>), 2.32 (s, 3H; bpy-CH<sub>3</sub>).

**<sup>31</sup>P NMR** (162 MHz, DMSO-d<sub>6</sub>) δ= 11.83.

**MS (ESI)** [M]<sup>+</sup> Calc for [C<sub>33</sub>H<sub>28</sub>N<sub>5</sub>O<sub>3</sub>P<sub>1</sub>Ru<sub>1</sub>Cl<sub>1</sub>]<sup>+</sup>, 710.0662. Found 766.1262.

**IR (neat, cm<sup>-1</sup>)** 826 (s), 880 (s), 959(s), 1131 (m), 1208 (m), 1239 (w), 1353 (w), 1391 (w), 1427 (w), 1475 (m), 1601(m), 2921 (w), 3059 (w).

#### 4.2.1.2 [P<sub>2</sub>W<sub>17</sub>O<sub>57</sub>{(RuTPY)<sub>2</sub>}



RuTPY (164 mg, 0.220 mmol), KCl (164 mg, 20.2 mmol), and K<sub>10</sub>-[P<sub>2</sub>W<sub>17</sub>O<sub>61</sub>] (0.50 g, 0.110 mmol) were dissolved in DMF (20 mL) and stirred. Dropwise additions of 12 M HCl (92 L, 1.104 mmol) were added while stirring, and the mixture was then heated to 85°C for 19 hours. Before filtration, the mixture was allowed to cool to RT. A large excess of ether (about 60 mL) was added to create a maroon-colored milky solution, which was then centrifuged to produce a maroon precipitate. The material was sonicated in ether, centrifuged, and then the process of centrifuging, decanting, and repeating was carried out until the precipitate resembled a free-flowing powder. The solid was gently heated in the air and then dried under a vacuum. A dark maroon solid yielded (530 mg, 84%)

<sup>1</sup>H NMR (400 MHz, DMSO-d<sub>6</sub>) δ=9.92 (d, *J*= 5.8 Hz, 2H), 9.21 (s, 4H), 8.93 (d, *J*= 8.1 Hz, 4H), 8.81 (d, *J*= 10.0 Hz, 2H), 8.53-8.45 (m, 10H), 8.08 – 7.93 (m, 4H), 7.66- 7.63 (m, 2H), 7.65 (m, 4H), 7.46 – 7.38 (m, 4H), 7.20-7.18 (m, 2H), 6.97- 6.89 (m, 2H), 2.75 (s, 6H, bpy-CH<sub>3</sub>), 2.33 (s, 6H; bpy-CH<sub>3</sub>).

<sup>31</sup>P NMR (162 MHz, DMSO-d<sub>6</sub>) δ= 14.33, -11.25, -12.88.

IR (neat, cm<sup>-1</sup>) 422 (s), 471 (s), 521 (s), 567 (s), 585 (s), 722 (br), 906 (s), 953 (s), 1085 (s), 1137 (w), 1250 (w), 1388 (m), 1410 (w), 1425 (w), 1464 (m), 1612 (m), 2921 (w)

## 5 Conclusion

Through the synthesis and isolating of an asymmetric Wells-Dawson hybrid POM, the synthesis of new, multifunctional hybrid materials based on molecular metal oxides has indeed been researched. Several synthetic approaches, including controlled hydrolysis of symmetric hybrid POM starting materials, were studied. Clear limits with these approaches were identified, and the attention was shifted to a one-pot synthesis methodology in which the design and functioning of two distinct ligands, as well as the efficiency of purifying symmetric and asymmetric hybrid products, were investigated. Purification and isolation attempts of an asymmetric hybrid POM product were unexpected and often unreplaceable. The Amine compound of the asymmetric Wells-Dawson hybrid POM has been initially separated by the use of improving selectivity by changing equivalents. This technique is far simpler and less costly than previously reported methods. Nevertheless, further research and analysis are required.

There are a variety of different methods of purifying asymmetric hybrids, and they will be successful depending on the molecular and its structure. Unfortunately, the separation procedure has been attempted using a few different solutions, and those solvents did not seem to be successful with this molecule. Furthermore, when we experimented with changing the concentration of the auxiliary chemicals, we received a remarkable result; but, because of a shortage of time, we could not attempt different concentrations and more approaches.

## 5.1 List of references

- (1) Thor Pope, M. *Heteropoly and Isopoly Oxometalates*; New York, USA, 1983.
- (2) Long, D.-L.; Tsunashima, R.; Cronin, L. Polyoxometalates: Building Blocks for Functional Nanoscale Systems. *Angew. Chem. Int. Ed Engl.* **2010**, *49* (10), 1736–1758. <https://doi.org/10.1002/anie.200902483>.
- (3) Clemente-Juan, J. M.; Coronado, E.; Gaita-Ariño, A. Magnetic Polyoxometalates: From Molecular Magnetism to Molecular Spintronics and Quantum Computing. *Chem. Soc. Rev.* **2012**, *41* (22), 7464. <https://doi.org/10.1039/c2cs35205b>.
- (4) Wang, S.-S.; Yang, G.-Y. Recent Advances in Polyoxometalate-Catalyzed Reactions. *Chem. Rev.* **2015**, *115* (11), 4893–4962. <https://doi.org/10.1021/cr500390v>.
- (5) Cameron, J. M.; Guillemot, G.; Galambos, T.; Amin, S. S.; Hampson, E.; Mall Haidaraly, K.; Newton, G. N.; Izzet, G. Supramolecular Assemblies of Organo-Functionalised Hybrid Polyoxometalates: From Functional Building Blocks to Hierarchical Nanomaterials. *Chem. Soc. Rev.* **2022**, *51* (1), 293–328. <https://doi.org/10.1039/D1CS00832C>.
- (6) Rhule, J. T.; Hill, C. L.; Judd, D. A.; Schinazi, R. F. Polyoxometalates in Medicine. *Chem. Rev.* **1998**, *98* (1), 327–358. <https://doi.org/10.1021/cr960396q>.
- (7) He, Q.; Zhang, Y.; Li, H.; Chen, Q. Rheological Properties of ABA-Type Copolymers Physically End-Cross-Linked by Polyoxometalate. *Macromolecules* **2020**, *53* (24), 10927–10941. <https://doi.org/10.1021/acs.macromol.0c01817>.
- (8) Song, Y.-F.; Tsunashima, R. Recent Advances on Polyoxometalate-Based Molecular and Composite Materials. *Chem. Soc. Rev.* **2012**, *41* (22), 7384. <https://doi.org/10.1039/c2cs35143a>.
- (9) Poepelmeier, K. R.; Reedijk, J. *Comprehensive Inorganic Chemistry II: From Elements to Applications*; Elsevier: Amsterdam [u.a.], 2013.
- (10) Lipscomb, W. N. Paratungstate Ion. *Inorg. Chem.* **1965**, *4* (1), 132–134. <https://doi.org/10.1021/ic50023a039>.
- (11) Hill, C. L.; Prosser-McCartha, C. M. Homogeneous Catalysis by Transition Metal Oxygen Anion Clusters. *Coord. Chem. Rev.* **1995**, *143*, 407–455. [https://doi.org/10.1016/0010-8545\(95\)01141-B](https://doi.org/10.1016/0010-8545(95)01141-B).
- (12) *Molecular Electronic Structures of Transition Metal Complexes. 1 / with Contrib. by J.P. Dahl*; Dahl, J. P., Ed.; Structure and bonding; Springer: Berlin Heidelberg, 2012.
- (13) Miras, H. N.; Cooper, G. J. T.; Long, D.-L.; Bögge, H.; Müller, A.; Streb, C.; Cronin, L. Unveiling the Transient Template in the Self-Assembly of a Molecular Oxide Nanowheel. *Science* **2010**, *327* (5961), 72–74. <https://doi.org/10.1126/science.1181735>.
- (14) Wang, Y.; Li, F.; Jiang, N.; Liu, X.; Xu, L. A “Directed Precursor Self-Assembly” Strategy for the Facile Synthesis of Heteropoly Blues: Crystal Structures, Formation Mechanism and Electron Distribution. *Dalton Trans.* **2019**, *48* (38), 14347–14353. <https://doi.org/10.1039/C9DT02789K>.
- (15) Long, D.-L.; Burkholder, E.; Cronin, L. Polyoxometalate Clusters, Nanostructures and Materials: From Self Assembly to Designer Materials and Devices. *Chem Soc Rev* **2007**, *36* (1), 105–121. <https://doi.org/10.1039/B502666K>.
- (16) Miras, H. N.; Yan, J.; Long, D.-L.; Cronin, L. Engineering Polyoxometalates with Emergent Properties. *Chem. Soc. Rev.* **2012**, *41* (22), 7403. <https://doi.org/10.1039/c2cs35190k>.

- (17) Misra, A.; Kozma, K.; Streb, C.; Nyman, M. Beyond Charge Balance: Counter-Cations in Polyoxometalate Chemistry. *Angew. Chem. Int. Ed.* **2020**, *59* (2), 596–612. <https://doi.org/10.1002/anie.201905600>.
- (18) Li, D.; Liu, Z.; Song, J.; Li, H.; Zhang, B.; Yin, P.; Zheng, Z. N.; Roberts, J. E.; Tsige, M.; Hill, C. L.; Liu, T. Cation Translocation around Single Polyoxometalate-Organic Hybrid Cluster Regulated by Electrostatic and Cation- $\pi$  Interactions. *Angew. Chem.* **2017**, *129* (12), 3342–3346. <https://doi.org/10.1002/ange.201612008>.
- (19) Keggin, J. F. Structure of the Molecule of 12-Phosphotungstic Acid. *Nature* **1933**, *131* (3321), 908–909. <https://doi.org/10.1038/131908b0>.
- (20) Lu, Y.-K.; Qu, Y.-Y.; Tian, M.-M.; Diao, C.-L.; Liu, Y.-Q.  $\mu_3$ -Dodecatungsto(V,VI)Aluminato- $\kappa^3 O : O' : O''$ -Tris[Aquabis(Ethylenediamine- $\kappa^2 N, N'$ )Copper(II)]. *Acta Crystallogr. Sect. E Struct. Rep. Online* **2011**, *67* (12), m1778–m1779. <https://doi.org/10.1107/S1600536811048288>.
- (21) Baker, L. C. W.; Figgis, J. S. New Fundamental Type of Inorganic Complex: Hybrid between Heteropoly and Conventional Coordination Complexes. Possibilities for Geometrical Isomerisms in 11-, 12-, 17-, and 18-Heteropoly Derivatives. *J. Am. Chem. Soc.* **1970**, *92* (12), 3794–3797. <https://doi.org/10.1021/ja00715a047>.
- (22) Grigoriev, V. A.; Hill, C. L.; Weinstock, I. A. Role of Cation Size in the Energy of Electron Transfer to 1:1 Polyoxometalate Ion Pairs  $\{(M^+)(X^{n+}VW_{11}O_{40})\}^{(8-n)-}$  ( $M = Li, Na, K$ ). *J. Am. Chem. Soc.* **2000**, *122* (14), 3544–3545. <https://doi.org/10.1021/ja993862c>.
- (23) Robert, F.; Tézé, A.; Hervé, G.; Jeannin, Y. The Crystal Structure of  $K_4(B1-SiMoW_{11}O_{40}) \cdot 9H_2O$ . *Acta Crystallogr. B* **1980**, *36* (1), 11–15. <https://doi.org/10.1107/S0567740880002336>.
- (24) Matsumoto, K. Y.; Kobayashi, A.; Sasaki, Y. The Crystal Structure of  $\beta$ - $K_4 SiW_{12} O_{40} \cdot 9H_2 O$  Containing an Isomer of the Keggin Ion. *Bull. Chem. Soc. Jpn.* **1975**, *48* (11), 3146–3151. <https://doi.org/10.1246/bcsj.48.3146>.
- (25) Tézé, A.; Cadot, E.; Béreau, V.; Hervé, G. About the Keggin Isomers: Crystal Structure of  $[N(C_4H_9)_4]_4$ - $\gamma$ - $[SiW_{12} O_{40}]$ , the  $\gamma$ -Isomer of the Keggin Ion. Synthesis and  $^{183}W$  NMR Characterization of the Mixed  $\gamma$ - $[SiMo_2 W_{10} O_{40}]^{n-}$  ( $n = 4$  or  $6$ ). *Inorg. Chem.* **2001**, *40* (9), 2000–2004. <https://doi.org/10.1021/ic000864l>.
- (26) Rowsell, J.; Nazar, L. F. Speciation and Thermal Transformation in Alumina Sols: Structures of the Polyhydroxyoxoaluminum Cluster  $[Al_{30} O_8 (OH)_{56} (H_2 O)_{26}]^{18+}$  and Its  $\delta$ -Keggin Moiety. *J. Am. Chem. Soc.* **2000**, *122* (15), 3777–3778. <https://doi.org/10.1021/ja993711+>.
- (27) Sloboda-Rozner, D.; Neimann, K.; Neumann, R. Aerobic Oxidation of Aldehydes Catalyzed by  $\epsilon$ -Keggin Type Polyoxometalates  $[Mo_{12}VO_39(M_2-OH)_{10}H_2\{XII(H_2O)_3\}_4]$  ( $X = Ni, Co, Mn$  and  $Cu$ ) as Heterogeneous Catalysts. *J. Mol. Catal. Chem.* **2007**, *262* (1–2), 109–113. <https://doi.org/10.1016/j.molcata.2006.08.046>.
- (28) Pope, M. T.; Jeannin, Y.; Fournier, M. *Heteropoly and Isopoly Oxometalates*; Inorganic Chemistry Concepts; Springer Berlin: Berlin, 2013.
- (29) Anyushin, A. V.; Kondinski, A.; Parac-Vogt, T. N. Hybrid Polyoxometalates as Post-Functionalization Platforms: From Fundamentals to Emerging Applications. *Chem. Soc. Rev.* **2020**, *49* (2), 382–432. <https://doi.org/10.1039/C8CS00854J>.
- (30) Canny, J.; Teze, A.; Thouvenot, R.; Herve, G. Disubstituted Tungstosilicates. 1. Synthesis, Stability, and Structure of the Lacunary Precursor Poly anion of a Tungstosilicate

- .Gamma.-SiW10O368-. *Inorg. Chem.* **1986**, 25 (13), 2114–2119.  
<https://doi.org/10.1021/ic00233a003>.
- (31) Dawson, B. The Structure of the 9(18)-Heteropoly Anion in Potassium 9(18)-Tungstophosphate,  $K_6(P_2W_{18}O_{62}) \cdot 14H_2O$ . *Acta Crystallogr.* **1953**, 6 (2), 113–126.  
<https://doi.org/10.1107/S0365110X53000466>.
- (32) The Structure and Formula of 12-Phosphotungstic Acid. *Proc. R. Soc. Lond. Ser. Contain. Pap. Math. Phys. Character* **1934**, 144 (851), 75–100.  
<https://doi.org/10.1098/rspa.1934.0035>.
- (33) Kondinski, A.; Parac-Vogt, T. N. Keggin Structure, Quo Vādis? *Front. Chem.* **2018**, 6, 346. <https://doi.org/10.3389/fchem.2018.00346>.
- (34) *Complexity in Chemistry and beyond: Interplay Theory and Experiment: New and Old Aspects of Complexity in Modern Research*; Hill, C. L., Musaev, D. G., Eds.; NATO science for peace and security series. B, Physics and biophysics; Springer: Dordrecht, 2012.
- (35) Matsunaga, S.; Miyamae, E.; Inoue, Y.; Nomiya, K.  $\beta, \beta$ -Isomer of Open-Wells–Dawson Polyoxometalate Containing a Tetra-Iron(III) Hydroxide Cluster:  $[ \{ Fe_4(H_2O)(OH)_5 \} (\beta, \beta - Si_2W_{18}O_{66}) ]^{9-}$ . *Inorganics* **2016**, 4 (2), 15. <https://doi.org/10.3390/inorganics4020015>.
- (36) Zhang, F.-Q.; Guan, W.; Yan, L.-K.; Zhang, Y.-T.; Xu, M.-T.; Hayfron-Benjamin, E.; Su, Z.-M. On the Origin of the Relative Stability of Wells–Dawson Isomers: A DFT Study of  $\alpha$ -,  $\beta$ -,  $\gamma$ -, A\*-, B\*-, and  $\Gamma^*$ - $[ (PO_4)_2W_{18}O_{54} ]^{6-}$  Anions. *Inorg. Chem.* **2011**, 50 (11), 4967–4977. <https://doi.org/10.1021/ic200203s>.
- (37) Janusson, E.; de Kler, N.; Vilà-Nadal, L.; Long, D.-L.; Cronin, L. Synthesis of Polyoxometalate Clusters Using Carbohydrates as Reducing Agents Leads to Isomer-Selection. *Chem. Commun.* **2019**, 55 (41), 5797–5800.  
<https://doi.org/10.1039/C9CC02361E>.
- (38) Nakajima, K.; Eda, K.; Himeno, S. Effect of the Central Oxocyanion Size on the Voltammetric Properties of Keggin-Type  $[XW_{12}O_{40}]^{n-}$  ( $n = 2-6$ ) Complexes. *Inorg. Chem.* **2010**, 49 (11), 5212–5215. <https://doi.org/10.1021/ic1003353>.
- (39) Li, B.; Li, W.; Li, H.; Wu, L. Ionic Complexes of Metal Oxide Clusters for Versatile Self-Assemblies. *Acc. Chem. Res.* **2017**, 50 (6), 1391–1399.  
<https://doi.org/10.1021/acs.accounts.7b00055>.
- (40) Liu, Q.; Wang, X. Polyoxometalate Clusters: Sub-Nanometer Building Blocks for Construction of Advanced Materials. *Matter* **2020**, 2 (4), 816–841.  
<https://doi.org/10.1016/j.matt.2020.01.020>.
- (41) Qi, W.; Wu, L. Polyoxometalate/Polymer Hybrid Materials: Fabrication and Properties: Polyoxometalate/Polymer Hybrid Materials. *Polym. Int.* **2009**, 58 (11), 1217–1225.  
<https://doi.org/10.1002/pi.2654>.
- (42) Gao, P.; Wu, Y.; Wu, L. Co-Assembly of Polyoxometalates and Peptides towards Biological Applications. *Soft Matter* **2016**, 12 (41), 8464–8479.  
<https://doi.org/10.1039/C6SM01433J>.
- (43) Zhang, B.; Zhao, M.; Qi, Y.; Tian, R.; Carter, B. B.; Zou, H.; Zhang, C.; Wang, C. The Intrinsic Enzyme Activities of the Classic Polyoxometalates. *Sci. Rep.* **2019**, 9 (1), 14832.  
<https://doi.org/10.1038/s41598-019-50539-9>.
- (44) Gao, N.; Sun, H.; Dong, K.; Ren, J.; Duan, T.; Xu, C.; Qu, X. Transition-Metal-Substituted Polyoxometalate Derivatives as Functional Anti-Amyloid Agents for

- Alzheimer's Disease. *Nat. Commun.* **2014**, *5* (1), 3422. <https://doi.org/10.1038/ncomms4422>.
- (45) Inoue, M.; Suzuki, T.; Fujita, Y.; Oda, M.; Matsumoto, N.; Yamase, T. Enhancement of Antibacterial Activity of Beta-Lactam Antibiotics by [P2W18O62]6-, [SiMo12O40]4-, and [PTi2W10O40]7- against Methicillin-Resistant and Vancomycin-Resistant *Staphylococcus Aureus*. *J. Inorg. Biochem.* **2006**, *100* (7), 1225–1233. <https://doi.org/10.1016/j.jinorgbio.2006.02.004>.
- (46) Timofeeva, M. N. Acid Catalysis by Heteropoly Acids. *Appl. Catal. Gen.* **2003**, *256* (1–2), 19–35. [https://doi.org/10.1016/S0926-860X\(03\)00386-7](https://doi.org/10.1016/S0926-860X(03)00386-7).
- (47) Kamata, K.; Sugahara, K. Base Catalysis by Mono- and Polyoxometalates. *Catalysts* **2017**, *7* (11), 345. <https://doi.org/10.3390/catal7110345>.
- (48) Zhang, Y.; Liu, J.; Li, S.-L.; Su, Z.-M.; Lan, Y.-Q. Polyoxometalate-Based Materials for Sustainable and Clean Energy Conversion and Storage. *EnergyChem* **2019**, *1* (3), 100021. <https://doi.org/10.1016/j.enchem.2019.100021>.
- (49) Omwoma, S.; Gore, C. T.; Ji, Y.; Hu, C.; Song, Y.-F. Environmentally Benign Polyoxometalate Materials. *Coord. Chem. Rev.* **2015**, *286*, 17–29. <https://doi.org/10.1016/j.ccr.2014.11.013>.
- (50) Cameron, J. M.; Wales, D. J.; Newton, G. N. Shining a Light on the Photo-Sensitisation of Organic–Inorganic Hybrid Polyoxometalates. *Dalton Trans.* **2018**, *47* (15), 5120–5136. <https://doi.org/10.1039/C8DT00400E>.
- (51) Papaconstantinou, E. Photochemistry of Polyoxometallates of Molybdenum and Tungsten and/or Vanadium. *Chem. Soc. Rev.* **1989**, *18*, 1. <https://doi.org/10.1039/cs9891800001>.
- (52) Streb, C. New Trends in Polyoxometalate Photoredox Chemistry: From Photosensitisation to Water Oxidation Catalysis. *Dalton Trans* **2012**, *41* (6), 1651–1659. <https://doi.org/10.1039/C1DT11220A>.
- (53) Kickelbick, G. Hybrid Materials—Past, Present and Future. *Hybrid Mater* **2014**, *1* (1), 39–51.
- (54) Sanchez, C.; Julián, B.; Belleville, P.; Popall, M. Applications of Hybrid Organic–Inorganic Nanocomposites. *J. Mater. Chem.* **2005**, *15* (35–36), 3559. <https://doi.org/10.1039/b509097k>.
- (55) Kibler, A. J.; Newton, G. N. Tuning the Electronic Structure of Organic–Inorganic Hybrid Polyoxometalates: The Crucial Role of the Covalent Linkage. *Polyhedron* **2018**, *154*, 1–20. <https://doi.org/10.1016/j.poly.2018.06.027>.
- (56) Schaming, D.; Costa-Coquelard, C.; Sorgues, S.; Ruhlmann, L.; Lampre, I. Photocatalytic Reduction of Ag2SO4 by Electrostatic Complexes Formed by Tetracationic Zinc Porphyrins and Tetracobalt Dawson-Derived Sandwich Polyanion. *Appl. Catal. Gen.* **2010**, *373* (1–2), 160–167. <https://doi.org/10.1016/j.apcata.2009.11.010>.
- (57) Martinetto, Y.; Pégot, B.; Roch-Marchal, C.; Cottyn-Boitte, B.; Floquet, S. Designing Functional Polyoxometalate-Based Ionic Liquid Crystals and Ionic Liquids. *Eur. J. Inorg. Chem.* **2020**, *2020* (3), 228–247. <https://doi.org/10.1002/ejic.201900990>.
- (58) Fay, N.; Hultgren, V. M.; Wedd, A. G.; Keyes, T. E.; Forster, R. J.; Leane, D.; Bond, A. M. Sensitization of Photo-Reduction of the Polyoxometalate Anions [S2M18O62]4<sup>-</sup> (M = Mo, W) in the Visible Spectral Region by the [Ru(Bpy)3]2<sup>+</sup> Cation. *Dalton Trans.* **2006**, No. 35, 4218. <https://doi.org/10.1039/b605663f>.

- (59) Kirchoff, B.; Rau, S.; Streb, C. Detecting and Preventing the Formation of Photosensitizer-Catalyst Colloids in Homogeneous Light-Driven Water Oxidation. *Eur. J. Inorg. Chem.* **2016**, 2016 (9), 1425–1429. <https://doi.org/10.1002/ejic.201600065>.
- (60) Favette, S.; Hasenknopf, B.; Vaissermann, J.; Gouzerh, P.; Roux, C. Assembly of a Polyoxometalate into an Anisotropic Gel. *Chem. Commun.* **2003**, No. 21, 2664. <https://doi.org/10.1039/b308889h>.
- (61) Monteiro, M. J. Design Strategies for Controlling the Molecular Weight and Rate Using Reversible Addition-Fragmentation Chain Transfer Mediated Living Radical Polymerization. *J. Polym. Sci. Part Polym. Chem.* **2005**, 43 (15), 3189–3204. <https://doi.org/10.1002/pola.20845>.
- (62) Dolbecq, A.; Dumas, E.; Mayer, C. R.; Mialane, P. Hybrid Organic–Inorganic Polyoxometalate Compounds: From Structural Diversity to Applications. *Chem. Rev.* **2010**, 110 (10), 6009–6048. <https://doi.org/10.1021/cr1000578>.
- (63) Proust, A.; Matt, B.; Villanneau, R.; Guillemot, G.; Gouzerh, P.; Izzet, G. Functionalization and Post-Functionalization: A Step towards Polyoxometalate-Based Materials. *Chem. Soc. Rev.* **2012**, 41 (22), 7605. <https://doi.org/10.1039/c2cs35119f>.
- (64) Anyushin, A. V.; Kondinski, A.; Parac-Vogt, T. N. Hybrid Polyoxometalates as Post-Functionalization Platforms: From Fundamentals to Emerging Applications. *Chem. Soc. Rev.* **2020**, 49 (2), 382–432. <https://doi.org/10.1039/C8CS00854J>.
- (65) Blazevic, A.; Rompel, A. The Anderson–Evans Polyoxometalate: From Inorganic Building Blocks via Hybrid Organic–Inorganic Structures to Tomorrows “Bio-POM.” *Coord. Chem. Rev.* **2016**, 307, 42–64. <https://doi.org/10.1016/j.ccr.2015.07.001>.
- (66) Bareyt, S.; Piligkos, S.; Hasenknopf, B.; Gouzerh, P.; Lacôte, E.; Thorimbert, S.; Malacria, M. Efficient Preparation of Functionalized Hybrid Organic/Inorganic Wells–Dawson-Type Polyoxotungstates. *J. Am. Chem. Soc.* **2005**, 127 (18), 6788–6794. <https://doi.org/10.1021/ja050397c>.
- (67) Sazani, G.; Pope, M. T. Organotin and Organogermanium Linkers for Simple, Direct Functionalization of Polyoxotungstates Electronic Supplementary Information (ESI) Available: Syntheses. See <http://www.rsc.org/Suppdata/Dt/B4/B402421d/>. *Dalton Trans.* **2004**, No. 13, 1989. <https://doi.org/10.1039/b402421d>.
- (68) Mayer, C. R.; Fournier, I.; Thouvenot, R. Bis- and Tetrakis(Organosilyl) Decatungstosilicate,  $[\gamma\text{-SiW}_{10}\text{O}_{36}(\text{RSi})_2\text{O}]_4^-$  and  $[\gamma\text{-SiW}_{10}\text{O}_{36}(\text{RSi})_4]_4^-$ : Synthesis and Structural Determination by Multinuclear NMR Spectroscopy and Matrix-Assisted Laser Desorption/Ionization Time-of-Flight Mass Spectrometry. *Chem. - Eur. J.* **2000**, 6 (1), 105–110. [https://doi.org/10.1002/\(SICI\)1521-3765\(20000103\)6:1<105::AID-CHEM105>3.0.CO;2-L](https://doi.org/10.1002/(SICI)1521-3765(20000103)6:1<105::AID-CHEM105>3.0.CO;2-L).
- (69) Niu, J.; Li, M.; Wang, J. Organosilyl Derivatives of Trivacant Tungstophosphate of General Formula  $\alpha\text{-A}[\text{PW}_9\text{O}_{34}(\text{RSiO})_3(\text{RSi})_3]_3^-$ . *J. Organomet. Chem.* **2003**, 675 (1–2), 84–90. [https://doi.org/10.1016/S0022-328X\(03\)00252-3](https://doi.org/10.1016/S0022-328X(03)00252-3).
- (70) Matt, B.; Renaudineau, S.; Chamoreau, L.-M.; Afonso, C.; Izzet, G.; Proust, A. Hybrid Polyoxometalates: Keggin and Dawson Silyl Derivatives as Versatile Platforms. *J. Org. Chem.* **2011**, 76 (9), 3107–3112. <https://doi.org/10.1021/jo102546v>.
- (71) Nomiya, K.; Togashi, Y.; Kasahara, Y.; Aoki, S.; Seki, H.; Noguchi, M.; Yoshida, S. Synthesis and Structure of Dawson Polyoxometalate-Based, Multifunctional, Inorganic–Organic Hybrid Compounds: Organogermeryl Complexes with One Terminal Functional

- Group and Organosilyl Analogues with Two Terminal Functional Groups. *Inorg. Chem.* **2011**, *50* (19), 9606–9619. <https://doi.org/10.1021/ic201336v>.
- (72) Villanneau, R.; Djamâa, A. B.; Chamoreau, L.; Gontard, G.; Proust, A. Bisorganophosphonyl and -Organoarsenyl Derivatives of Heteropolytungstates as Hard Ligands for Early-Transition-Metal and Lanthanide Cations. *Eur. J. Inorg. Chem.* **2013**, *2013* (10–11), 1815–1820. <https://doi.org/10.1002/ejic.201201257>.
- (73) Kim, G. S.; Hagen, K. S.; Hill, C. L. Synthesis, Structure, Spectroscopic Properties, and Hydrolytic Chemistry of Organophosphonoyl Polyoxotungstates of Formula  $[C_6H_5P(O)]_2X_n+W_{11}O_{39}(8-n)^-$  ( $X_{n+} = P^{5+}, Si^{4+}$ ). *Inorg. Chem.* **1992**, *31* (25), 5316–5324. <https://doi.org/10.1021/ic00051a025>.
- (74) Mayer, C. R.; Herson, P.; Thouvenot, R. Organic–Inorganic Hybrids Based on Polyoxometalates. 5. <sup>1</sup> Synthesis and Structural Characterization of Bis(Organophosphoryl)Decatungstosilicates  $[\gamma-SiW_{10}O_{36}((RPO)_2)]^{4-}$ . *Inorg. Chem.* **1999**, *38* (26), 6152–6158. <https://doi.org/10.1021/ic990724f>.
- (75) Cameron, J. M.; Fujimoto, S.; Kastner, K.; Wei, R.-J.; Robinson, D.; Sans, V.; Newton, G. N.; Oshio, H. H. Orbital Engineering: Photoactivation of an Organofunctionalized Polyoxotungstate. *Chem. - Eur. J.* **2017**, *23* (1), 47–50. <https://doi.org/10.1002/chem.201605021>.
- (76) Oms, O.; Hakouk, K.; Dessapt, R.; Deniard, P.; Jobic, S.; Dolbecq, A.; Palacin, T.; Nadjo, L.; Keita, B.; Marrot, J.; Mialane, P. Photo- and Electrochromic Properties of Covalently Connected Symmetrical and Unsymmetrical Spiropyran–Polyoxometalate Dyads. *Chem. Commun.* **2012**, *48* (99), 12103. <https://doi.org/10.1039/c2cc35376h>.
- (77) Saad, A.; Oms, O.; Dolbecq, A.; Menet, C.; Dessapt, R.; Serier-Brault, H.; Allard, E.; Baczkó, K.; Mialane, P. A High Fatigue Resistant, Photoswitchable Fluorescent Spiropyran–Polyoxometalate–BODIPY Single-Molecule. *Chem. Commun.* **2015**, *51* (89), 16088–16091. <https://doi.org/10.1039/C5CC06217A>.
- (78) Saad, A.; Oms, O.; Marrot, J.; Dolbecq, A.; Hakouk, K.; El Bekkachi, H.; Jobic, S.; Deniard, P.; Dessapt, R.; Garrot, D.; Boukheddaden, K.; Liu, R.; Zhang, G.; Keita, B.; Mialane, P. Design and Optical Investigations of a Spironaphthoxazine/Polyoxometalate/Spiropyran Triad. *J Mater Chem C* **2014**, *2* (24), 4748–4758. <https://doi.org/10.1039/C4TC00378K>.
- (79) Boulmier, A.; Vacher, A.; Zang, D.; Yang, S.; Saad, A.; Marrot, J.; Oms, O.; Mialane, P.; Ledoux, I.; Ruhlmann, L.; Lorcy, D.; Dolbecq, A. Anderson-Type Polyoxometalates Functionalized by Tetrathiafulvalene Groups: Synthesis, Electrochemical Studies, and NLO Properties. *Inorg. Chem.* **2018**, *57* (7), 3742–3752. <https://doi.org/10.1021/acs.inorgchem.7b02976>.
- (80) Wu, P.; Yin, P.; Zhang, J.; Hao, J.; Xiao, Z.; Wei, Y. Single-Side Organically Functionalized Anderson-Type Polyoxometalates. *Chem. - Eur. J.* **2011**, *17* (43), 12002–12005. <https://doi.org/10.1002/chem.201101552>.
- (81) Zhang, J.; Luo, J.; Wang, P.; Ding, B.; Huang, Y.; Zhao, Z.; Zhang, J.; Wei, Y. Step-by-Step Strategy from Achiral Precursors to Polyoxometalates-Based Chiral Organic–Inorganic Hybrids. *Inorg. Chem.* **2015**, *54* (6), 2551–2559. <https://doi.org/10.1021/ic502622k>.
- (82) Micoine, K.; Malacria, M.; Lacôte, E.; Thorimbert, S.; Hasenknopf, B. Regioselective Double Organic Functionalization of Polyoxotungstates through Electrophilic Addition of

- Aromatic Isocyanates to  $[P_2W_{17}O_{61}(SnR)]^{7-}$ . *Eur. J. Inorg. Chem.* **2013**, 2013 (10–11), 1737–1741. <https://doi.org/10.1002/ejic.201201147>.
- (83) Boglio, C.; Micoine, K.; Derat, É.; Thouvenot, R.; Hasenknopf, B.; Thorimbert, S.; Lacôte, E.; Malacria, M. Regioselective Activation of Oxo Ligands in Functionalized Dawson Polyoxotungstates. *J. Am. Chem. Soc.* **2008**, *130* (13), 4553–4561. <https://doi.org/10.1021/ja800072q>.
- (84) Santoni, M.-P.; Hanan, G. S.; Hasenknopf, B. Covalent Multi-Component Systems of Polyoxometalates and Metal Complexes: Toward Multi-Functional Organic–Inorganic Hybrids in Molecular and Material Sciences. *Coord. Chem. Rev.* **2014**, *281*, 64–85. <https://doi.org/10.1016/j.ccr.2014.09.003>.
- (85) Odobel, F.; Séverac, M.; Pellegrin, Y.; Blart, E.; Fosse, C.; Cannizzo, C.; Mayer, C. R.; Elliott, K. J.; Harriman, A. Coupled Sensitizer-Catalyst Dyads: Electron-Transfer Reactions in a Perylene-Polyoxometalate Conjugate. *Chem. - Eur. J.* **2009**, *15* (13), 3130–3138. <https://doi.org/10.1002/chem.200801880>.
- (86) Tagliavini, V.; Honisch, C.; Serrati, S.; Azzariti, A.; Bonchio, M.; Ruzza, P.; Carraro, M. Enhancing the Biological Activity of Polyoxometalate–Peptide Nano-Fibrils by Spacer Design. *RSC Adv.* **2021**, *11* (9), 4952–4957. <https://doi.org/10.1039/D0RA10218K>.
- (87) Gumerova, N. I.; Blazevic, A.; Caldera Fraile, T.; Roller, A.; Giester, G.; Rompel, A. Synthesis and Characterization of Hybrid Anderson Hexamolybdoaluminates(III) Functionalized with Indometacin or Cinnamic Acid. *Acta Crystallogr. Sect. C Struct. Chem.* **2018**, *74* (Pt 11), 1378–1383. <https://doi.org/10.1107/S2053229618012536>.
- (88) Stuckart, M.; Monakhov, K. Yu. Polyoxometalates as Components of Supramolecular Assemblies. *Chem. Sci.* **2019**, *10* (16), 4364–4376. <https://doi.org/10.1039/C9SC00979E>.
- (89) Yvon, C.; Macdonell, A.; Buchwald, S.; Surman, A. J.; Follet, N.; Alex, J.; Long, D.-L.; Cronin, L. A Collection of Robust Methodologies for the Preparation of Asymmetric Hybrid Mn–Anderson Polyoxometalates for Multifunctional Materials. *Chem Sci* **2013**, *4* (10), 3810–3817. <https://doi.org/10.1039/C3SC51618K>.
- (90) Yvon, C.; Surman, A. J.; Hutin, M.; Alex, J.; Smith, B. O.; Long, D.-L.; Cronin, L. Polyoxometalate Clusters Integrated into Peptide Chains and as Inorganic Amino Acids: Solution- and Solid-Phase Approaches. *Angew. Chem. Int. Ed.* **2014**, *53* (13), 3336–3341. <https://doi.org/10.1002/anie.201311135>.
- (91) Kang, S.; Ono, R. J.; Bielawski, C. W. Synthesis of Poly(3-Hexylthiophene)- Block - Poly(Ethylene)- Block -Poly(3-Hexylthiophene) via a Combination of Ring-Opening Olefin Metathesis Polymerization and Grignard Metathesis Polymerization. *J. Polym. Sci. Part Polym. Chem.* **2013**, *51* (18), 3810–3817. <https://doi.org/10.1002/pola.26798>.
- (92) Macdonell, A.; Johnson, N. A. B.; Surman, A. J.; Cronin, L. Configurable Nanosized Metal Oxide Oligomers via Precise “Click” Coupling Control of Hybrid Polyoxometalates. *J. Am. Chem. Soc.* **2015**, *137* (17), 5662–5665. <https://doi.org/10.1021/jacs.5b02466>.
- (93) Song, Y.-F.; Long, D.-L.; Kelly, S. E.; Cronin, L. Sorting the Assemblies of Unsymmetrically Covalently Functionalized Mn-Anderson Polyoxometalate Clusters with Mass Spectrometry. *Inorg. Chem.* **2008**, *47* (20), 9137–9139. <https://doi.org/10.1021/ic801366r>.
- (94) Liu, B.; Yang, J.; Yang, M.; Wang, Y.; Xia, N.; Zhang, Z.; Zheng, P.; Wang, W.; Lieberwirth, I.; Kübel, C. Polyoxometalate Cluster-Contained Hybrid Gelator and Hybrid

- Organogel: A New Concept of Softening of Polyoxometalate Clusters. *Soft Matter* **2011**, *7* (6), 2317. <https://doi.org/10.1039/c1sm05032j>.
- (95) Wang, X.-L.; Wang, Y.-L.; Miao, W.-K.; Hu, M.-B.; Tang, J.; Yu, W.; Hou, Z.-Y.; Zheng, P.; Wang, W. Langmuir and Langmuir-Blodgett Films of Hybrid Amphiphiles with a Polyoxometalate Headgroup. *Langmuir ACS J. Surf. Colloids* **2013**, *29* (22), 6537–6545. <https://doi.org/10.1021/la401136a>.
- (96) Lahootun, V.; Besson, C.; Villanneau, R.; Villain, F.; Chamoreau, L.-M.; Boubekour, K.; Blanchard, S.; Thouvenot, R.; Proust, A. Synthesis and Characterization of the Keggin-Type Ruthenium-Nitrido Derivative [PW<sub>11</sub>O<sub>39</sub>{RuN}]<sup>4-</sup> and Evidence of Its Electrophilic Reactivity. *J. Am. Chem. Soc.* **2007**, *129* (22), 7127–7135. <https://doi.org/10.1021/ja071137t>.
- (97) Dablemont, C.; Hamaker, C. G.; Thouvenot, R.; Sojka, Z.; Che, M.; Maatta, E. A.; Proust, A. Functionalization of Heteropolyanions—Osmium and Rhenium Nitrido Derivatives of Keggin- and Dawson-Type Polyoxotungstates: Synthesis, Characterization and Multinuclear (183W,15N) NMR, EPR, IR, and UV/Vis Fingerprints. *Chem. - Eur. J.* **2006**, *12* (36), 9150–9160. <https://doi.org/10.1002/chem.200600934>.
- (98) Mehr, S. H. M.; Craven, M.; Leonov, A. I.; Keenan, G.; Cronin, L. A Universal System for Digitization and Automatic Execution of the Chemical Synthesis Literature. *Science* **2020**, *370* (6512), 101–108. <https://doi.org/10.1126/science.abc2986>.
- (99) Steiner, S.; Wolf, J.; Glatzel, S.; Andreou, A.; Granda, J. M.; Keenan, G.; Hinkley, T.; Aragon-Camarasa, G.; Kitson, P. J.; Angelone, D.; Cronin, L. Organic Synthesis in a Modular Robotic System Driven by a Chemical Programming Language. *Science* **2019**, *363* (6423), eaav2211. <https://doi.org/10.1126/science.aav2211>.
- (100) Merrifield, R. B. Automated Synthesis of Peptides: Solid-Phase Peptide Synthesis, a Simple and Rapid Synthetic Method, Has Now Been Automated. *Science* **1965**, *150* (3693), 178–185. <https://doi.org/10.1126/science.150.3693.178>.
- (101) Plante, O. J.; Palmacci, E. R.; Seeberger, P. H. Automated Solid-Phase Synthesis of Oligosaccharides. *Science* **2001**, *291* (5508), 1523–1527. <https://doi.org/10.1126/science.1057324>.
- (102) Alvarado-Urbina, G.; Sathe, G. M.; Liu, W.-C.; Gillen, M. F.; Duck, P. D.; Bender, R.; Ogilvie, K. K. Automated Synthesis of Gene Fragments. *Science* **1981**, *214* (4518), 270–274. <https://doi.org/10.1126/science.6169150>.
- (103) Liu, C.; Xie, J.; Wu, W.; Wang, M.; Chen, W.; Idres, S. B.; Rong, J.; Deng, L.-W.; Khan, S. A.; Wu, J. Automated Synthesis of Prexasertib and Derivatives Enabled by Continuous-Flow Solid-Phase Synthesis. *Nat. Chem.* **2021**, *13* (5), 451–457. <https://doi.org/10.1038/s41557-021-00662-w>.
- (104) Li, J.; Ballmer, S. G.; Gillis, E. P.; Fujii, S.; Schmidt, M. J.; Palazzolo, A. M. E.; Lehmann, J. W.; Morehouse, G. F.; Burke, M. D. Synthesis of Many Different Types of Organic Small Molecules Using One Automated Process. *Science* **2015**, *347* (6227), 1221–1226. <https://doi.org/10.1126/science.aaa5414>.
- (105) Pyles, H.; Zhang, S.; De Yoreo, J. J.; Baker, D. Controlling Protein Assembly on Inorganic Crystals through Designed Protein Interfaces. *Nature* **2019**, *571* (7764), 251–256. <https://doi.org/10.1038/s41586-019-1361-6>.
- (106) Addadi, L.; Joester, D.; Nudelman, F.; Weiner, S. Mollusk Shell Formation: A Source of New Concepts for Understanding Biomineralization Processes. *Chem. - Eur. J.* **2006**, *12* (4), 980–987. <https://doi.org/10.1002/chem.200500980>.

- (107) Hamley, I. W. The Amyloid Beta Peptide: A Chemist's Perspective. Role in Alzheimer's and Fibrillization. *Chem. Rev.* **2012**, *112* (10), 5147–5192. <https://doi.org/10.1021/cr3000994>.
- (108) Soria-Carrera, H.; Franco-Castillo, I.; Romero, P.; Martín, S.; Fuente, J. M.; Mitchell, S. G.; Martín-Rapún, R. On-POM Ring-Opening Polymerisation of *N*-Carboxyanhydrides. *Angew. Chem. Int. Ed.* **2021**, *60* (7), 3449–3453. <https://doi.org/10.1002/anie.202013563>.
- (109) Pope, M. T.; Müller, A. Polyoxometalate Chemistry: An Old Field with New Dimensions in Several Disciplines. *Angew. Chem. Int. Ed. Engl.* **1991**, *30* (1), 34–48. <https://doi.org/10.1002/anie.199100341>.
- (110) Liu, T.; Diemann, E.; Li, H.; Dress, A. W. M.; Müller, A. Self-Assembly in Aqueous Solution of Wheel-Shaped Mo<sub>154</sub> Oxide Clusters into Vesicles. *Nature* **2003**, *426* (6962), 59–62. <https://doi.org/10.1038/nature02036>.
- (111) Chen, X.; Zhang, G.; Li, B.; Wu, L. An Integrated Giant Polyoxometalate Complex for Photothermally Enhanced Catalytic Oxidation. *Sci. Adv.* **2021**, *7* (30), eabf8413. <https://doi.org/10.1126/sciadv.abf8413>.
- (112) Chen, J.-J.; Symes, M. D.; Cronin, L. Highly Reduced and Protonated Aqueous Solutions of [P<sub>2</sub>W<sub>18</sub>O<sub>62</sub>]<sup>6-</sup> for on-Demand Hydrogen Generation and Energy Storage. *Nat. Chem.* **2018**, *10* (10), 1042–1047. <https://doi.org/10.1038/s41557-018-0109-5>.
- (113) She, S.; Xuan, W.; Bell, N. L.; Pow, R.; Ribo, E. G.; Sinclair, Z.; Long, D.-L.; Cronin, L. Peptide Sequence Mediated Self-Assembly of Molybdenum Blue Nanowheel Superstructures. *Chem. Sci.* **2021**, *12* (7), 2427–2432. <https://doi.org/10.1039/D0SC06098D>.
- (114) Bareyt, S.; Piligkos, S.; Hasenknopf, B.; Gouzerh, P.; Lacôte, E.; Thorimbert, S.; Malacria, M. Highly Efficient Peptide Bond Formation to Functionalized Wells-Dawson-Type Polyoxotungstates. *Angew. Chem. Int. Ed.* **2003**, *42* (29), 3404–3406. <https://doi.org/10.1002/anie.200351346>.
- (115) Xiao, Z.; Chen, K.; Wu, B.; Li, W.; Wu, P.; Wei, Y. An Easy Way to Construct Polyoxovanadate-Based Organic–Inorganic Hybrids by Stepwise Functionalization. *Eur. J. Inorg. Chem.* **2016**, *2016* (6), 808–811. <https://doi.org/10.1002/ejic.201501297>.
- (116) Makrygenni, O.; Secret, E.; Michel, A.; Brouri, D.; Dupuis, V.; Proust, A.; Siaugue, J.-M.; Villanneau, R. Heteropolytungstate-Decorated Core-Shell Magnetic Nanoparticles: A Covalent Strategy for Polyoxometalate-Based Hybrid Nanomaterials. *J. Colloid Interface Sci.* **2018**, *514*, 49–58. <https://doi.org/10.1016/j.jcis.2017.12.019>.
- (117) Graham, C. R.; Finke, R. G. The Classic Wells–Dawson Polyoxometalate, K<sub>6</sub> [α-P<sub>2</sub>W<sub>18</sub>O<sub>62</sub>]-14H<sub>2</sub>O. Answering an 88 Year-Old Question: What Is Its Preferred, Optimum Synthesis? *Inorg. Chem.* **2008**, *47* (9), 3679–3686. <https://doi.org/10.1021/ic702295y>.
- (118) Ginsberg, A. P. *Inorganic Syntheses*; Inorganic syntheses; J. Wiley & sons: New York Chichester Brisbane [etc.], 1990.
- (119) Gottlieb, H. E.; Kotlyar, V.; Nudelman, A. NMR Chemical Shifts of Common Laboratory Solvents as Trace Impurities. *J. Org. Chem.* **1997**, *62* (21), 7512–7515. <https://doi.org/10.1021/jo971176v>.
- (120) Morera, E.; Ortar, G. A Palladium-Catalyzed Carbonylative Route to Primary Amides. *Tetrahedron Lett.* **1998**, *39* (18), 2835–2838. [https://doi.org/10.1016/S0040-4039\(98\)00259-7](https://doi.org/10.1016/S0040-4039(98)00259-7).
- (121) Schnyder, A.; Beller, M.; Mehlretter, G.; Nsenda, T.; Studer, M.; Indolese, A. F. Synthesis of Primary Aromatic Amides by Aminocarbonylation of Aryl Halides Using

- Formamide as an Ammonia Synthon. *J. Org. Chem.* **2001**, *66* (12), 4311–4315.  
<https://doi.org/10.1021/jo015577t>.
- (122) Pascual-Borràs, M.; López, X.; Poblet, J. M. Accurate Calculation of  $^{31}\text{P}$  NMR Chemical Shifts in Polyoxometalates. *Phys. Chem. Chem. Phys.* **2015**, *17* (14), 8723–8731.  
<https://doi.org/10.1039/C4CP05016A>.
- (123) Krueve, A.; Kaupmees, K.; Liigand, J.; Oss, M.; Leito, I. Sodium Adduct Formation Efficiency in ESI Source: Sodium Adduct Formation Efficiency in ESI Source. *J. Mass Spectrom.* **2013**, *48* (6), 695–702. <https://doi.org/10.1002/jms.3218>.
- (124) Jia, Q.; Zhang, Y.; Cao, J. Characterization of Polyoxometalates by Electrospray Ionization Mass Spectrometry. *Sci. China Chem.* **2015**, *58* (7), 1206–1210.  
<https://doi.org/10.1007/s11426-015-5355-4>.
- (125) Borràs-Almenar, J. J.; Coronado, E.; Müller, A.; Pope, M. T. *Polyoxometalate Molecular Science*; Springer Netherlands : Imprint : Springer: Dordrecht, 2003.
- (126) Pope, M. T.; Papaconstantinou, E. Heteropoly Blues. II. Reduction of 2:18-Tungstates. *Inorg. Chem.* **1967**, *6* (6), 1147–1152. <https://doi.org/10.1021/ic50052a018>.
- (127) Elgrishi, N.; Rountree, K. J.; McCarthy, B. D.; Rountree, E. S.; Eisenhart, T. T.; Dempsey, J. L. A Practical Beginner's Guide to Cyclic Voltammetry. *J. Chem. Educ.* **2018**, *95* (2), 197–206. <https://doi.org/10.1021/acs.jchemed.7b00361>.
- (128) Cameron, J. M.; Fujimoto, S.; Wei, R.-J.; Newton, G. N.; Oshio, H. Post-Functionalization of a Photoactive Hybrid Polyoxotungstate. *Dalton Trans.* **2018**, *47* (31), 10590–10594.  
<https://doi.org/10.1039/C8DT01253A>.
- (129) Hampson, E.; Cameron, J. M.; Amin, S.; Kyo, J.; Watts, J. A.; Oshio, H.; Newton, G. N. Asymmetric Hybrid Polyoxometalates: A Platform for Multifunctional Redox-Active Nanomaterials. *Angew. Chem. Int. Ed.* **2019**, *58* (50), 18281–18285.  
<https://doi.org/10.1002/anie.201912046>.
- (130) Liu, Z.; Huang, F.; Wu, P.; Wang, Q.; Yu, Z. Amide Bond Formation Assisted by Vicinal Alkylthio Migration in Enaminones: Metal- and CO-Free Synthesis of  $\alpha,\beta$ -Unsaturated Amides. *J. Org. Chem.* **2018**, *83* (10), 5731–5750.  
<https://doi.org/10.1021/acs.joc.8b00775>.
- (131) Schowen, R. L.; Jayaraman, H.; Kershner, L. Catalytic Efficiencies in Amide Hydrolysis. The Two-Step Mechanism  $^{1,2}$ . *J. Am. Chem. Soc.* **1966**, *88* (14), 3373–3375.  
<https://doi.org/10.1021/ja00966a034>.
- (132) Borràs-Almenar, J. J.; Coronado, E.; Müller, A.; Pope, M. T. *Polyoxometalate Molecular Science*; Springer Netherlands : Imprint : Springer: Dordrecht, 2003.
- (133) Chen, W.; Tong, U.; Zeng, T.; Streb, C.; Song, Y.-F. Reversible Photodimerization of Coumarin-Modified Wells–Dawson Anions. *J. Mater. Chem. C* **2015**, *3* (17), 4388–4393.  
<https://doi.org/10.1039/C5TC00379B>.
- (134) Ravelli, D.; Fagnoni, M.; Fukuyama, T.; Nishikawa, T.; Ryu, I. Site-Selective C–H Functionalization by Decatungstate Anion Photocatalysis: Synergistic Control by Polar and Steric Effects Expands the Reaction Scope. *ACS Catal.* **2018**, *8* (1), 701–713.  
<https://doi.org/10.1021/acscatal.7b03354>.
- (135) Wild, A.; Winter, A.; Schlütter, F.; Schubert, U. S. Advances in the Field of  $\pi$ -Conjugated 2,2':6',2''-Terpyridines. *Chem Soc Rev* **2011**, *40* (3), 1459–1511.  
<https://doi.org/10.1039/C0CS00074D>.
- (136) Sauvage, J. P.; Collin, J. P.; Chambron, J. C.; Guillerez, S.; Coudret, C.; Balzani, V.; Barigelli, F.; De Cola, L.; Flamigni, L. Ruthenium(II) and Osmium(II) Bis(Terpyridine)

- Complexes in Covalently-Linked Multicomponent Systems: Synthesis, Electrochemical Behavior, Absorption Spectra, and Photochemical and Photophysical Properties. *Chem. Rev.* **1994**, *94* (4), 993–1019. <https://doi.org/10.1021/cr00028a006>.
- (137) Mutai, T.; Cheon, J.-D.; Arita, S.; Araki, K. Phenyl-Substituted 2,2':6',2''-Terpyridine as a New Series of Fluorescent Compounds—Their Photophysical Properties and Fluorescence Tuning. *J. Chem. Soc. Perkin Trans. 2* **2001**, No. 7, 1045–1050. <https://doi.org/10.1039/b102685m>.
- (138) Jørgensen, M.; Krebs, F. C. Stepwise Unidirectional Synthesis of Oligo Phenylene Vinylenes with a Series of Monomers. Use in Plastic Solar Cells. *J. Org. Chem.* **2005**, *70* (15), 6004–6017. <https://doi.org/10.1021/jo0506783>.
- (139) Hagemann, O.; Jørgensen, M.; Krebs, F. C. Synthesis of an All-in-One Molecule (for Organic Solar Cells). *J. Org. Chem.* **2006**, *71* (15), 5546–5559. <https://doi.org/10.1021/jo060491r>.
- (140) Amin, S.; Cameron, J. M.; Watts, J. A.; Walsh, D. A.; Sans, V.; Newton, G. N. Effects of Chain Length on the Size, Stability, and Electronic Structure of Redox-Active Organic–Inorganic Hybrid Polyoxometalate Micelles. *Mol. Syst. Des. Eng.* **2019**, *4* (5), 995–999. <https://doi.org/10.1039/C9ME00060G>.
- (141) Clayden, J.; Greeves, N.; Warren, S. G. *Organic Chemistry*, 2nd ed.; Oxford University Press: Oxford; New York, 2012.
- (142) Balthazor, T. M.; Grabiak, R. C. Nickel-Catalyzed Arbuzov Reaction: Mechanistic Observations. *J. Org. Chem.* **1980**, *45* (26), 5425–5426. <https://doi.org/10.1021/jo01314a059>.
- (143) Matt, B.; Coudret, C.; Viala, C.; Jouvenot, D.; Loiseau, F.; Izzet, G.; Proust, A. Elaboration of Covalently Linked Polyoxometalates with Ruthenium and Pyrene Chromophores and Characterization of Their Photophysical Properties. *Inorg. Chem.* **2011**, *50* (16), 7761–7768. <https://doi.org/10.1021/ic200906b>.
- (144) Barthelmes, K.; Winter, A.; Schubert, U. S. Dyads and Triads Based on Phenothiazine, Bis(Terpyridine)Ruthenium(II) Complexes, and Fullerene. *Eur. J. Inorg. Chem.* **2016**, *2016* (32), 5132–5142. <https://doi.org/10.1002/ejic.201600793>.
- (145) Johnson, B. A.; Agarwala, H.; White, T. A.; Mijangos, E.; Maji, S.; Ott, S. Judicious Ligand Design in Ruthenium Polypyridyl CO<sub>2</sub> Reduction Catalysts to Enhance Reactivity by Steric and Electronic Effects. *Chem. - Eur. J.* **2016**, *22* (42), 14870–14880. <https://doi.org/10.1002/chem.201601612>.
- (146) Winter, A.; Schubert, U. S. Metal-Terpyridine Complexes in Catalytic Application – A Spotlight on the Last Decade. *ChemCatChem* **2020**, *12* (11), 2890–2941. <https://doi.org/10.1002/cctc.201902290>.
- (147) Winter, A.; Schubert, U. S. Synthesis and Characterization of Metallo-Supramolecular Polymers. *Chem. Soc. Rev.* **2016**, *45* (19), 5311–5357. <https://doi.org/10.1039/C6CS00182C>.
- (148) Serp, P.; Hernandez, M.; Richard, B.; Kalck, P. A Facile Route to Carbonylhalogenometal Complexes (M = Rh, Ir, Ru, Pt) by Dimethylformamide Decarbonylation. *Eur. J. Inorg. Chem.* **2001**, *2001* (9), 2327–2336. [https://doi.org/10.1002/1099-0682\(200109\)2001:9<2327::AID-EJIC2327>3.0.CO;2-D](https://doi.org/10.1002/1099-0682(200109)2001:9<2327::AID-EJIC2327>3.0.CO;2-D).
- (149) Benavides, P. A.; Matias, T. A.; Araki, K. Unexpected Lability of the [Ru<sup>III</sup>(Phtpy)Cl<sub>3</sub>] Complex. *Dalton Trans.* **2017**, *46* (44), 15567–15572. <https://doi.org/10.1039/C7DT03658B>.

- (150) Haukka, M.; Kiviaho, J.; Ahlgren, M.; Pakkanen, T. A. Studies on Catalytically Active Ruthenium Carbonyl Bipyridine Systems. Synthesis and Structural Characterization of  $[\text{Ru}(\text{Bpy})(\text{CO})_2\text{Cl}_2]$ ,  $[\text{Ru}(\text{Bpy})(\text{CO})_2\text{Cl}(\text{C}(\text{O})\text{OCH}_3)]$ ,  $[\text{Ru}(\text{Bpy})(\text{CO})_2\text{Cl}]_2$ , and  $[\text{Ru}(\text{Bpy})(\text{CO})_2\text{ClH}]$  (Bpy = 2,2'-Bipyridine). *Organometallics* **1995**, *14* (2), 825–833. <https://doi.org/10.1021/om00002a033>.
- (151) Homanen, P.; Haukka, M.; Pakkanen, T. A.; Pursiainen, J.; Laitinen, R. H. Ruthenium(II) Bipyridine Complexes: Synthesis and Characterization of  $\text{Ru}(\text{Bpy})(\text{CO})_2(\text{SCN})_2$ ,  $\text{Ru}(\text{Dmbpy})(\text{CO})_2\text{Cl}_2$ , and  $\text{Ru}(\text{Dmbpy})(\text{CO})_2(\text{NCS})\text{H}$  (Bpy = 2,2'-Bipyridine; Dmbpy = 6,6'-Dimethyl-2,2'-Bipyridine). *Organometallics* **1996**, *15* (19), 4081–4084. <https://doi.org/10.1021/om9602724>.